



Norwegian University of
Science and Technology

A song of Host and Virus:
Studying Phage Plaque Development on Bacterial
Lawns

Aslak Todal

January 24th, 2020

Chemical Engineering and Biotechnology

Submission date: January 2020

Supervisor Eivind Almaas, IBT

Co-supervisor Nikolay Martyushenko, IBT

Norwegian University of Science and Technology
Department of Chemical Engineering

Preface

Phew! I have learned a lot during this process. However, I'm deeply thankful for having been in the dark about just how complex some of this would get, as I couldn't have imagined finding myself in the position of having to explain how diffusion in an extra spatial dimension would play into the progression viral proliferation when I first tried to create a time laps video of plaque formation.

I would like to extend my gratitude to my supervisor Eivind Almaas and my co-supervisor Nikolay Martyushenko; for always having faith in my work and giving me the freedom and labspace to pursue new ideas.

A special thank you to my girlfriend Lisa Yvonne Mele, the trained anthropologist who volunteered to edit this monstrosity.

One of the great things about books is sometimes there are some fantastic pictures.

George W. Bush

Declaration of Compliance

I hereby declare I have not cheated.

Aslak Todal

Trondheim, January 24th, 2020

Abstract

This thesis presents novel methods, equipment, and a mathematical model for the study of bacteriophage plaque development on bacterial lawns in semi-solid agar. The Cellfiebooth system, which I developed and first presented in my previous report "Fluorescence Imaging of the Pre-Visible Stage of Bacteriophage Plaque Formation" [1] is used as the method for measuring plaque development. The system is based on determining the distribution of DNA released by phage-induced bacterial lysis. The developed model is a reaction-diffusion model and considers the diffusion of both nutrient and phage, while focusing on the shape and growth of plaques in bacterial lawns. Comparing the experimental and theoretical results, it was found that the diffusion of nutrient from within the plaque is a vital driver for the late expansion of plaques. It was also found that the bacterial host can change growth strategy during the experiment, and that this will have severe consequences for plaque morphology. In addition, a new protocol was developed for determining the burst size, lysis time and standard deviation in the lysis time of a phage strain, all in a single experiment. I hope that the presented advances in the continuous measurement and modelling of viral plaque development, can be useful for readers aspiring to progress in the field of phage therapy.

Sammendrag

I denne masteroppgaven presenteres nye metoder, utstyr og en matematisk modell for undersøkelse av utviklingen av bakteriofagplakk i semisolid agar fylt med bakterier. Cellfiebooth-systemet, opprinnelig utviklet og introdusert i prosjektoppgaven «Fluorescence Imaging of the Pre-Visible Stage of Bacteriophage Plaque Formation» [1], anvendes for å måle dannelsen av plakk. Systemet er basert på måling av DNA-distribusjon som følge av bakteriolyse induisert av bakteriofager. Den utviklede reaksjon- og diffusjonsmodellen forholder seg til diffusjonen av både næring og bakteriofager, og tar høyde for plakkens form og vekst. Gjennom komparasjon av eksperimentelle og teoretiske resultater, stadfestes det at diffusjon av næring fra plakkens innside er en vital driver for sen plakkekspansjon. Det blir også etablert at bakterieverter kan endre vekststrategi underveis i eksperimenters forløp, og at dette da vil ha alvorlige konsekvenser for plakkens morfologi. I tillegg utvikles en ny protokoll for bestemmelse av antall nye virus fra en infeksjon, tidsrommet mellom infeksjon og lysis, samt standardavvik for tidsrommet mellom infeksjon og lysis—alt i ett eksperiment. Jeg håper de presenterte utviklingene innen kontinuerlig måling og modellering av viral plakkutvikling kan være nyttig for lesere med som har fremgang innen bakteriofagterapi som hensikt.

Table of Content

1	Introduction	1
2	Theory	5
2.1	Virus, phages and their propagation	5
2.1.1	Phages	6
2.1.2	Plaques	8
2.2	Bacteria, Escherichia coli, and growth	9
2.3	Modelling	11
2.3.1	Is it useful?	11
2.3.2	Reaction-diffusion models	13
2.3.3	Viral reaction and diffusion	15
2.4	Numerical analysis	16
2.5	Why is everything normally distributed?	18
2.5.1	Normal distribution	18
2.5.2	Gamma distribution	19
2.5.3	Central limit theorem	20
3	Method	22
3.1	Bacterial and viral strains	22
3.2	Cellfiebooth	22
3.2.1	Protocol	22
3.2.2	Test for bacterial fluorescence	24
3.2.3	Changes to the Cellfiebooth system	24
3.3	Characterisation of growth rate of bacteria immobilised in soft agar	25
3.4	Characterisation of viral burst size and lysis time	27
3.5	Mathematical model	29
4	Results and analysis	35
4.1	Characterisation of growth rate	35
4.2	Burst size and eclipse time	39
4.3	Test for bacterial fluorescence	46
4.4	Cellfiebooth and model results	48
4.4.1	Experimental run 1.1 with DH5 α	48
4.4.2	Experimental run 1.2 with DH5 α	69
4.4.3	Experimental run 1.3 with DH5 α	89
4.4.4	Experimental run 2.1 with BL21	92
5	Discussion	104
5.1	Burst size and lysis time	104
5.2	Characterisation of growth rate	105
5.3	Cellfiebooth and model results	106

5.3.1	Cellfiebooth	106
5.3.2	Model	107
5.3.3	Cellfiebooth and model in relation to previously exper- imental and theoretical attempts to characterise the formation of plaques	110
5.3.4	Run 1.3	113
6	Conclusion	115
	References	117
	Appendix	125
A	Protocol for making M9 broth	125
A.1	M9 5x stock	125
A.2	M9 1x working solutions	125
B	Characterisation of growth rate - additional data	126
C	Burst size and lysis time - additional data	127
D	Observed effects from Cellfiebooth regarding measurement of light	130

List of Figures

1	Infected bacterial cells filled with capsomeres and phage DNA. Illustration by Ingemund Skålnes through personal communications. December 25th, 2019.	5
2	The lytic cycle of a phage. Bacteria, DNA and virus not drawn to scale. By Ingemund Skålnes through personal communications. 25 December 2019.	7
3	The different phases of bacterial growth. The lower curve shows the log bacterial density, while the upper curve shows the growth rate at the same stages. Figure originally published in Monods 1949 paper[53].	10
4	Growth rate of <i>M. tuberculosis</i> in Dubos' medium, as a function of glucose concentration. Figure originally published in Monods 1949 paper[53].	11
5	Turing patterns generated by numerically solving the FitzHugh–Nagumo equation. Generated in python. Source code under MIT License[69].	14
6	The results from table 1	17
7	Probability density for normal distribution. "Standard deviation diagram" by Dan Kernler CC BY 4.0[88].	19
8	Gamma distribution for different shape parameters. Figure was generated in python, by me.	20
9	Picture of the Cellfiebooth hardware with light-source on. The camera (1) is on top of the cupboard and the lens is sticking in and focusing on the Petri dish (2). The light source (3) is under faced up, but not directly against the camera. A cardboard box (4) covers the camera under an experimental run to avoid light pollution.	23
10	Example of experimental data evaluating against a model in a spreadsheet.	26
11	Example figure of how burst size is determined. The sketch shows the rate of change in bacterial concentration with regards to time. The two lines correspond to bacterial solutions inoculated with phages, where the bacterial concentrations are initially equal. The initial phage concentration in the blue line is the initial phage concentration in the red line diluted by a factor of the burst size of the phage inoculated. The letters A, B, C, and D correspond to the area beneath the graphs. The ratio between A and B are equal to C and D.	28
12	Simplified state map over the model.	29
13	Complete state map over the model.	30

14	Growth of DH5a. Scatter plot showing the average of the bacterial concentration given in OD ₆₀₀ for different initial bacterial concentrations. The results appear as lines due to the high amount of data points. The experiment was done with ten replicates for each dilutions and the graphs show the average of the dilutions. Error bars are not included as the largest standard deviation was 0.029.	36
15	Growth of BL21. Scatter plot showing the average bacterial concentration given in OD ₆₀₀ for different initial bacterial concentrations. Error bars are given for every tenth data point. The results appear as lines due to the high amount of data points	36
16	Comparison of experimental data with mathematical model. <i>E. coli</i> strain BL21 in sloppy agar with different start concentrations.	38
17	Comparison of experimental data with mathematical model. <i>E. coli</i> strain DH5α in sloppy agar with different start concentrations.	38
18	Cell concentration measured in OD ₆₀₀ for DH5α introduced to different concentrations of the phage. The lines represent the average from an experiment conducted with seven replicates. The largest variance was 0.077. The early values, especially for the control, are affected by dew in the machine.	40
19	Cell concentration measured in OD ₆₀₀ for BL21 was introduced to different concentrations of the phage. The lines are the average from the experiment done with seven replicates. Largest variance was 0.033. The early values are affected by dew in the machine.	41
20	Change in OD ₆₀₀ over time for DH5a introduced to different concentrations of phages. Data is filtered with five point average. Every other dilution is shown. The dilutions not included follow the same pattern as displayed and can be found in appendix C	42
21	Change in OD ₆₀₀ over time for BL21 introduced to different concentrations of phages.	43
22	The gamma distribution fitted to the first negative peaks for BL21 introduced different concentrations of phage. This was done to find the deviation in lysis time and the results are shown in table 6	44
23	The gamma distribution fitted to the first negative peaks for DH5α introduced different concentrations of phage. This was done to find the deviation in lysis time and the results are shown in table 6.	44

24	Cellfiebooth results at different time points. The number in the series is given in the left corner of the image.	46
25	Both images were captured and processed with Cellfiebooth. The light intensity has been scaled by a factor of 40 to make the effect visible to the naked eye. The left side is with Gel-Green and the right side is without.	47
26	Change in light intensity over time in the bacterial lawn in experiment 1.1.	49
27	DH5 α with initial OD ₆₀₀ = 0.086. The number in the series is given in the left corner of the image. There are six minutes between each number. Data were captured before the improvements mentioned in 3.2.3 A fungus started growing at the bottom of the Petri dish. The plaques in box A and B are studied. closer	50
28	Closer look at the data from box b in figure 27 presented in a grayscale heatmap. The data were treated with a Gaussian filter with sigma = 5.	51
29	Experimental data in box B at 16 hours, compared to the model.	52
30	Experimental data in box B at 23 hours, 48 min compared to the model.	53
31	Experimental data in box B at 31 hours, 36 min compared to the model.	54
32	Experimental data in box B at 39 hours, 24 min compared to the model.	55
33	Experimental data in box B at 47 hours, 12 min compared to the model.	56
34	Experimental data in box B at 55 hours, 48 min compared to the model.	57
35	Radial profile of plaque in box B in the experimental result found by calculating the radial average.	58
36	Radial profile for the theoretical results.	59
37	Closer look at the data from box A in figure 27 presented in a grayscale heatmap. The data were treated with a Gaussian filter with sigma = 5.	61
38	Experimental data in box A at 16 hours, compared to the model.	62
39	Experimental data in box A at 23 hours and 48 min, compared to the model.	63
40	Experimental data in box A at 31 hours and 36 min, compared to the model.	64
41	Experimental data in box A at 39 hours 24 min, compared to the model.	65
42	Experimental data in box A at 46 hours and 36 min, compared to the model.	66
43	Experimental data in box A at 55 hours, compared to the model.	67

44	Change in light intensity over time in the bacterial lawn in experiment 1.2.	69
45	DH5 α with initial OD ₆₀₀ = 0.333. The number in the series is given in the left corner of the image. Six minutes between each number. The plaques in box C and D are studied closer	70
46	Closer look at the data from box C in figure 45 presented in a grayscale heatmap. The data were treated with a Gaussian filter with sigma = 5.	71
47	Experimental data in box C at 9 hours, compared to the model.	72
48	Experimental data in box C at 25 hours and 12 min, compared to the model.	73
49	Experimental data in box C at 41 hours and 24 min, compared to the model.	74
50	Experimental data in box C at 57 hours and 36 min, compared to the model.	75
51	Experimental data in box C at 73 hours and 48 min, compared to the model.	76
52	Experimental data in box C at 90 hours, compared to the model.	77
53	Radial profile of plaque in box C in the experimental result found by calculating the radial average. The radial profile for image nr. 414 show a clear double peak, and the following images show a saddle point where the first local maximum was measured.	79
54	Radial profile of plaque in box C in the theoretical result. The model predicts that the plaque stops expanding completely after 25 hours, and little to no change happens past this point.	80
55	Radial profile of the infected bacteria in box C in the theoretical result. The model predicts that the bacteria continues to be infected, but as new phages are not produced and the amount of phages decrease for each bacteria that is infected the rate of expansion in infected bacteria decreases as well.	80
56	Closer look at the data from box D in figure 45 presented in a grayscale heatmap. The data were treated with a Gaussian filter with sigma = 5.	81
57	Experimental data in box D at 9 hours, compared to the model.	82
58	Experimental data in box D at 25 hours and 12 min, compared to the model.	83
59	Experimental data in box D at 41 hours and 24 min, compared to the model.	84
60	Experimental data in box D at 57 hours and 36 min, compared to the model.	85
61	Experimental data in box D at 73 hours and 48 min, compared to the model.	86
62	Experimental data in box D at 90 hours, compared to the model.	87

63	Change in light intensity over time in different parts of the bacterial lawn in experiment 1.3. The graph show local variations in the bacterial growth curve.	90
64	DH5 α with unknown initial bacterial concentration. The number in the series is given in the left corner of the image. Six minutes between each number. The two plaques that merge create a double ring while the plaques that are seemingly unaffected by neighbouring plaques do not.	91
65	Change in light intensity over time in the bacterial lawn in experiment 2.1.	93
66	BL21 with initial OD ₆₀₀ = 0.808. The number in the series is given in the left corner of the image. Six minutes between each number. Data captured before the improvements mentioned in 3.2.3. Box E is studied closer.	94
67	Closer look at the data from box E in figure 66 presented in a grayscale heatmap. The data were treated with a Gaussian filter with sigma = 5.	95
68	Experimental data in box E at 5 hours, compared to the model.	96
69	Experimental data in box E at 19 hours, compared to the model.	97
70	Experimental data in box E at 33 hours, compared to the model.	98
71	Experimental data in box E at 47 hours, compared to the model.	99
72	Experimental data in box E at 61 hours, compared to the model.	100
73	Experimental data in box E at 75 hours, compared to the model.	101
74	Radial profile of plaque in box E in the experimental result found by calculating the radial average.	102
75	Radial profile of plaque in box in the theoretical result. The model predicts that the plaque stops expanding completely after 20 hours, and little to no change happens past this point.	103
76	Growth curve for <i>E. coli</i> BL21. The dashed line shows the modelled growth for the same seeding OD. All models have the same constants related to growth kinetics.	126
77	Growth curve for <i>E. coli</i> DH5 α . The dashed line shows the modelled growth for the same seeding OD. All models have the same constants related to growth kinetics.	127
78	Rate of change in OD ₆₀₀ over time for BL21 introduced to different concentrations of phages. Odd number dilutions. . .	128
79	Rate of change in OD ₆₀₀ over time for DH5a introduced to different concentrations of phages. Data filtered with 5 point average. Odd number dilutions.	128
80	Change in OD when the <i>E. coli</i> strain DH5 α is introduced to different concentrations of the UP phage.	129
81	515 nm longpass filter on top of 465 nm shortpass filter with LED lights on behind.	130
82	Light source directly under Petri dish in Cellfiebooth.	131

List of Tables

1	Euler's method for $y' = x + y$ for x from 0 to 1 with step-size $h = 0.2$	17
2	Overview of all constants used in the model and where they come from.	34
3	Growth constants found for each bacteria. The variance to the experimental data is shown in table 4	37
4	The variance, R^2 , between the model and experimental data for each dilution.	37
5	Ratio between the areas under first and second infection cycle and second and third infection cycle. The values are not displayed when one of the infection cycles were not present, or not strong enough to be measured.	43
6	The standard deviation in lysis time for the phage in DH5 α and BL21. Standard deviation in phage lysis time was identified by fitting the gamma distribution to the first negative peak, which is shown in figure 23 and 22. The R^2 for the fitted gamma distribution.	45
7	Burst size and lysis time for the phage in relation to the two different hosts.	45
8	Average pixel value for the different boxes in Figure 25.	47
9	Overview of the experimental runs included in the thesis.	48

1 Introduction

A little bit of history and a lot of discovery

During the austral summer of 1996-1997, an Australian research team travelled to the Antarctic[2]. There they sought out the lakes Fryxell, Hoare, and Joyce and retrieved water and ice samples at different depths. The lakes, placed at roughly 77°6' south, are covered by ice all year, and multi-cellular organisms are virtually absent[2]. With sub-zero temperatures all year long, and virtually no sunlight penetrating the 4 to 5 meter thick layer of ice, one would expect there to be few, *if any*, viruses and microbes present. Staggeringly, the samples from the ice and waters of these lakes showed otherwise. The research team discovered an abundance of viruses! Even their deepest samples, at 35m, contained over a million viruses per millilitre, with an average virus to bacteria ratio of 52.7.

The Naica mine is located 112 km south east of Chihuahua city in northern Mexico[3]. While it is one of the most important silver and lead deposits in the world, it is probably most famous for the Cave of the Crystals. This cave is connected to the mine at a depth of 300 meters, and the ceiling, wall and floor are completely draped with clear translucent gypsum crystals. The cave contains some of the largest natural crystals in the world, and only a handful of researchers have been allowed to enter since its discovery.[3, 4]. One of the privileged researchers having been permitted access to the cave, is the geologist Juan Manuel García-Ruiz and his team. What they found was that the cave was formed by volcanoes, 26 million years ago[3, 4]. The volcanic magma kept the cave steady at a high temperature of 54°C over hundreds of thousands of years. As it turns out, these conditions provided an ideal environment for the slow growing crystals to reach the ginormous size that earned them the status as the world's largest natural grown crystal.

Another group of researchers allowed to visit the exclusive cave, was Curtis Suttle and his team[5, 6]. While they must have been impressed by the crystals in the cave, they had little professional interest in them. Instead, they retrieved a water sample and brought it back home to their lab. Suttle's work is mainly in virology, and he was curious to see if there were organisms sturdy enough to survive in the harsh conditions of the cave. As the cave has been biologically cut off from the outside world for millions of years, you would think Suttle and his team were on a wild goose chase. They did not find any geese, but their findings certainly revealed life. The samples revealed 200 million viruses in each drop of water collected from the cave[4-6].

We find viruses almost wherever we look for them; in acidic hot springs, in antarctic lakes and in the deep sea[7, 8]. Even when we look in familiar, less known locations like human lungs—where it has been assumed we would not

find viruses—new ones are discovered.

In 2009, Dana Wilner, a biologist at San Diego State University, wished to look for viruses in the lungs of patients with cystic fibrosis. The occasion for this inquiry was that microbes and viruses had earlier been implicated in chronic pulmonary diseases[9]. She had five patients with cystic fibrosis and five healthy individuals (i.e. the control group) cough up sputum in cups. She brought the generously contributed sputum back to her lab, and placed the samples under a microscope. Looking through the microscope lens, she was met by surprising sights. All her samples were brimming with viruses. On average there were 175 different species of viruses per sample, 90% of which were completely unknown. After this study, the severely erroneous assumption that lungs of healthy individuals are sterile, was abruptly debunked.

We live on a planet of viruses.

Carl Zimmer

It is difficult to overstate the extent to which viruses are an integral part of our life on earth. Wherever we have found life, we have found viruses[1, 4, 8]. It is estimated that the ocean contains $1 \cdot 10^{31}$ virus particles, making them the most abundant biological entity in water[4, 8]. As astronomical as these numbers may sound, it has since been implied they are an underestimation, as the techniques commonly used to measure the amount of viruses in seawater often miss RNA viruses. These are estimated to represent between 38% - 63% of the total amount of viruses in the sea[10]. If you are reading this thesis on the toilet, you probably inhale between 500 and 6000 viruses for every breath you take (assuming you are an average-quantity breather inhaling half a litre of air per breath)[11]. I would advice you not to let these numbers make you nervous, as hyperventilating certainly will not lower the number of viruses joining the lively virion party going down in your lungs.

We are not familiar with the origin of viruses. One of the three main hypothesis today's virologists are working with, is the "Virus First" Hypothesis[12]. As the name insinuates, this hypothesis suggests that viruses predate all other lifeforms on earth[12, 13]. Today it is common knowledge that viruses are everywhere around (as well as inside of) us, and have been God knows how long. In a historically sense however, we have not been aware of them for long[14]. Yes, humans have probably been more and less uncomfortably aware of the effects and consequences of viral presence, but without the conceptualisation of such a thing as a virus. Viruses were first discovered late in the 19th century [15], and the often smaller bacteria specific viruses called *bacteriophages* or *phages* for short, were first discovered or identified by Félix Hubert d'Herelle in 1917[16].

d'Herelle was going about his business cultivating bacteria in Petri dishes, when zones of clearing in the otherwise opaque bacterial lawn piqued his interest. When these zones of clearing (now termed plaques) turned out to be bacteria specific viruses, the discovery entirely shifted the course of his career. He goes on to discover that the phages work as an antimicrobial agent, and that they are an astonishing *thousand times* more effective than the antimicrobial agents available [17]. d'Herelle develops the concept of phage therapy. By taking advantage of the high selectivity of phages, d'Herelle is able to administer phages therapeutically to cure bacterial infections. Amazingly, the phages would destroy the pathogenic bacteria, while remaining completely innocuous to the human host cells[17]. The same certainly cannot be said of the other antimicrobial agents that were available at that time. The technique worked, and for a time d'Herelle experienced both commercial and political success. d'Herelle was however a controversial character within the scientific community. He was very outspoken about his "heretical" theories which considered phages to be a common guest in all creatures and the underling reason to how we spontaneously recover from diseases. Even going so far as to claim bad hygiene being the cure for diseases caused by bad hygiene, citing that the lowest cholera mortality in India was found in Campbell Hospital, which was a hospital for poor people[17]. As phage therapy became popular within the soviet union, his technique experienced the effect of "soviet taint" in the west, and "d'Herelles Cure" became "Stalin's Cure". [17, 18]. These factors, along with the rise of antibiotics, forced his research into complete obscurity. It almost goes without saying that antibiotics went on to claim the position as the cure-all wonder drug for all your microbial complications [17, 19, 20].

Unfortunately, due to the surge of antibiotic-resistant bacteria in recent time, antibiotics have begun to loose their previous "super-potency"[21]. Because of this, phages are experiencing a rising relevance in the medical field[22].

Where we stand today

New findings suggest that phages are even more complex than we have thought. For instance, a 2017 Israeli study originally looking at quorum sensing in bacteria during bacteriophage infection, stumbled upon a six amino acid long peptide; a signal molecule produced by the phage[23, 24]. As it turns out, this signal molecule has the function of coordinating when the virus will utilise the lysogenic pathway and lie dormant in the host-DNA, as well as when it will use the lytic pathway and break out of the host. These findings demonstrate phages having a "social life", and solidify our understanding of phages as a more complex biological system, rather than simple cellular machines. As of today, there are 12,000 complete phage genomes on

GeneBank [dec. 2019]. Comparing those numbers to the tens of millions of different species of phages believed to exist out there, no wonder a researcher can spit on their microscope and discover species never seen before[9, 25].

There is *much* to learn about what is going on at the ultramicroscopic level. There is reason to believe that better understanding the interactions between phages and bacteria will be a crucial element to the scientific comprehension of our ecology and environment. As I have touched upon, the implications of this research are especially great for the medical field. Eager to contribute, I will start my study of the interaction between bacteria and bacteriophages by following d'Herelles footsteps. Like d'Herelle, my studies are commenced by studying plaques, however with 100 years of technological and scientific advancement in my toolbox.

Phages and their ability to form plaques were first discovered over a hundred years ago by d'Herelle[26]. Today, the morphology of plaques is used as basis for selection of phages in therapeutic use[27]. However, research into how these plaques form has been lacking. The mathematical models presented have not been empirically tested, most observations being anecdotal[28]. Neither is there much, if any, work done continuously measuring plaque formation. Attempting to reduce this lack of knowledge, I have done just that. This thesis presents my methods and findings. **Using a novel technique I developed and presented in my report "Fluorescence imaging of the pre-visible stage of bacteriophage plaque formation", I continuously measure plaque formation. I will also attempt to explain the dynamic between the bacterial hosts, phages and the available nutrient. Aiding the explanation, I will be using a self-developed mathematical model[1].**

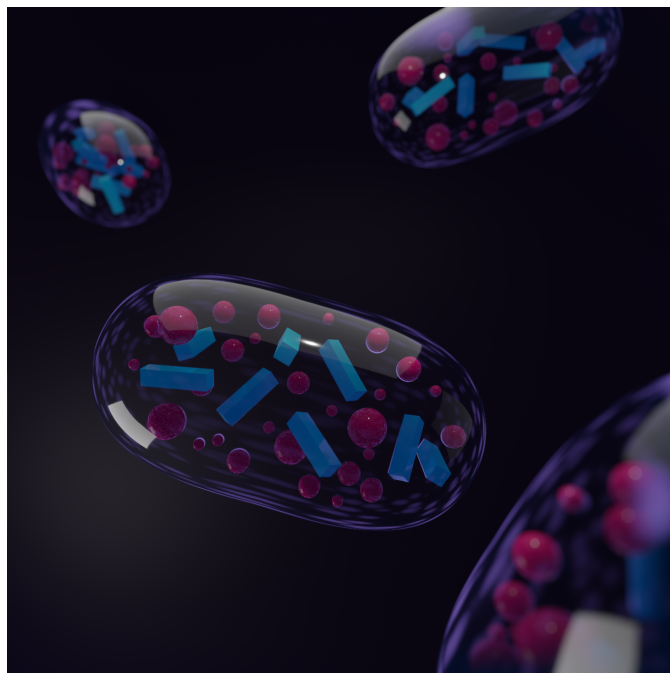


Figure 1: Infected bacterial cells filled with capsomeres and phage DNA. Illustration by Ingemund Skålnes through personal communications. December 25th, 2019.

2 Theory

2.1 Virus, phages and their propagation

Viruses are small infectious agent that are not able to replicate independently[29, 30]. They are *obligate intracellular parasites*, and rely on entering a suitable living cell (i.e. host) to carry out their replication cycle through the process termed *infection*[29, 31]. Viruses do possess their own genetic information, making them independent from their host organisms[29]. In its extracellular form– *virus particle* or *virion*–the virus is a microscopic particle containing nucleic acids wrapped in proteins and sometimes other macromolecules, depending on virus type. In this extracellular form, the virus is metabolically inert; a state where no respiration or biosynthesis occurs. This translates to the virus particle’s incapability to (i) elude threats or danger, (ii) repair itself when damaged, and (iii) replicate itself. It is unable to do anything that requires energy, and simply "floats around" in its environment. When the virus particle comes into contact with a viable host, it will latch on to the surface of the host and inject the viral genome into the host, effectively infecting it[29, 32].

Viruses can be classified by the host they infect as well as by their genome [29, 33]. A *virus that infects bacteria* is called a *bacteriophage*—or *phage* for short—from the greek word *phagein*; "to eat".

2.1.1 Phages

A briefer version of the following introduction to bacteriophages was first presented in my report "Fluorescence imaging of the pre-visible stage of bacteriophage plaque formation"[1]. Phages—like all other viruses—are obligate intracellular parasites. Just like other viruses then, phages have no way of replicating until contact with a host cell has occurred. In order to successfully replicate, a phage needs to infect a host, effectively "hijacking" its cellular machinery and coercing it into production of viral components [34]. Although phages are dependent on their host cells, they still have various possible life cycles. The most common of these alternative life cycles being the lytic and the lysogenic life cycles[35].

The steps of the lytic life cycle is show in figure 2. The protein cape commonly referred to as *capsomere* is shown in red. Shown in green is the viral DNA, and the grey represents the bacterial host cell. The first step of infection is the *attachment phase*, which is the most common basis for host specificity[29]. The virion has one or more proteins on the outside that interacts with specific cell surfaces called receptors. The receptors are normal surface components of the bacteria such as proteins, carbohydrates, lipids or complexes of these. These receptors carry out normal functions for the cell, e.g. the receptor for the phage T1, which serves as an iron-uptake protein for he host cell[29]. Step two is the *penetration step*. The attachment of the virion causes a change in both the host and phage respective surfaces that results in penetration. As a minimum, the viral genome needs to enter the host cell, while some phages are dependent on some enzymes to enter as well to be able to carry out the viral replication[29]. Step three begins once the virus and eventual necessary enzymes have entered the cell. The replication process is initiated by the synthesising of the viral genome and proteins. The viral proteins can be grouped into two broad categories. The first category is the *early proteins*, which are synthesised soon after injection and are necessary for the replication of virus nucleic acids. The second broad category is *late proteins*, which include the protein coat of the virion. The early proteins are typically enzymes, while the late proteins are structural components synthesised in much larger amounts. The time between the penetration and the first complete virion is called the *eclipse period* and is characterised by the lack of presence of any infecting agents[29, 36]. Step four is characterised by assembly of the viral coating and packing of DNA. This often happens spontaneously through electrostatics, Van der Waals, and hydrogen bonding

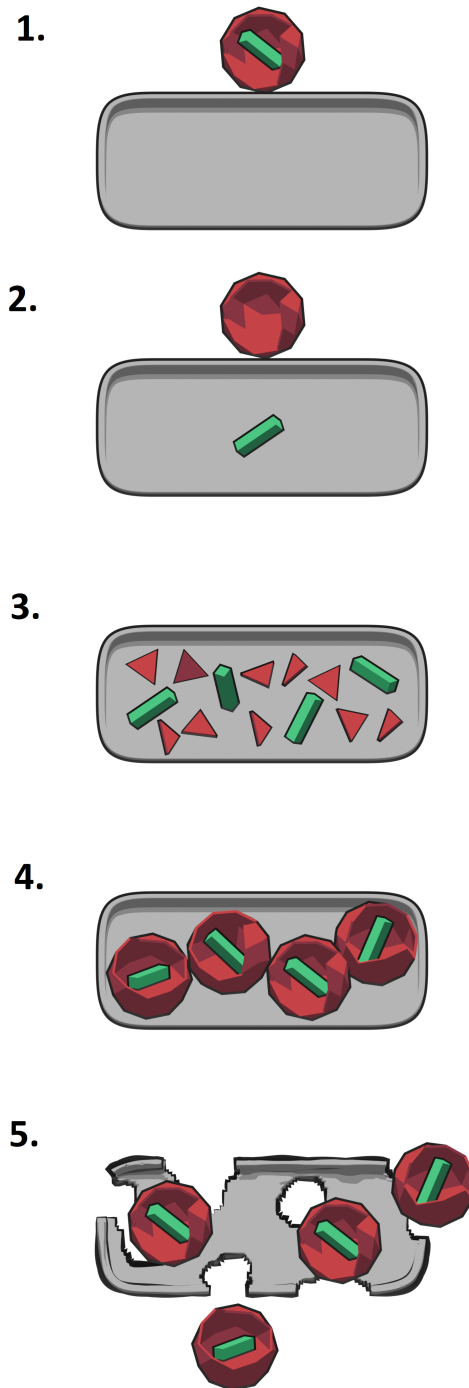


Figure 2: The lytic cycle of a phage. Bacteria, DNA and virus not drawn to scale. By Ingemund Skálnes through personal communications. 25 December 2019.

interactions between the different viral sub-units [37]. The last step, step five, is the release of virions. The virus produces enzymes called lysozymes that break up the bacterial surface and release the newly formed virions into the environment[29, 38].

The lysogenic life cycle involves the viral genome being inserted into the bacterial chromosome (or into the bacterial cell as a plasmid) by infecting the host. By inserting itself as a genetic element into the bacterial cell, the phage is able to lay dormant for thousands of host generations, with the viral genome being replicated along with the hosts[29]. Phage genome in this state is termed *prophage*[29, 39]. Phages in this state can affect the host by expressing genes either introduced by the phage or genes not usually expressed by the host, effectively altering the phenotype of the host[40]. This is a process termed *lysogenic conversion*. With the exception of lysogenic conversion, the prophage lies dormant until it is induced[39]. Upon induction, the prophage proceeds on a typically lytic pathway; rapidly producing new virions and releasing the produced progeny through lysing the cell wall of the host. While many a phage follows either the lytic or the lysogenic life cycle, the *temperate phages* are able to "select" either of the two when infecting a host[39]. They will not be relevant for this thesis, but an introduction to phage theory should at least mention the lesser known life cycles *pseudolyso-genicity* and *chronic infection life cycle*. These are generally unexplored and rather controversial concepts in phage biology as per today. [41–43].

Since their grande entrée into scientific conceptualisation, phages and phage derived proteins have become an important tool in molecular laboratories all over the world[29]. In many ways, the study of phages can be said to have formed the backbone of molecular biology[44]. To exemplify; phages were an integral part of demonstrating DNA as genetic material and proving Darwins natural selection. Also, phage-derived enzymes are extensively used for common laboratory protocols [29, 44–46].

2.1.2 Plaques

In virology one often encounters the need to quantify the number of infectious virions within a solution[29, 47]. This is commonly done by performing a double agar overlay plaque assay. Even though it dates 100 years back to d'Herelles first observation of phages, the technique is still considered one of the most effective ways of achieving direct quantification of infectious virions[26, 47]. The standard plaque assay protocol is ubiquitous enough that it can be found in introductory microbiology textbooks like Brock's "Biology of Microorganisms"[29]. The protocol is performed by having three parts molten nutrient agar mixed with one part bacterial broth in the exponential phase, and a phage sample diluted to contain between one and three hundred

plaque forming units (PFU). This mixture is mixed properly using a vortex, and poured over a Petri dish with agar. The agar plate with the mixture is left to incubate overnight. The bacteria are immobilised in the agar, while the smaller phages are free to spread as they proliferate. This results in see-through spots (i.e. plaques) in the otherwise opaque bacterial lawn, where phages have lysed and annihilated all surrounding bacteria. These plaques are then either counted or isolated, depending on the intention. The morphology of these plaques are also used to assess the efficiency of phages when selecting viral strains for phage therapy[48].

2.2 Bacteria, *Escherichia coli*, and growth

In section 2.1, I elaborated on how bacteriophages depend on their hosts to carry out their life cycles. Studying these bacteria specific viruses without introducing and making certain efforts to understand their hosts, would leave us with an incomplete impression.

Escherichia coli (shortened to *E. coli*) is a gram negative, rod-shaped bacterium that belongs to the Enterobacteriaceae family [29, 49]. Members of this genus are near universal inhabitants of the intestinal tract of humans and other warm-blooded animals[29]. The *E. coli* bacteria are well characterised, facultative anaerobe, and fast growing in a wide range of media[29, 49]. Owing to these attributes, they have been extensively utilised as a model in research and teaching since the 1940s[49]. Different strains of *E. coli* are used for different purposes, e.g. the *DH5 α* , for cloning and *BL21* for recombinant protein expression[49–51]. Their specific use is due to their *genotypes*. *BL21*, among other properties, lacks common proteases which would degrade the proteins *BL21* is made to produce, and *DH5 α* lacks endonucleases that would degrade transformed genes [51]. While growing optimally at 37 °C, the *E. coli* grows at a wide range of temperature, and is found to be proliferating at temperatures as high as 53 °C[49, 52].

Bacteria, such as *E. coli*, reproduce through binary fission. This means that a single cell divides into two identical daughter cells[29]. Under favourable conditions, the bacteria can reproduce with a generation time of 20 minutes[49]. Knowing this, we can derive a simple model for the growth rate shown in equation 1, where N is the concentration of bacteria, N_0 is the starting concentration of bacteria and t_g is the number of generation times passed.

$$N = N_0 \cdot 2^{t_g} \tag{1}$$

Equation 1 shows us that the growth of bacteria is exponential, doubling every generation time[53]. This model is only accurate for optimal growth when the bacteria are not limited by temperature, nutrients, space, or competition. In 1949, Jaques Monod presented his equation, dubbed the Monod

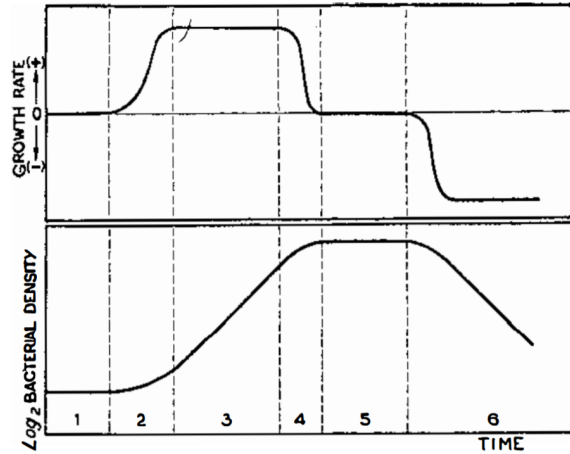


Figure 3: The different phases of bacterial growth. The lower curve shows the log bacterial density, while the upper curve shows the growth rate at the same stages. Figure originally published in Monods 1949 paper[53].

equation, which related the bacterial growth rate to the nutrient concentration[53]. This equation has the same form as the Michaelis-Menten equation, which models enzyme kinetics. While the Michaelis-Menten equation is based on theoretical assumptions, the Monod equation is based on empirical data, which he presents in his paper. The Monod equation is show in equation 2, where μ is the growth rate, μ_{max} is the maximal growth rate, S is the substrate concentration, and K_S is the half velocity constant, which is the value of S when $\frac{\mu}{\mu_{max}} = 0.5$.

$$\mu = \mu_{max} \frac{S}{K_S + S} \quad (2)$$

Figure 3, from Monods 1949 paper displays the typical phases of growth for a bacterial culture growing in a batch in a lab setting where the environment is ideal and controlled, and the only thing limiting the bacteria is nutrient and space. The Monod paper divides the life of cultures into six different phases, while most modern microbiology textbooks divide it into four phases[29, 53, 54]. Phase 1 and 2 are the *lag phase* and *acceleration phase*, respectively, and are usually treated as just the lag phase[29]. Here the bacteria is inoculated into the media and spends time biosynthesising the appropriate enzymes or repairs, if the cells have been damaged. The next phase (phase 3) is the *exponential phase*. Here the bacteria grows exponentially, dividing at the maximal rate allowed by their genetics and environment. The exponential phase is the only phase modelled by the term given in equation 1. Phase 4 and 5 are the *retardation phase* and *stationary phase*, usually treated as

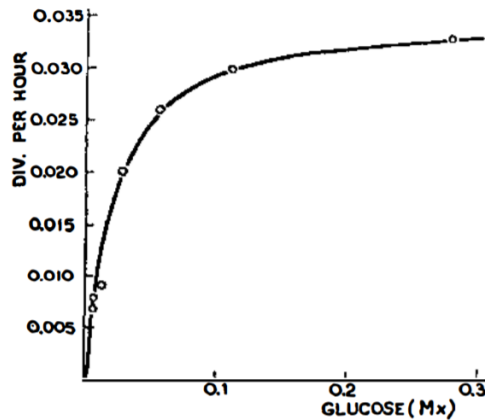


Figure 4: Growth rate of *M. tuberculosis* in Dubos' medium, as a function of glucose concentration. Figure originally published in Monods 1949 paper[53].

just the *stationary phase*. Here the exponential growth ceases due either to lack of limiting substrates or to accumulation of growth limiting waste products[29].

The Monod equation allows us to reliably model the life of bacterial cultures from the exponential phase till stationary, by encompassing the access of limiting substrates. In the beginning when the limiting substrate S is considerably larger than K_S , we can approximate $K_S + S \approx S$ and the fraction $\frac{S}{K_S + S}$ becomes $\frac{S}{S}$ which is 1, and the term in equation 2; becomes $\mu = \mu_{max}$. Under these conditions the growth rate is equal the max growth rate. The growth rate of a bacteria is plotted as a function of its limiting substrate in figure 4. The solid line is the Monod equation while the dots are experimentally measured growth rates. The figure shows the growth rate converging towards a maximum growth rate as the concentration of limiting substrate is increased.

2.3 Modelling

2.3.1 Is it useful?

Modelling is not some complex, purely scientific action. In fact it is something each and every one of us does every day. If you held the door for someone today, you *modelled* how this gesture would play out. You gazed back at the person behind you and *modelled* how the other person would reach and enter said door. Your eyes quickly registered the information needed to measure the distance between the door and the other person, as well as the speed at which this person was moving. You then did some quick

modelling in your mind resulting in an estimate of the different ways it could play out if you held the door or not. Maybe holding the door would seem like a nice gesture, or maybe the other person was so far away that holding the door would force the other person into an awkward half-sprint, half-walk motion, making the whole gesture a testament to the dysfunctional social dynamic between the two of you. The model does not give you a definitive answer to your door-holding dilemma. What it does give you is an estimate of the consequences. The estimation gives you more data for your door holding parameter, and hopefully allows you to at least maintain your social equilibrium. Perhaps contrary to layman conceptualisations of modelling as a complex, "scientific" endeavour, modelling in order to predict and control ones circumstances is a constant action of the human mind; continuous and inevitable.

Mathematical modelling is used extensively in natural science and engineering[55, 56]. In this type of modelling, we mimic reality by using the language of mathematics[57]. These models can be composed by a set of linear, algebraic, or differential equations[55]. The models are constructed on the basis of practical observations and our current understanding of how these practical observations came to be[56]. A model's purpose is to mimic a process or phenomenon, and the value of a model is measured by how much perceived insight is gained into the phenomenon. This makes the creation of a model an iterative process, as a model is created, evaluated and changed[58]. However, this does not imply that the purpose or aim of all models is perfect mimicking of reality. "All models are wrong, but some are useful". This aphorism is generally attributed to the statistician George Box, who repeated it in his many articles and books[59, 60]. To understand this aphorism, we can consider a simple example. The ideal gas law, shown in equation 3, was first stated by Émile Clapeyron in 1834[61, 62]. Here V is volume, P the pressure, n the number of moles of gas, and R the ideal gas constant.

$$V = \frac{nRT}{P} \quad (3)$$

The law shows how volume, pressure and temperature affect each other in an ideal gas. There is no such thing as an ideal gas in nature, and we will never have a gas that behaves exactly according to the law. This makes the model "wrong". That does not mean that the law is not useful. It is in fact very useful, as it provides an accurate estimate under the right conditions, and provides valuable insight into the physical behaviour of gasses. As G. Box himself writes in a 1979 article: "For such a model there is no need to ask the question 'Is the model true?'. If 'truth' is to be the 'whole truth' the answer must be 'No'. The only question of interest is 'Is the model illuminating and useful?'"[63].

Other examples of (more or less "true") mathematical models are Newton's

laws of motion, Faraday’s law of electromagnetic induction, Maxwell equations in electromagnetism and - most relevant to this thesis - the *reaction-diffusion model*. [55, 64–66].

2.3.2 Reaction-diffusion models

In his seminal paper, Alan Turing theoretically demonstrated a system of reacting and diffusing chemicals spontaneously forming a spatial pattern [66, 67]. To explore this emergence, Turing considered a system of two chemicals; one being an activator and the other an inhibitor. The activator would stimulate the production of the inhibitor, and the inhibitor depleted or stopped the production of the activator. He showed that a system with an inhibitor with greater diffusion than the activator would result in diffusion-driven instability. As diffusion is commonly considered an homogenising process, processes of diffusion-driven instability can seem counter-intuitive [67]. To better understand diffusion-driven instability, we can consider a simple auto-catalytic process of $A + B \longrightarrow 2B$ as explained by Maini et al. (1997) [67]. An unstirred reactor filled with chemical A and no B would obviously gain no reaction. If the reactor was seeded with chemical B, but B is immobilised while A is able to diffuse, the reaction would only occur where B was seeded. Eventually, the reaction would consume all chemical A and the reactor would be left with spots consisting of a high concentration of B [67]. If, however, there was a supply of A across the domain in addition to a decay step for B to limit its growth, it would be possible to achieve a balance between supply and diffusion for A. This could balance the decay of B in the spots, and provide a steady-state, long-lived pattern, with high concentrations of A in between the spots and high concentration of B in the spots. The exact pattern of spots would still be highly dependent on where the initial seeding occurs. Turing makes two predictions. The first prediction is that this structure will develop spontaneously even from an initially close to homogeneous distribution of A and B, provided that A diffuses faster than B. The second prediction he makes is that the final pattern will not necessarily depend on the initial disturbance if B has a non-zero diffusivity—the spots adjusting their position to the demands of the local “supply and demand” occurring due to diffusion and reaction.

$$\frac{\partial \mathbf{u}}{\partial t} = D_u \frac{\partial^2 \mathbf{u}}{\partial x^2} + \mathbf{R}_u \quad (4)$$

The general reaction-diffusion equation is shown in equation 4. Here the term $\frac{\partial \mathbf{u}}{\partial t}$ represents the change in concentration of component \mathbf{u} over time, $D_u \frac{\partial^2 \mathbf{u}}{\partial x^2}$ represents the spatial diffusion of component \mathbf{u} , and \mathbf{R}_u represents the net rate of formation and consumption of the same component [68].

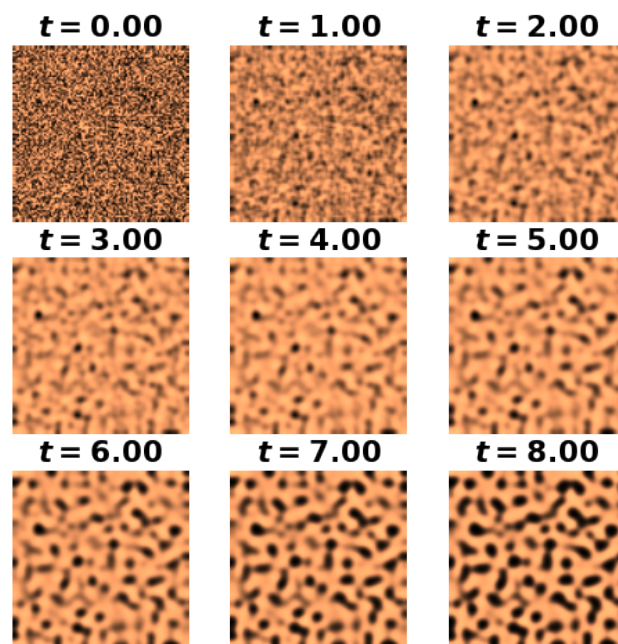


Figure 5: Turing patterns generated by numerically solving the FitzHugh–Nagumo equation. Generated in python. Source code under MIT License[69].

Turing suggested that reaction-diffusion systems could be the basis of many biological phenomena, such as the patterns of a "dappling" (horse with spots on their coat), phyllotaxis (leaf arrangement), and gastrulation (early embryonic development)[66, 67, 70]. I made Figure 5 by modifying a python code that numerically solves the FitzHugh-Nagumo equation; a reaction-diffusion system[69]. The figure shows how a stable Turing pattern emerges over time, and one can see the pattern on the figure bearing resemblance to the coat of a cheetah, leopard or jaguar.

While reaction-diffusion systems may seem like a viable explanation for the emergence of biological patterns, they have in many cases (e.g. the segmentation of body parts in *Drosophila Melongaster* [fruit fly]), been found not to be the underlying force[67, 71]. To quote Maini et al. (1997) "... although RD theory provides a very elegant mechanism for segmentation, nature appears to have chosen a much less elegant way of doing it!". Relevantly, reaction-diffusion systems do seem to be the underlying cause is in the formation and enlargement of viral plaques.

2.3.3 Viral reaction and diffusion

The first reaction-diffusion system describing plaque formation and enlargement was introduced by Yin and McCaskill (1992) [72, 73]. Their incentive for developing this model was derivation of a formula for the radial expansion of plaques. This work was a continuation on work initiated by Koch in 1964. Using heuristic arguments, Koch suggested that that the radial expansion of plaques could be described by the equation $c = a(\frac{D}{L})^{\frac{1}{2}}$, where c is the radial propagation velocity of the expanding plaque, D is the viral diffusivity through the mixed medium, L is the lysis time for the phage and a is a constant[72, 74].

The system Yin and McCaskill developed had three components: the host bacteria (B), free virus particles (V), and the infected bacteria (I). The model is governed by three reactions: the adsorption of phages with the rate constant k_1 , the desorption of phages k_{-1} , and the burst rate of infected bacteria. Y represents the yield of virus particles, and is a constant. How the reactions and components in the model relate to each other is shown in equation 5.



An alternative reaction diffusion model was later derived by Ortega-Cejas et. al, which incorporates a time delay to better mimic the lysis time effect[75]. What these models have in common is the importance the viral adsorption rate (k_1) is given in the model. As of today, there are few empirical tests

of the models[76, 77]. The empirical test that have been performed find the models failing to capture qualitative aspects of the experimental results found[28].

2.4 Numerical analysis

A lot of theory in this thesis has been dedicated to differential equations and their solutions, without elaborating how these equations are solved. While most equations encountered during primary education are analytically solvable with an absolute and finite solution, this most certainly is not true for all equations[78]. As an example, consider the following problem: professor Yin has 2 apples, professor Abedon has 3 apples, how many apples do they have amongst one another? This problem is analytically solvable. We know the answer is *exactly five*: five apples is *the answer* for the stated problem. In science and engineering on the other hand, we often encounter equations to which it is impossible to find *the* absolute solution using the analytical tools available[78]. In such cases, we have to settle with an approximate solution, often acquired through *numerical analysis*.

Euler's method is an example of a method for numerical analysis. The method is a first-order numerical procedure for solving ordinary differential equations (ODEs) with a given initial value[78]. This method yields approximate solution values at variables with equal distance. Euler's method is summed up in equation 6. It is based on the assumption of local linearity and approximates the solutions for an ODE by starting from a known initial value $y(x_0)$, then approximating the next value step-wise with each step having an x-value h larger than the last.

$$y(x + h) \approx y(x) + h \cdot y'(x + h) \quad (6)$$

The following example is borrowed from the book "Advanced engineering mathematics"[78], and shows how the ODE in equation 7 can be solved given the real solution being $y = e^x - x - 1$.

$$y' = y + xy(0) = 0 \quad (7)$$

Table 1 shows equation 7 solved using step-size $h = 0.2$. n shows the number of iterations, x_n the x value used, y_n the approximated solution and $y(x_n)$ the real solution. The error column shows the difference between the solutions found through Euler's method and the real solution. The approximated solution and real solutions are plotted in figure 6.

Errors in numerical methods are related to the step-size h . The smaller h is, the smaller the error. This also leads to a larger number of steps that need to

Table 1: Euler’s method for $y' = x + y$ for x from 0 to 1 with step-size $h = 0.2$

n	x_n	y_n	$y(x_n)$	error
0	0	0.000	0.000	0.000
1	0.2	0.000	0.021	0.021
2	0.4	0.040	0.092	0.052
3	0.6	0.128	0.222	0.094
4	0.8	0.274	0.426	0.152
5	1	0.488	0.718	0.230

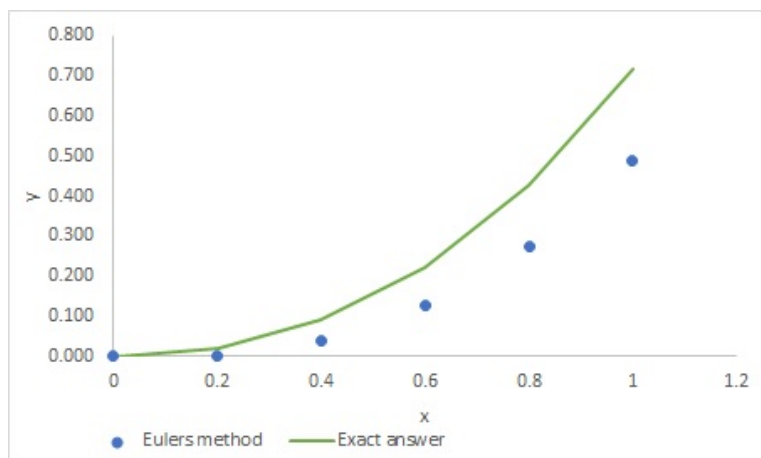


Figure 6: The results from table 1

be calculated[79]. There are alternative algorithms rendering a lower error with the same step-size as Euler’s, even still the maximum step-size with a stable solution will always be dependent on the numerical stability of the system of equations.

A system of equations is numerically unstable when the numerical solutions change drastically but the exact solution does not. Numerical instability can be avoided by using a smaller step-size or alternative methods. If an equation includes terms that can yield rapid variation in the solution, it is considered to be a stiff equation[79],

$$\delta t < \frac{(\delta x)^2}{2 \cdot D} \quad (8)$$

Various methods have been developed to analyse the stability of a numerical system[80]. Widely used is the *Von Neumann stability analysis*, which is based on the decomposition of the errors into Fourier series[80, 81]. The Von Neumann stability analysis for diffusion is shown in equation 8, where δt is the step size for time, δx is the spatial step size and D is the diffusion

constant. The analysis tell us that the step size in time (δt) must be *smaller* than the square of the spatial step size (δx) divided by the diffusion constant times two.

2.5 Why is everything normally distributed?

Calculus is an incomparable tool for analysing and working with the sort of determinism one frequently comes across in engineering, science and economics[82, 83]. The all-encompassing importance of calculus can be exemplified by noticing how preposterous may seem the need to add a citation to the previous statement. While most of us could probably agree on the greatness of calculus, it does however fall short when we encounter the need to deal with the randomness (or stochasticity) of natural phenomena. And randomness does appear a lot in nature. The variations found in the weight of eggs, the number of protein molecules produced from a single mRNA before it is degraded, and the size of deer antlers are some examples of stochasticity appearing in nature[82–85]. To deal with this randomness, we need tools from statistics and probability.

Even though the examples mentioned above seem somewhat random (pun intended), we can still safely predict something about the outcome. We know the likelihood of a chicken laying an egg weighing 50 grams and laying an egg weighing 2 kilograms, is not equal. This brings us to the concept of *probability*. Probability is defined as a value between 0 and 1 that denotes the likelihood of an event occurring[82, 83]. In the classical example of a coin flip, the possible outcomes (*sample space*) are either heads or tails, and the two possible outcomes are equally likely with a 0.5 probability for each outcome[82, 83].

Returning to the example of the weight of chicken eggs, we notice that listing the probability for all outcomes becomes impossible, as the sample space of all possible weights of an egg is *not discreet* (with a set of only particular possible values), but *continuous* (with a set of numbers within a range). This is where we turn to probability distributions¹. A probability distribution is a mathematical function that provides the probabilities of occurrence of different possible outcomes in an experiment.

2.5.1 Normal distribution

We know from C. J. Adams' 1998 paper "A model relating egg weight and distribution to age of hen and season" that the weight of a chicken egg follows

¹Note that probability densities also exist for discreet functions. In the case of a single coin toss it would be a histogram with two equally large bars.

a normal distribution, and that the average weight of a chicken egg is about 50 grams with a standard deviation of 0.8 grams[86]. The density function for a normal distribution is shown in equation 9, where μ is the mean of the distribution, and σ is the standard deviation plotted in figure 9.

$$f(x) = \frac{1}{\sigma\sqrt{2\pi}} e^{-\frac{(x-\mu)^2}{2\sigma^2}} \quad (9)$$

From the graph in figure 9, we see that the mean is the most frequent value, 50 % of the measurements will lie above and 50 % will lie below[82, 83, 87]. The normal distribution is symmetrical around the mean, and the frequency decreases at a varying, but predictable rate as one moves away from the middle value. An example of this symmetry is the probability of a sample being between μ and $\mu + \sigma$ is equal to the probability of the sample being between $\mu - \sigma$ and μ . We also see that 68% of samples will be within range of the mean \pm the standard deviation. From the egg example, this would translate to the probability of a randomly chosen egg to weigh within the range [49.2, 50.8] to be 68%.

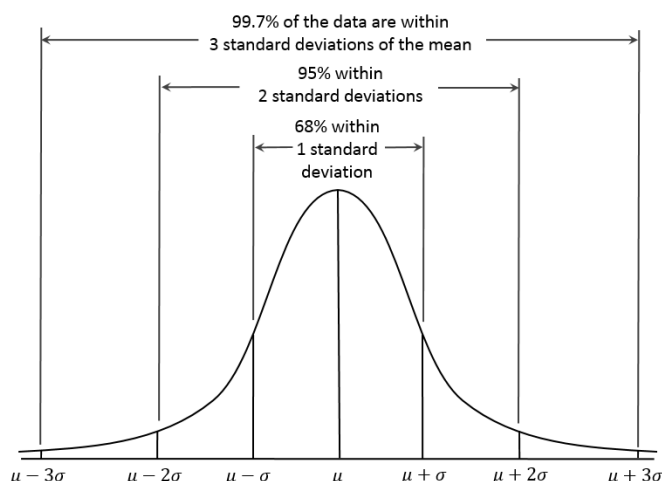


Figure 7: Probability density for normal distribution. "Standard deviation diagram" by Dan Kernler CC BY 4.0[88].

2.5.2 Gamma distribution

The gamma distribution is a continuous distribution function with two positive shape parameters[82, 89]. The two shape parameters for the gamma distribution are shape parameter; α and the rate parameter; β . The probability density function for gamma distribution is given in equation 10. The mean of a gamma distribution is $\frac{\alpha}{\beta}$ and the variance is $\frac{\alpha}{\beta^2}$ [82].

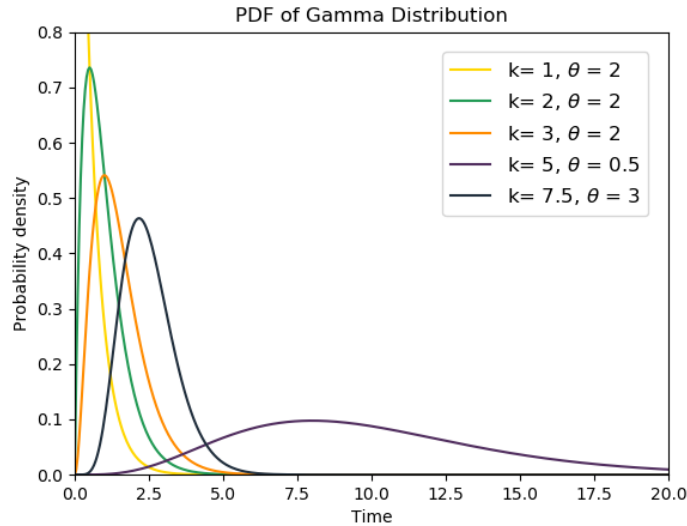


Figure 8: Gamma distribution for different shape parameters. Figure was generated in python, by me.

$$f(x; \alpha, \beta) = \frac{\beta^\alpha \cdot x^{\alpha-1} e^{-\beta \cdot x}}{\Gamma(\alpha)} \quad x > 0, \quad \alpha, \beta > 0 \quad (10)$$

In contrast to the normal distribution, we see from figure 8 that the gamma distribution is skewed and asymmetric. The gamma distribution is often used as the probability model for waiting times[82, 90]. An example of this is in "life testing", where time until death is the random variable, which frequently has a gamma distribution[90]. The gamma distribution has also been frequently used in biology. It can be used to predict the probability of developing cancer as you age, the amount of pollen found in air, and a wide range of molecular mechanisms relevant for gene switching and transcription initiation[84, 91, 92].

2.5.3 Central limit theorem

While there is a vast amount of different probability distributions, the normal distribution shows up the most, and its importance can hardly be overstated [83, 93]. Large parts of statistics theory is based on the assumption that observed quantities are normally distributed[83, p. 871]. This is due to the *central limit theorem*. The central limit theorem states that when a large number of independent and identically distributed random variables with finite mean and variances is added up—after suitable scaling—the distribution of the resulting quantity is approximately normally distributed. Errors in ex-

perimental measurements are often the sum of many small factors, as clearly illustrated by Catherine A. Peters' example of an experimentalist measuring temperature; "... the manufacturer of a thermometer may not have calibrated it very well so the temperature markings do not exactly match the corresponding level of mercury. There may be impurities in the mercury so that it does not expand and contract in a reproducible fashion. The experimentalist's line of sight causes parallax error in reading the markings. The temperature varies slightly over the time period of the measurement. The temperature varies spatially in the region where the experimentalist would like to record the temperature. Collectively, these errors add up to generate the imprecision in an experimental measurement." [94].

In biology, outcomes like height, weight, or litter size are often emerged properties from the sum of many small-scale processes, so, because of the central limit theorem, the distribution of these properties typically approaches the normal curve [83, 93]. The wide spread use of the central limit theorem in biological research can be illustrated by how the theorem has been used in calculating microbial risk assessment for food borne illnesses, in the study of restriction sites in genomes, as well as in the study of polygenic trait values over a pedigree [95–97].

3 Method

3.1 Bacterial and viral strains

The *E. coli* strains DH5 α and BL21 were selected due to their high growth rate, and because they are susceptible hosts for the phages that happened to be available in the laboratory I had daily access to during the research period. The phage strain used was U-phage, and was gifted by the PhageAge project². The U-phage has a host range that includes both BL21 and DH5 α .

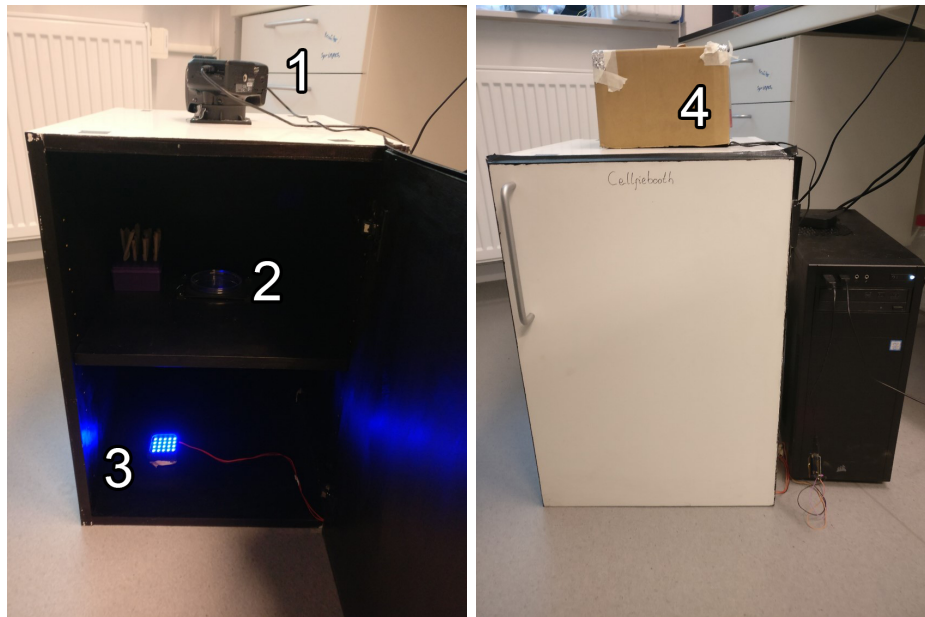
3.2 Cellfiebooth

3.2.1 Protocol

In this thesis, I have utilised the self-developed Cellfiebooth system first presented in my report "Fluorescence imaging of the pre-visible stage of bacteriophage plaque formation". It was used to experimentally measure viral plaque development in bacterial lawn[1]. The fundamental principle of the system is measurement of phage-induced cell lysis as a function of free DNA in the agar, which is stained by a fluorescent dye. This is achieved by the experimental setup shown in figure 9.

Creating the Cellfiebooth system, I built on the established protocol for plaque assay described in section 2.1.2. I constructed a device that measured the concentration of dead bacteria in the Petri dish, and developed the software needed to run the experiments and analyze the results. As most growth media contains components that are auto-fluorescent, the nutrient media used is a modified M9 minimal media (protocol given in Appendix A). The soft agar overlay contains 3x the working solution of the fluorescent dye GelGreen, which is the concentration the manufacturer recommends to achieve the strongest fluorescence[98]. The GelGreen dye is fluorescent when it creates a dimer with DNA. As it is a large molecule, it will not enter bacterial cells or phage particles, and only affects the DNA freely available in the solution from the lysis of phages. To photograph this fluorescence, the Cellfiebooth is isolated from ambient or disturbing light[1, 98]. The inside of the Cellfiebooth is painted black, all openings are fitted with black tape, and the camera opening is covered by a cardboard box, as shown in figure 9b (4). The light source, shown in figure 9a (1), is fitted with a shortpass light filter with 538 nm cut on that inhibits light with a wavelength lower than 538 nm from passing through it. The camera, shown in figure 9a (3), is fitted with a longpass light filter with a 530 nm cut off. The longpass filter hinders

²I have been a part of the PhageAge project in various roles since it started as an iGEM team in 2017.



(a) Door open.

(b) Door closed and camera covered.

Figure 9: Picture of the Cellfiebooth hardware with light-source on. The camera (1) is on top of the cupboard and the lens is sticking in and focusing on the Petri dish (2). The light source (3) is under faced up, but not directly against the camera. A cardboard box (4) covers the camera under an experimental run to avoid light pollution.

light with a wavelength higher than 530 nm from passing through the filter. Together, these two filters hinders most to all light coming directly from the light source from being registered by the camera. The DNA - GelGreen dimers in the Petri dish, which emit light at a wavelength of between 500 to 600 nm, provide the only light in the system that penetrates the filter at the top and is registered by the camera.

The following is a list of the required supplies, and the protocol for performing the experiment:

- Heater
- Cellfiebooth
- 13 mL centrifuge tubes
- Diluted phage sample
- GelGreen
- Vortex

1. Two 13 mL centrifuge tubes are added 3 mL M9 soft agar and 1.2

μL GelGreen x10 000. The solution is thoroughly mixed and kept at 50 °C with a heat block for a few minutes to dissolve all precipitated GelGreen.

2. The tubes are removed from the heat block and are added 1 mL bacterial broth in exponential phase, and 100 μL diluted phage sample. The solution is again thoroughly mixed.
3. The solution is poured over a Petri dish filled with M9 agar and left to settle (30 to 60 seconds)
4. One Petri dish is placed in the Cellfiebooth where it will be measured for fluorescence at steady intervals over a predetermined time period (usually every 5 minutes for 48 to 90 hours), while the other is kept as a biological replicate.

For further details on the protocol, hardware and software related to the Cellfiebooth, see my report "Fluorescence imaging of the pre-visible stage of bacteriophage plaque formation" [1].

3.2.2 Test for bacterial fluorescence

GelGreen reacting fluorescent with bacteria was tested for by cultivating a bacteria in M9 soft agar on a Petri dish where half the Petri dish contained GelGreen, while the other half is without. This was achieved by cutting a plastic rectangle out of an empty plastic Petri dish. The rectangle was soaked in 70% ethanol solution and dried off before it was placed upright in the middle of Petri dish filled with M9 - agar. The rectangle was pushed into the agar-gel to avoid sloppy agar from flowing and contaminating the GelGreen-free side of the Petri dish. Two 13 mL centrifuge tubes were filled with 1.5 mL sloppy M9 and 0.5 mL DH5 α strain of *E. coli* in exponential phase. One of the tubes was filled with 0.6 μL 10 000X GelGreen. Both tubes were then vortexed and poured onto their respective side of the Petri dish. Pictures were then captured in the Cellfiebooth, and then again 19 hours later when the bacterial lawn had appeared.

3.2.3 Changes to the Cellfiebooth system

Some improvements have been made to the Cellfiebooth system since the initial version presented in the report[1]. These modifications were implemented both as general efforts toward optimising the precision of the system, and as an improvement-motivated reaction to the outcome of the experiment described in Section 3.2.2. The Canon EOS 500D camera was replaced by a Nikon d750. In the independent audio and image quality measurements

DxOmark, the Nikon camera performs 1.48 times better on the overall score and 4.45 times better in low light, marking a considerable improvement[99, 100].

The light filter fitted to the camera has been changed from a filter with 495 cut on to 530 nm cut on. This in order to block out light that scattered as the light from the light-source hit the bacterial lawn. This is more thoroughly elaborated upon in section 5.3.1 as this experiment revealed that the bacterial lawn is visible in the Cellfiebooth due to light scattering.

In addition to these changes, I detected and fixed some minor bugs in the Cellfiebooth software.

3.3 Characterisation of growth rate of bacteria immobilised in soft agar

Accurate measures of the growth rate of the *E. coli* strains BL21 and DH5 α in M9 soft agar is required for the model. These values were acquired experimentally. Since the initial bacterial concentration can vary, I studied the bacterial growth for different initial bacterial concentration. The Cellfiebooth is kept at 21 °C, but the multiplate reader used has 28 °C as the lowest stable temperature, so the bacteria were studied at 28 °C.

M9 broth was inoculated with BL21 and incubated at 37 °C for 6-7 hours. The broth was then diluted in a four-step two-fold dilution, using M9 broth. For each dilution the absorbance was measured at 600nm (OD₆₀₀), and 0.5 mL broth was extracted and mixed with 1.5 mL M9 soft agar. This mixture has the same concentration of agar as the soft agar overlay used in the Cellfiebooth. Each dilution of bacterial broth mixed with soft agar was then poured into wells in a 96 well-plate and placed in a microplate reader (tecan infinite m200 pro) where the OD₆₀₀ is measured in 5 minute intervals over 40 hours, and the temperature is kept at a constant 28 °C.

The maximal growth rate μ_{\max} , nutrient yield γ , and half velocity constant K_m were found separately for both bacterial strains by fitting a model that follows the Monod kinetics, using the Microsoft Excel solver function. A model in which bacterial concentration and nutrient content was equal to the seeding point in the experimental setup was created for each dilution. A screenshot from my work before the model fitting was done is used as an example in figure 10. Here the columns "Raw sample" and "Dilution 1" are experimental results, while columns "Model raw", "Nutrients", "Model 1" and "Nutrients 1" are theoretical results. The models for the different dilutions all follow Monod kinetics with the same μ_{\max} , γ , and K_m , as seen in the "variables" cells E11 to G11 in the figure. The discrepancies between the models and experimental results were calculated for each time point and

	A	B	C	D	E	F	G	H
1								
2								
3			Raw sample	Dilution 1	Dilution 2	Dilution 3	Dilution 4	
4	OD yield		0.404225007	0.385250006	0.411700007	0.427525021	0.393100012	
5	Yield OD/gram N		146.9909115	140.0909112	149.7090933	155.463644	142.9454589	
6	N0 [g/mL]			Max	155.463644			
7	0.00275			Min	140.0909112			
8								
9					Variables			
10					y [od/(g/ml)] Km		u_max [h^-1]	
11					100	0.0001	0.000015	
12		Sum of diff	R^2					
13	Model raw	2436.742507	0.738779781		Boundaries			
14	Model 1	3054.570608	0.713723457		y	<=	186.5563729	
15	Model 2	3634.393785	0.65968421		y	>=	112.072729	
16	Model 3	3802.771897	0.64389415		Km	>=	1E-10	
17	Model 4	2835.3404	0.639287128		u_max	>=	1E-10	
18	SQD	15763.8192			u_max	<=	0.0001	
19								
20	Time [h]	Raw sample	Model raw	Nutrients	Difference	Dilution 1	Model 1	Nutrient 1
25	0.316055556	0.332725003	0.332725003	0.00275	0	0.263950005	0.263950005	0.002
26	0.395027778	0.334925003	0.338823042	0.00268902	0.003898039	0.264958921	0.268787566	0.0027016
27	0.474	0.337349996	0.345027906	0.002626971	0.00767791	0.267499994	0.2696146	0.0026933
28	0.552972222	0.339924999	0.351341052	0.00256384	0.011416054	0.269424994	0.270329707	0.0026862
29	0.631944444	0.342724994	0.357763914	0.002499611	0.01503892	0.271300003	0.27095972	0.0026799
30	0.710916667	0.345825009	0.364297889	0.002434271	0.01847288	0.273374997	0.271522777	0.0026742
31	0.789888889	0.349049993	0.370944335	0.002367807	0.021894342	0.275500007	0.272031716	0.0026691
32	0.868861111	0.352499999	0.377704553	0.002300204	0.025204554	0.277674995	0.272496093	0.0026645
33	0.947833333	0.355850004	0.384579785	0.002231452	0.028729781	0.280025005	0.272923089	0.0026602
34	1.026805556	0.358975008	0.391571189	0.002161538	0.032596181	0.282375	0.273318403	0.0026563
35	1.105777778	0.362199999	0.398679831	0.002090452	0.036479831	0.284900002	0.273686564	0.0026526

Figure 10: Example of experimental data evaluating against a model in a spreadsheet.

summed (cells B13-B17). The square sum of all the differences sums was used as objective function (cell B18).

The boundaries are shown in the box E13 to G18. The lower and upper boundaries for the yield constant were set by calculating a theoretical yield for each run. The theoretical yield is based on an assumption that all nutrient in the mix was used to grow bacteria. This theoretical yield was calculated in box A3 to G5, where the total change in OD₆₀₀ was found (OD yield) and the theoretical yield constant $Y_{XS} \left[\frac{OD_{600}}{g} \right]$ was calculated. The upper bound was set to be $1.2 \cdot \max y_{theory}$ and the lower bound was set to be $0.8 \cdot \min y$. The lower limits for K_m and μ_{max} are set to be $1 \cdot 10^{-10}$ as a way to keep the variables non-zero. The upper limit for μ_{max} is set to 0.5 since a higher growth rate would make the model unstable and a higher a higher growth rate would not fit the results. The solver method used was GRG-nonlinear, using multistart with a population size of 100.

3.4 Characterisation of viral burst size and lysis time

This protocol for characterising burst size and eclipse time was developed by Nikolay Martyushenko and me. It is based on continuously measuring bacterial concentration in series of solutions with different concentrations of phage particles, where the highest concentrations are at least equal parts phage particles and bacterial cells. Phage sample was amplified by adding 100 μL raw phage sample to 3 mL bacterial broth in exponential phase and incubated for a couple of hours until the solution was transparent. An eight-step two-fold serial dilution was made from the amplified phage sample. The core idea behind the method is that the values pertaining to bursts have to be periodic with respect to phage dilution, since a dilution by the burst size should yield an equal change in bacterial concentration, just translated by the lysis time. This is illustrated in figure 11, where the red and blue lines show the rate of change in bacteria. The two solutions have equal initial bacterial concentration, but the initial phage concentration in the solution represented by the blue line is the initial phage concentration of red line diluted by the burst size of the phage. In the red line we see that there are two cycles of infections, while the blue line has three cycles. As a result of this, after the first infection cycle for the blue line, the phage concentration is equal to the initial phage concentration for the red line, and the following infection cycles will behave equal to the infection cycles to the red.

The variance for lysis time was found by fitting a gamma distribution to the negative peak in the rate of change in bacterial concentration. This was only done for the first infection cycle, as interference from both the first and third infection cycle affects the shape of the second infection cycle.

For this experiment to work, the span of different dilutions need to include phage concentration that give one, two and three infection cycles.

BL21 and DH5 α were inoculated separately in M9 broth, and incubated until they reached an exponential growth phase. The OD₆₀₀ was measured. 500 μL bacterial broth was mixed with 1.5 mL M9 soft agar and 100 μL phage sample from the first dilution step. The ratio between soft agar and bacterial broth is the same as in the Cellfiebooth. This is to mimic the environment the phage and host experience there. This solution was mixed and added in wells on a 96 well microplate. This was done for all phage dilutions and both bacteria. The 96 well microplate was then placed in a tecan infinite m200 pro, where the OD₆₀₀ was measured with steady intervals over 16 hours.

The change in OD₆₀₀ was found by identifying the numerical differentiation of the data. The lysis time was then determined by calculating the time between the first and second negative peak for change in OD₆₀₀, for dilutions with two infection cycles. The burst size was found by first calculating the

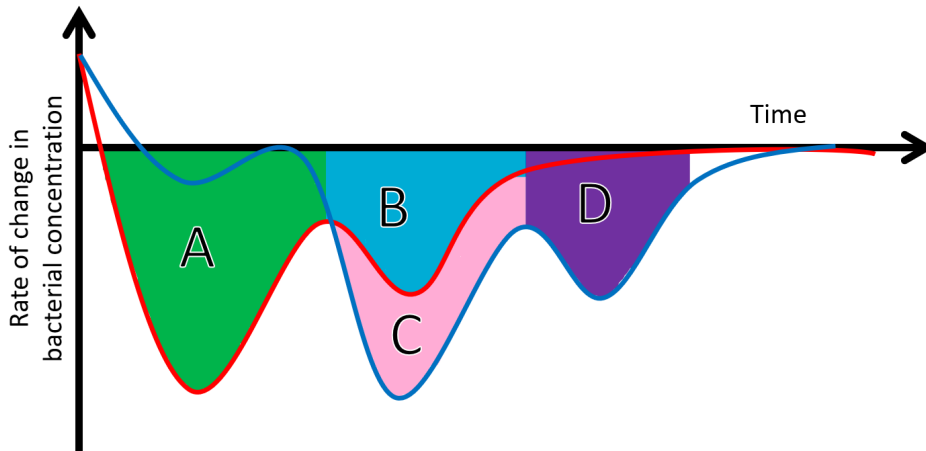


Figure 11: Example figure of how burst size is determined. The sketch shows the rate of change in bacterial concentration with regards to time. The two lines correspond to bacterial solutions inoculated with phages, where the bacterial concentrations are initially equal. The initial phage concentration in the blue line is the initial phage concentration in the red line diluted by a factor of the burst size of the phage inoculated. The letters A, B, C, and D correspond to the area beneath the graphs. The ratio between A and B are equal to C and D.

area under the graph for each negative peak and then comparing the ratio between the first and second, and the second and third infection cycle for each dilution. The technique builds on the assumption that two bacteria and phage solutions—where the phage concentration in one is equal to the other diluted with the burst size of the phage—will behave almost equally. The exception being that the solution with diluted phage concentration will have an offset of one lysis time. Here the ratio between the area under the first and second infection cycle in the original solution behaves just like the ratio between the area under the second and third infection cycle in the diluted solution. By finding the ratio between the infection cycles for all dilutions and plotting them, we can extrapolate the burst size from finding the offset between the two lines where the ratio is close to 1, as it will be the most precise here.

The standard deviation to the lysis time was found by fitting a gamma distribution to the first negative peak in rate of change in bacterial concentration. The standard deviation of this gamma distribution is equal to the standard deviation of the lysis time of the phage. As the phages are thoroughly mixed when they are first introduced to the bacteria, we can assume that the time of infection for the first infection cycle is equal for all bacteria and phages. As the following infection cycles are initiated by the previous cycles, standard deviation of the following infection cycles will not yield a good approximation of the standard deviation for the lysis time.

3.5 Mathematical model

The model used to explore the emergent properties of phage-host in this thesis is a diffusion-reaction model. A simplified map over this model is shown in figure 12, where we see a summary of what is happening in the model. Bacteria grow by mitosis; where a cell splits into two equal parts. As a consequence, the influx rate of new bacteria is dependent on the amount of bacteria already present in the model, which is why the influx of bacteria is shown as an arrow from itself. When a bacteria and a phage meet, both are removed from the model and become an infected bacterium. This infected bacterium will then burst through lysis and release new phage and free DNA to the system.

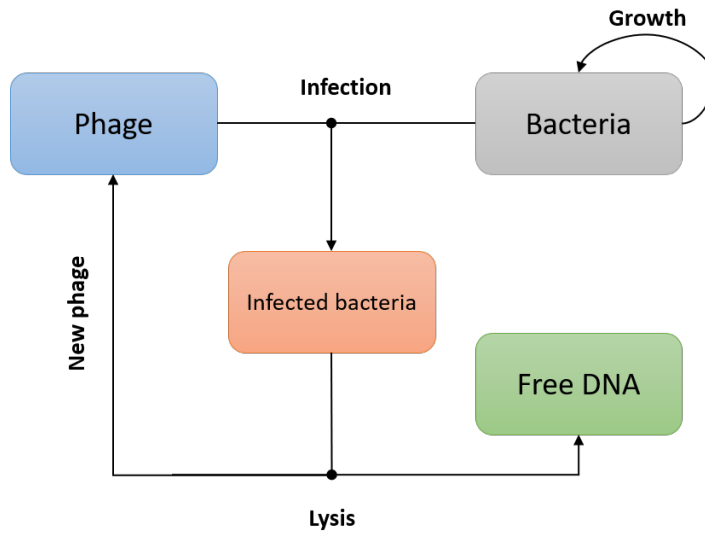


Figure 12: Simplified state map over the model.

The complete model does however include a few more components, and the complete state map is shown in figure 13. Here, *nutrition* is introduced as a new element, *diffusion* is introduced as a new effect, and the infected bacteria state is split up into multiple stages. These alterations all affect the model, but the introduction of diffusion is the greatest conceptual change. To understand the model, we can imagine a grid where each cell has to consider their own state map individually. Through diffusion, the neighbouring cells will now affect each other, by nutrients and phage freely diffusing from cells with higher concentration to cells with lower concentration.

Consider an arbitrary cell at the position (i, j) . If the concentration of phage is higher in cell $(i, j-1)$ and the concentration of nutrition is lower in cell $(i+1, j)$, then some phage particles will flow over from cell $(i, j-1)$ to (i, j) and nutrition will flow from (i, j) to $(i+1, j)$. Now, the reaction in

(i, j) will be affected by a lower nutrition concentration and a higher phage concentration.

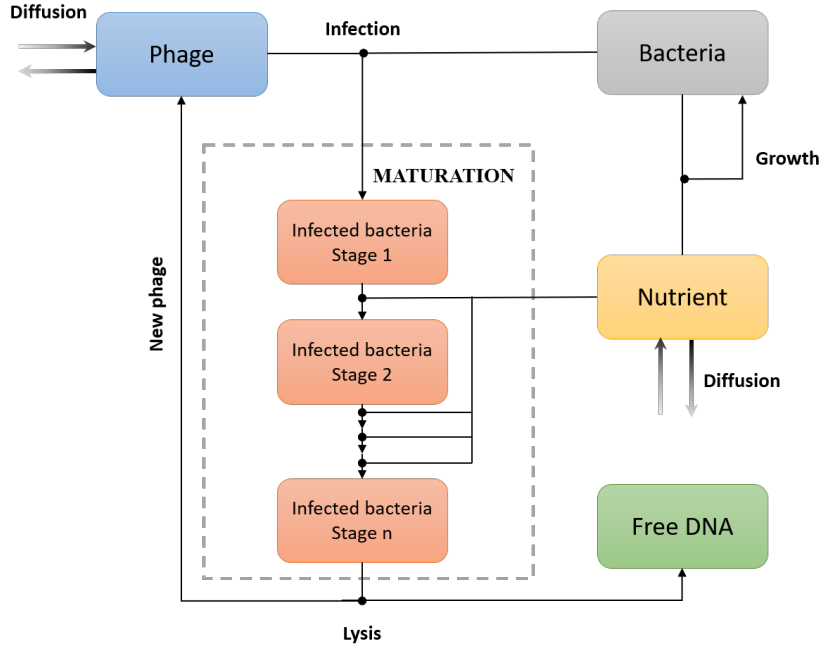


Figure 13: Complete state map over the model.

The infection of a bacterium is split into multiple stages. This is done to properly mimic the effects happening in real life. An infected bacteria would never release immediately after an infection. The biosynthesis of a phage takes time, and the lysis of infected bacteria is controlled by the phages. The rate of which the infected bacteria moves through each stage of infection is decided by the concentration of infected cells at the given stage multiplied with a rate constant k_1 and the Monod equation.

The model is governed by the partial differential equations presented in equation 11 to equation 15. The states, like $B(x,y,t)$ for bacteria, are written with a capital letter for short and the nabla notation (∇) represents the gradient $\nabla = (\frac{\partial}{\partial x} + \frac{\partial}{\partial y})$. D_N and D_P are the diffusion constants for nutrient and phage respectively.

$$\frac{\partial B}{\partial t} = \left(\mu_{max} \frac{N}{K_s + N} \right) \cdot B - \alpha B P \quad (11)$$

$$\frac{\partial N}{\partial t} = -\gamma \left(\frac{N}{K_s + N} \right) \cdot \left(\mu_{max} \cdot B + k_i \cdot \sum_{i=1}^n I_i \right) + D_N \cdot \nabla N \quad (12)$$

$$\frac{\partial P}{\partial t} = \beta \cdot I_n \cdot k_I \cdot \frac{N}{N + K_s} - \alpha B P + D_P \cdot \nabla P \quad (13)$$

$$\frac{\partial I}{\partial t} : \begin{cases} \frac{\partial I_1}{\partial t} = \alpha \cdot B \cdot P - I_1 \cdot k_I \cdot \frac{N}{N+K_s} \\ \frac{\partial I_2}{\partial t} = I_1 \cdot k_I \cdot \frac{N}{N+K_s} - I_2 \cdot k_I \cdot \frac{N}{N+K_s} \\ \dots \\ \dot{I}_n = I_{n-1} \cdot k_I \cdot \frac{N}{N+K_s} - I_n \cdot k_I \cdot \frac{N}{N+K_s} \end{cases} \quad (14)$$

$$\frac{\partial D_{DNA}}{\partial t} = I_n \cdot k_I \cdot \frac{N}{N + K_s} \quad (15)$$

Every capitalised variable is a component from the state map in figure 13 with the exception of the diffusion constants D_N and D_P . As this is quite a large and extensive model, a step-wise rendition of each expression explaining the origin and effect of each term will be most beneficial way to explain the model and the root of each expression. Equation 11 determines the change in bacterial concentration. Equation 16 shows how the equation takes different affects into account. The bacterial growth is governed by the existing bacterial concentration multiplied with Monod equation, where μ_{max} is maximum growth rate, N is the nutrient concentration, and K_s is the half velocity constant[53]. Loss of bacteria is governed by the loss of bacteria due to infection. Here α is the adsorption rate and represents the chance of infection, P is the concentration of phages and B is the concentration of bacteria.

$$\frac{\partial B}{\partial t} = \underbrace{\left(\mu_{max} \frac{N}{K_M + N} \right) \cdot B}_{\substack{\text{Bacterial growth,} \\ \text{governed by the Monod} \\ \text{equation}}} - \underbrace{\alpha \cdot B \cdot P}_{\substack{\text{Loss of} \\ \text{bacteria due} \\ \text{to infection}}} \quad (16)$$

Change in nutrient concentration is governed by two effects, as shown in equation 17. The first term is the effect of both infected and uninfected bacteria consuming nutrients. The Monod equation is multiplied with the bacterial growth rate and γ , where γ is the yield constant that represents how many grams of nutrients are consumed for each gram of new bacteria. These growth kinetic constants are assumed to be the same for infected and uninfected bacteria. The second is diffusion of nutrients, as nutrients in the

agar are glucose and casamino acids, which are small enough to diffuse freely in the agar.

$$\frac{\partial N}{\partial t} = - \underbrace{\gamma \cdot \left(\frac{N}{K_s + N} \right) \cdot \left(\mu_{max} \cdot B + k_I \cdot \sum_{i=1}^n I_i \right)}_{\text{Nutrient consumed by infected and uninfected bacteria}} + \underbrace{D_N \nabla N}_{\text{Diffusion of nutrients}} \quad (17)$$

The change in phage concentration is governed by three different terms, as shown in equation 18. The first term is the influx of new phages to the system by infected bacteria bursting. This term is similar to the last term in \dot{I}_n representing the number of infected bacteria leaving the last stage and bursting multiplied with β , which is a constant that constitutes the burst size of an infected bacteria. The next term represents the loss of phages due to infection where α is the adsorption rate and represents the chance of infection, multiplied with the concentration of bacteria and phage. The last term constitutes the diffusion of phages, and is the diffusion constant for phages, multiplied with the phage concentration and the gradient.

$$\frac{\partial P}{\partial t} = \underbrace{\beta \cdot I_n \cdot k_I \cdot \frac{N}{N + K_m}}_{\text{Bursting of infected bacteria}} - \underbrace{\alpha B P}_{\text{Loss of phage from infection}} + \underbrace{D_P \nabla P}_{\text{Diffusion of phages}} \quad (18)$$

The change in concentration of infected bacteria differs from the other equations, as it is governed by a series of equations, instead of one equation. The infection is split into several stages, which the infected bacteria need to go through before it bursts and releases phages into the system. This segmentation of the infection stage is done as a way to incorporate the lysis time into the model. Each stage of infection follows a gamma distribution. When the number of infection stages is sufficiently high, the summed distribution of all infected bacteria stages becomes a normal distribution due to the Central Limit Theorem. The rate constant k_I and the number of infection stages n is calculated from the variance and mean lysis time of the phage used. From the theory about gamma distributions we know that the mean is $\mu = \frac{\alpha}{\beta}$ and the variance is $\sigma^2 = \frac{\alpha}{\beta^2}$. Inserting the rate constant k_I for the rate parameter β and the number of stages n for the shape parameter α we can algebraically manipulate the equations for mean and variance to arrive at the expressions for n and k_I showed in equation 19 and 20. With these expressions, finding the fitting rate and number of stages becomes a question of finding the mean lysis time and variance of this lysis time. This is found through my own experimental work which is described in section 3.4.

$$k_I = \frac{\mu_T}{\sigma_T^2} \quad (19) \quad n = \frac{\mu_T^2}{\sigma_T^2} \quad (20)$$

The first stage in the collection of equations for infected bacteria consists of two terms, where the first constitutes the influx of stage 1 infected bacteria. This term is the concentration of phage particles multiplied by the concentration of susceptible bacteria as well as the constant α , which represents the chance of infection. The second term is the rate of which the infected bacteria moves through stages. This is rate is decided by a rate constant k_I as well as the Monod equation. The Monod equation is included as the infected bacteria is dependent on absorbing nutrition to produce phage-particles.

$$\frac{\partial I_1}{\partial t} = \underbrace{\alpha \cdot B \cdot P}_{\substack{\text{Bacteria} \\ \text{becoming} \\ \text{infected}}} - \underbrace{I_1 \cdot k_I \cdot \frac{N}{N + K_s}}_{\substack{\text{Infected bacteria} \\ \text{moving to the next} \\ \text{stage of infection}}} \quad (21)$$

The second infection stage until the last follow the equation shown in equation 22. The first term constitutes the influx of infected bacteria from the previous stage, and the second term constitutes the out flux of infected bacteria to the next stage or bursting for the last stage.

$$\frac{\partial I_i}{\partial t} = \underbrace{I_{i-1} \cdot k_I \cdot \frac{N}{N + K_s}}_{\substack{\text{Infected bacteria} \\ \text{moving to the next} \\ \text{stage of infection}}} - \underbrace{I_i \cdot k_I \cdot \frac{N}{N + K_s}}_{\substack{\text{Infected bacteria} \\ \text{moving to the next} \\ \text{stage of infection}}} \quad (22)$$

Change in the amount of DNA in the system is governed by a single term, as shown in equation 23. This term represents the lysis of bacteria by phages.

$$\frac{\partial D_{DNA}}{\partial t} = + \underbrace{I_n \cdot k_I \cdot \frac{N}{N + K_s}}_{\substack{\text{DNA released} \\ \text{from lysis of} \\ \text{infected bacteria}}} \quad (23)$$

The model was solved using Eulers method in python. An adaptive time-step was not used as the model consists of stiff equations. The stiffness is due to the rapid change The step size for time (dt) was set using equation 24, which is the Von Neuman stability analysis done for diffusion in two dimensions multiplied by 0.8. The step size is multiplied by 0.8 to make sure the step size is low enough to avoid numerical instability.

$$\delta t = \frac{\delta x^2}{4 \cdot D} \cdot 0.8 \quad (24)$$

The constants used in the model and their origin is summed up in Table 2. The diffusion constants and absorption rate are retrieved from literature, while the rest is found through experimental results. These will be further discussed in the result and discussion sections.

Table 2: Overview of all constants used in the model and where they come from.

	Symbol	Bl21	unit	source
Bacterial growth rate	μ_{max}	$1.99 \cdot 10^{-1}$	h^{-1}	This thesis
Half velocity constant	K_m	$2.12 \cdot 10^{-3}$	g/gDW	This thesis
Nutrial yield	γ	$2.32 \cdot 10^{-2}$	g/gDW	This thesis
Burst size	μ_T	95 ± 5	$\text{phage} \cdot \text{cell}^{-1}$	This thesis
Lysis time	μ_T	42 ± 2	min	This thesis
STD - lysis time	σ_T	$6.2 \pm .2$	h^{-1}	This thesis
DH5a				
Bacterial growth rate	μ_{max}	$1.34 \cdot 10^{-1}$	h^{-1}	This thesis
Half velocity constant	K_m	$2.30 \cdot 10^{-3}$	g/gDW	This thesis
Nutrial yield	γ	$1.90 \cdot 10^{-2}$	g/gDW	This thesis
Burst size	β	85 ± 5	$\text{phage} \cdot \text{cell}^{-1}$	This thesis
Lysis time	μ_T	78 ± 4	min	This thesis
STD - lysis time	σ_T	17 ± 2	h^{-1}	This thesis
Common				
Rate const. for inf. stages	k_i	$6 \cdot 10^{-9}$	$\text{phage}^{-1} \cdot \text{cell}^{-1} \cdot \text{mL}^{-1} \cdot \text{h}^{-1}$	[46]
Diffusion constant for nutrition	D_N	$2.16 \cdot 10^{-2}$	$\text{cm}^2 \cdot \text{h}^{-1}$	[101]
Diffusion constant for phage	D_P	$4.32 \cdot 10^{-5}$	$\text{cm}^2 \cdot \text{h}^{-1}$	[102]

4 Results and analysis

I commence the following chapter by introducing my lab results concerning the characterisation of bacterial and phage strain used in this thesis, as the values found through these experiments are used in my model. Following that, I present the results related to the characterisation of the Cellfiebooth system, as the results from this characterisation is relevant to the interpretation of the results from Cellfiebooth. Wrapping up the chapter, I present the results from the Cellfiebooth alongside the modelling, as these are of mutual relevance to one another.

4.1 Characterisation of growth rate

The experimental data are shown for four different dilutions in figure 14 and 15. The data were fitted to a bacterial growth model that follows Monod kinetics. The theoretical results are presented alongside the three first dilutions in figure 16 and 17. The experimental data are shown as dots, while the theoretical data are shown as dashed lines. As described in section 3.3, this experiment was carried out by mixing the bacterial broth with molten soft agar and pouring it into the wells in a multiplate. Due to the temperature changes caused by warm, soft agar being cooled down in the multiplate; dew formed on the lid of the multiplate. This caused substantial noise in the first five data points, leading to the exclusion of these measurements from the model fitting. The excluded data points constitute only the first half hour of the experiment. The dew subsided after the first half hour, and the rest of the data show clear trends with little noise.

The model was fitted to the experimental data for the raw bacteria sample and the first two dilutions. The decision not to include all the dilutions in the model fitting, came from discovering that the model proved to fit the higher dilutions much better than the smaller ones. Including the smaller dilutions would have yielded a worse overall result, rather than a good fit for the higher start concentrations and a worse fit for the lower concentrations. The bad fit is probably a consequence of limitations to the equipment used for experimental measurements. The multiplate reader is simply not precise enough to measure the low bacterial concentration in the early stages of the run, whence bacterial seeding concentration is low.

The experimental data for the growth curve for BL21, shown in figure 15, are considerably more varied than the same data for DH5 α . This is because the experiment was done on two separate occasions, with four replicates for each run, and the data presented is the average plus the variance. All the experimental data for the growth of DH5 α , on the other hand, was measured in a single experiment where each dilution had eight replicates. Both display

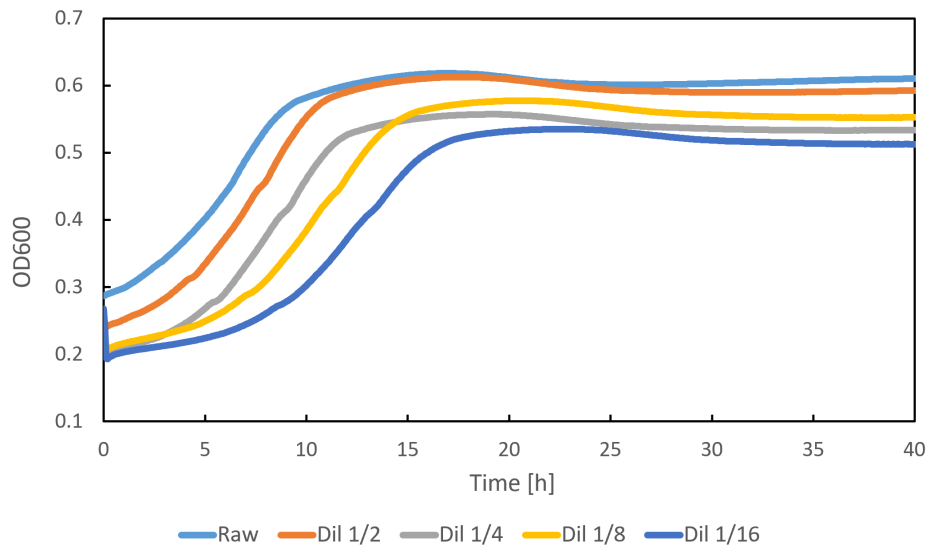


Figure 14: Growth of DH5a. Scatter plot showing the average of the bacterial concentration given in OD₆₀₀ for different initial bacterial concentrations. The results appear as lines due to the high amount of data points. The experiment was done with ten replicates for each dilutions and the graphs show the average of the dilutions. Error bars are not included as the largest standard deviation was 0.029.

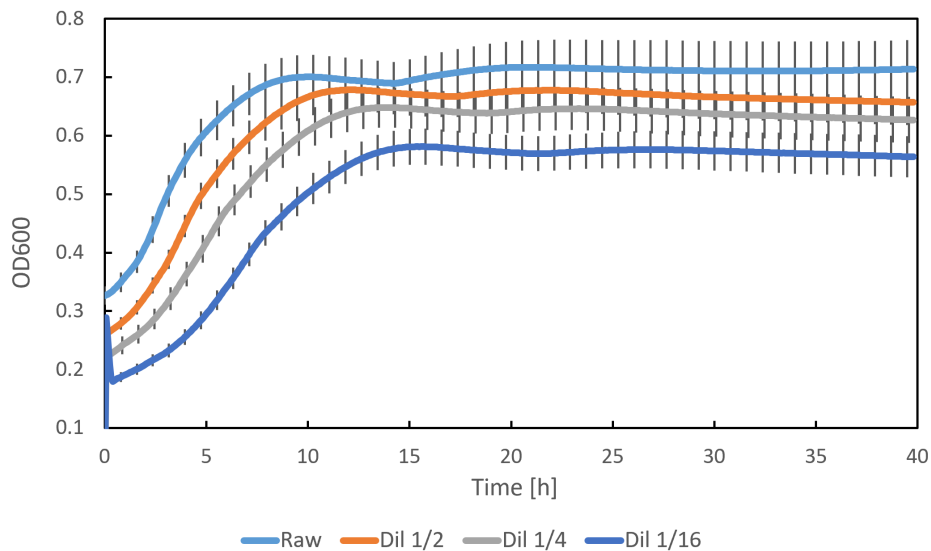


Figure 15: Growth of BL21. Scatter plot showing the average bacterial concentration given in OD₆₀₀ for different initial bacterial concentrations. Error bars are given for every tenth data point. The results appear as lines due to the high amount of data points

expected behaviour. BL21 grows a bit faster and reaches a higher end OD₆₀₀ than DH5 α , which corresponds with the literature[103]. The growth curve of DH5 α shown in figure 14 displays interesting results, as the end concentration for Dil 1/8 is higher than the end concentration of Dil 1/4. My expectation would be to find the pattern of higher start dilution giving higher end dilution to apply here, as it does in the BL21 experiment. There is no obvious cause or explanation to this phenomena, but the difference in end concentration is not too large, and it may simply be a result of human error.

The growth kinetic constants found are presented in table 3. K_m and γ are given in gram nutrient per gram bacterial dry weight.

	BL21	DH5a	unit
μ_{\max}	$1.99 \cdot 10^{-1}$	$1.34 \cdot 10^{-1}$	h^{-1}
K_m	$2.12 \cdot 10^{-3}$	$2.30 \cdot 10^{-3}$	g/gDW
γ	$2.32 \cdot 10^{-2}$	$1.90 \cdot 10^{-2}$	g/gDW

Table 3: Growth constants found for each bacteria. The variance to the experimental data is shown in table 4

The Table 4 shows the variance, R^2 , between the experimental data and theoretical data that uses the found kinetic growth constants and equal starting conditions. Both theoretical and experimental data for all dilutions can be found in Appendix B.

	BL21	DH5a
Raw	0.983	0.991
Dilution 1	0.992	0.983
Dilution 2	0.996	0.978
Dilution 3	0.997	0.950
Dilution 4	0.997	0.928

Table 4: The variance, R^2 , between the model and experimental data for each dilution.

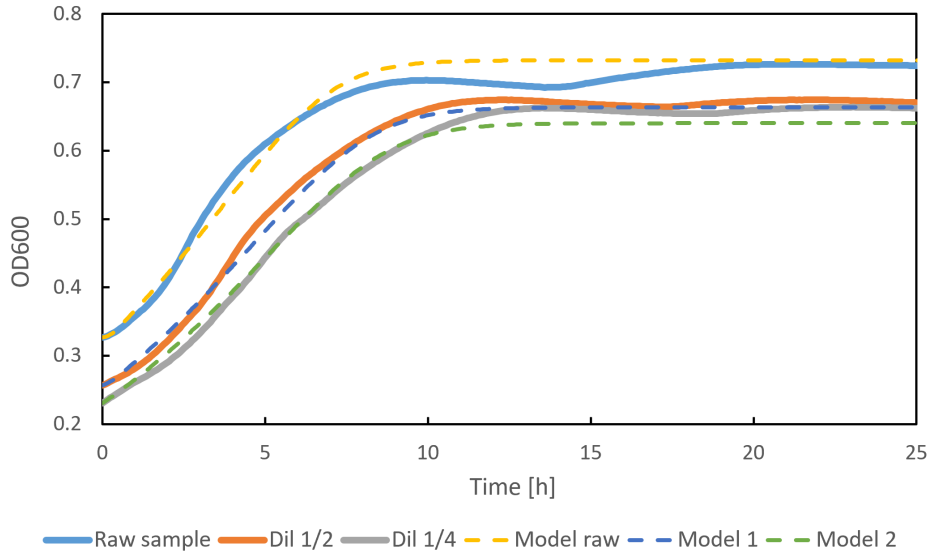


Figure 16: Comparison of experimental data with mathematical model. *E. coli* strain BL21 in sloppy agar with different start concentrations.

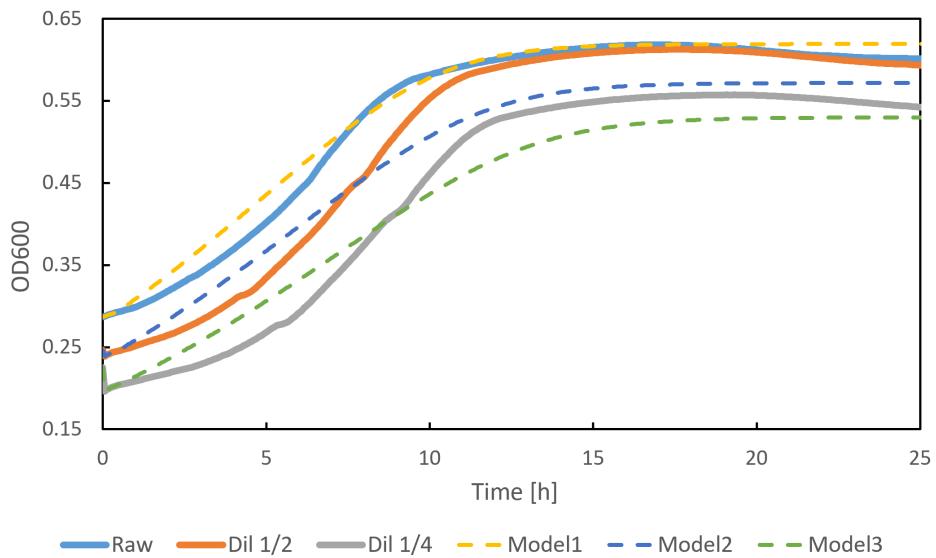


Figure 17: Comparison of experimental data with mathematical model. *E. coli* strain DH5α in sloppy agar with different start concentrations.

4.2 Burst size and eclipse time

I carried out the experiment as described in section 3.4 for both DH5 α and BL21. The multiplate contained eight biological replicates for all dilutions. The temperature was set to 28 °C throughout the experiment. The graphs in figure 18 and 19 show the change in OD₆₀₀ for each run. As described in section 3.4, the different concentrations were made in a two-fold serial dilution, and each dilution is named after the concentration of phages in relation to the raw dilution. For example, "Dil 1/16" contains 1/16 of the phages in "Raw". The dilution series made was used for both bacterial strains. This means the concentration in "Dil 1/4" in the DH5 α experiment contained the same amount of phage particles as "Dil 1/4" in the BL21 experiment at the point of seeding. As the starting bacterial solution was not entirely identical, the results are not comparable on all levels.

From the graphs in figure 18 and 19, we see that the introduction of phages result in a decline in measured OD₆₀₀. This is due to the phage lysing the infected bacteria. The measurements are taken at steady intervals over 16 hours. All concentrations of phages end in a constant OD₆₀₀ that does not change beyond what is shown, while the control containing no phage particles continuous to growth as expected. This suggests that all bacterial cells present are lysed by the phages. As it turns out; the lower the initial phage concentration - the longer it takes before OD₆₀₀ reach a steady state. This is as expected, as the phages will need time to proliferate if the amount of phages present is not sufficient to infect all bacteria.

Figure 20 shows a graph of the rate of change in OD₆₀₀ over time, for all equal number dilutions. Odd numbered dilutions show the same trends and can be found in the appendix 80. The change in OD₆₀₀ over time represents the rate of which bacteria grow and die. The data for DH5 α was treated with five point moving average to filter out noise. This was not necessary for the data for BL21. In "Raw", where the bacteria is introduced to the highest concentration of phage particles, we can only observe a single peak. This suggests that the number of phages present were equal or higher than the number of bacteria in the mix, and all bacteria were infected and lysed at the same time with a normally distributed variation. "Dil 1/4" shows a weak second peak, while "Dil 1/16" shows two distinct peaks before reaching zero. This suggests that the initial concentration of phages did not infect all bacteria present. However, as the infected bacteria were lysed and released a new wave of phage particles to the solution, the rest of the bacteria were infected and subsequently lysed. The trend continues and "Dil 1/64" and lower seem to have three waves of infection or more. The same trend was observed for BL21 and in the odd numbered dilution. The lower amount of data noise in BL21 seems to stem from the BL21 experiment having a higher

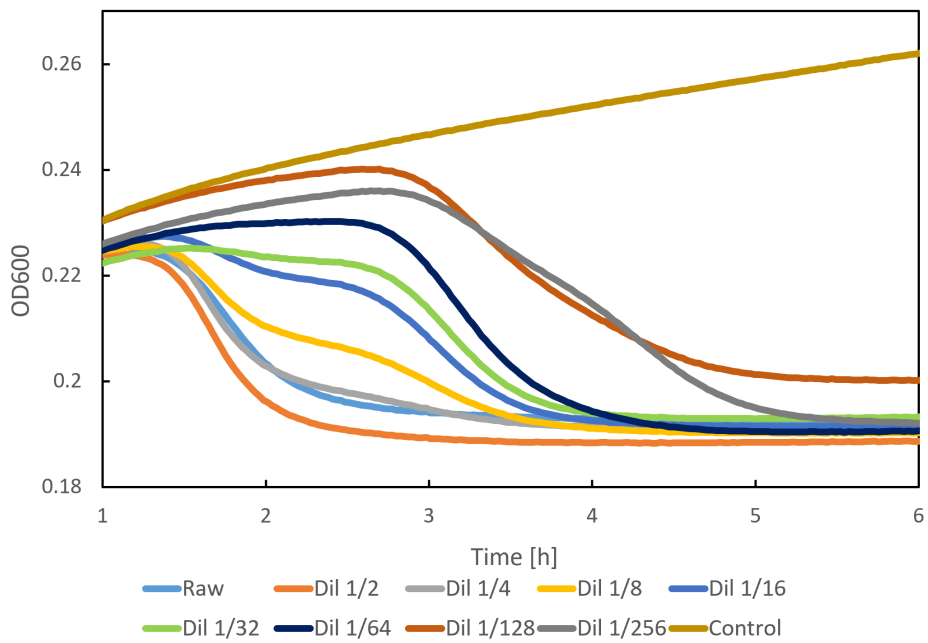


Figure 18: Cell concentration measured in OD₆₀₀ for DH5 α introduced to different concentrations of the phage. The lines represent the average from an experiment conducted with seven replicates. The largest variance was 0.077. The early values, especially for the control, are affected by dew in the machine.

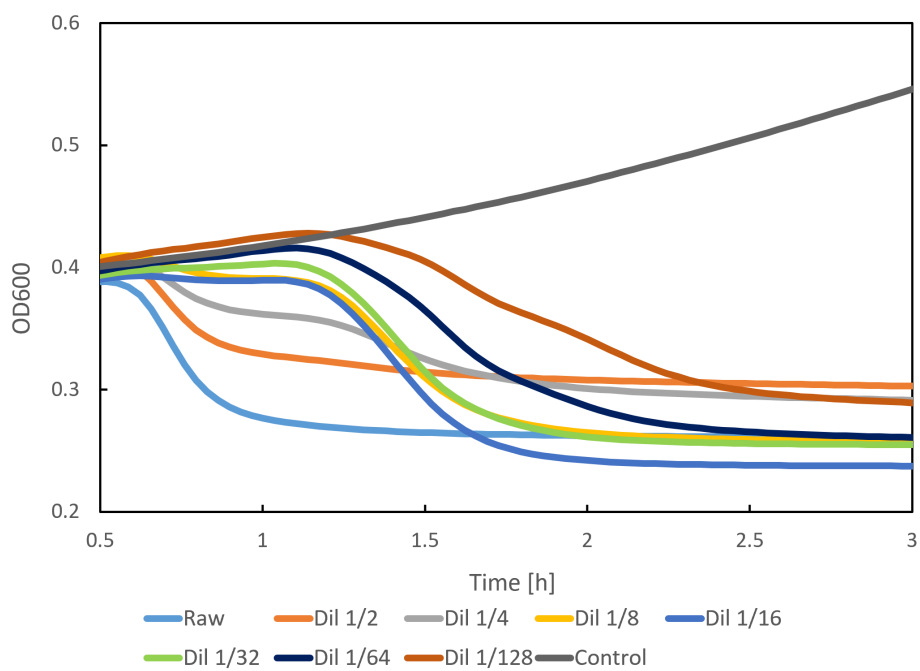


Figure 19: Cell concentration measured in OD₆₀₀ for BL21 was introduced to different concentrations of the phage. The lines are the average from the experiment done with seven replicates. Largest variance was 0.033. The early values are affected by dew in the machine.

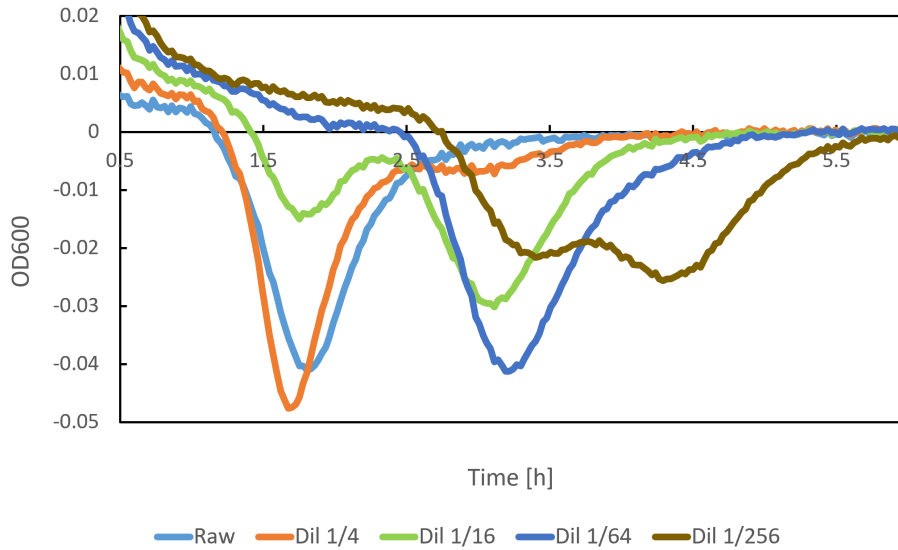


Figure 20: Change in OD_{600} over time for DH5a introduced to different concentrations of phages. Data is filtered with five point average. Every other dilution is shown. The dilutions not included follow the same pattern as displayed and can be found in appendix C

initial concentration of bacterial cells at the beginning of the experiment. The lysis time was found by calculating the time between the negative peaks for the dilutions where both peaks are prominent. This was "Dil 1/4", "Dil 1/8", and "Dil 1/16" for BL21, and dilution "Dil 1/8", "Dil 1/16", and "Dil 1/32" for DH5 α . The results are presented in table 7. The standard variation in lysis time was found by fitting a gamma distribution to the first negative peak in rate of change in bacterial concentration (first infection cycle) for the three dilutions with the highest initial phage concentration. Figure 22 and 23 show the gamma distribution and the negative peaks they are fitted to, and table 6 shows the variance in R^2 between the experimental results and the found gamma distribution.

The growth of control bacteria is stable throughout the period of interest. As mentioned in section 3.4, the core idea behind the method is that values pertaining to bursts have to be periodic with respect to phage dilution. This is because a dilution by the burst size should yield similar infection cycles translated by the lysis time.

The ratio between the area under the negative peaks in figure 21 and 20 are presented in table 5. The distance between the lines reveals the burst size the phage obtains for each bacterial strain, and the values are most accurate when the ratio is close to one. The burst size was extrapolated from these values, and the results are presented in Table 7.

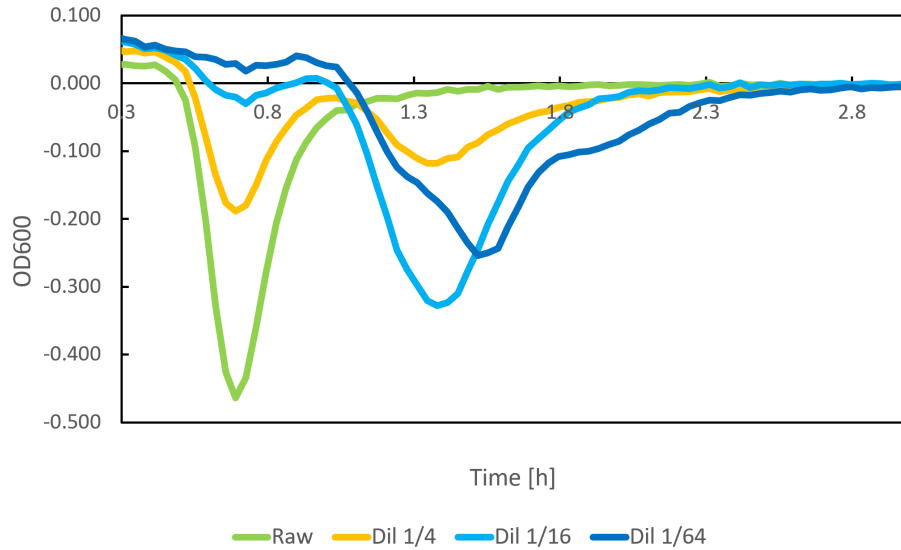


Figure 21: Change in OD_{600} over time for BL21 introduced to different concentrations of phages.

Table 5: Ratio between the areas under first and second infection cycle and second and third infection cycle. The values are not displayed when one of the infection cycles were not present, or not strong enough to be measured.

Ratio	BL21		DH5 α	
	First and second	Second and third	First and second	Second and third
1	10.85	-	-	-
2	4.37	-	10.75	-
4	0.78	-	3.89	13.05
8	0.12	-	1.15	7.82
16	-	12.19	0.27	9.91
32	-	8.55	-0.02	9.64
64	-	2.46	-	4.17
128	-	0.92	-	1.24
256	-	-	-	0.56

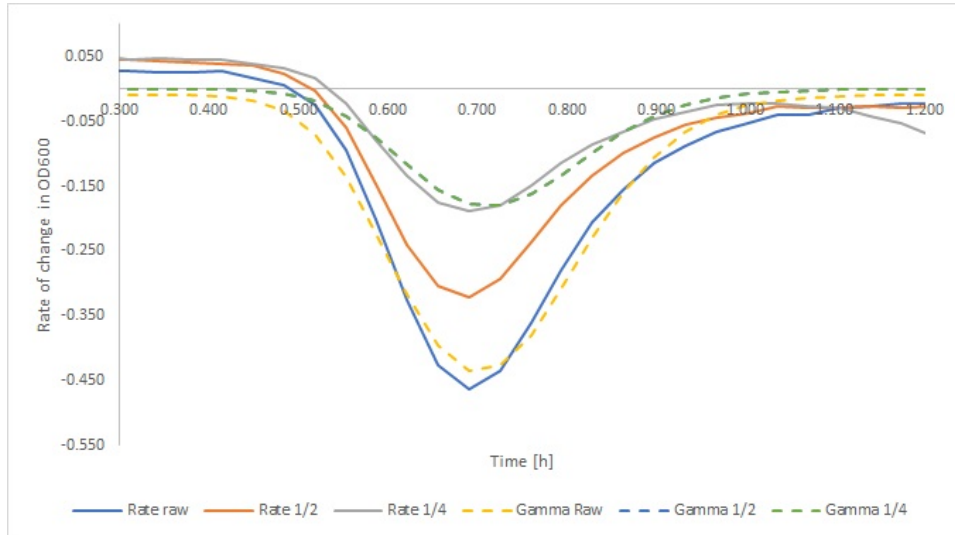


Figure 22: The gamma distribution fitted to the first negative peaks for BL21 introduced different concentrations of phage. This was done to find the deviation in lysis time and the results are shown in table 6

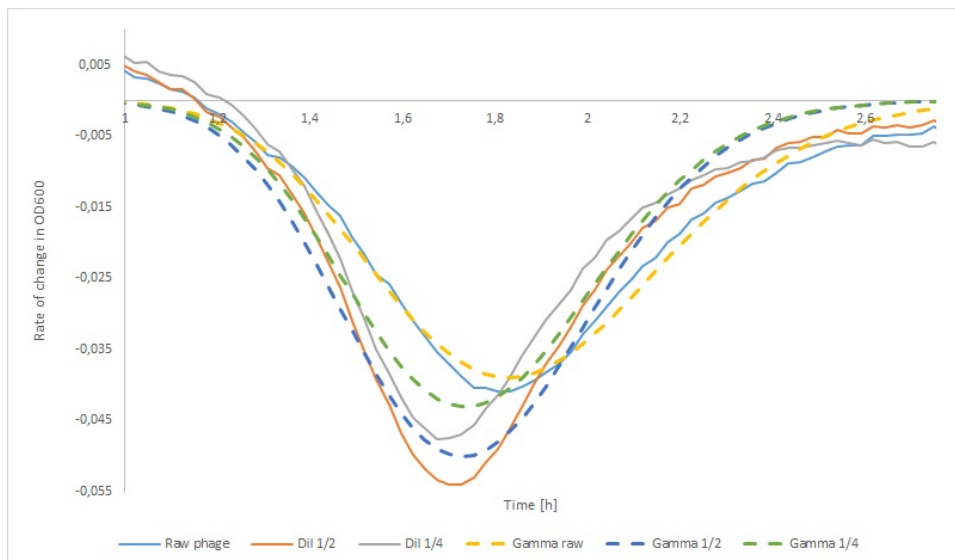


Figure 23: The gamma distribution fitted to the first negative peaks for DH5α introduced different concentrations of phage. This was done to find the deviation in lysis time and the results are shown in table 6.

Table 6: The standard deviation in lysis time for the phage in DH5 α and BL21. Standard deviation in phage lysis time was identified by fitting the gamma distribution to the first negative peak, which is shown in figure 23 and 22. The R^2 for the fitted gamma distribution.

	BL21		DH5 α	
	σ_T	R^2	σ_T	R^2
Raw	6.29	0.972	18.7	0.985
Dil 1/2	6.00	0.938	16.0	0.979
Dil 1/4	6.04	0.931	16.0	0.925
Average	6.1 ± 0.2		17 ± 2	

Table 7: Burst size and lysis time for the phage in relation to the two different hosts.

	BL21	DH5 α	unit
Burst size	85 ± 5	95 ± 5	phage \cdot cell $^{-1}$
Lysis time	42 ± 2	78 ± 4	min
Standard deviation in lysis time	6.1 ± 0.2	17 ± 2	min

4.3 Test for bacterial fluorescence

From analysing the results generated with Cellfiebooth, I observed the bacterial lawn becoming more visible as time progressed. This effect is illustrated in Figure 24, where two Cellfiebooth measurements from different time points in the same run are placed side by side. As previously elaborated, the Cellfiebooth system is based on the fluorescent dye GelGreen being activated by creating a dimer with DNA flowing in the agar. The DNA is present in the system due to bacteria being lysed by phages. I arrived at two hypotheses aiming to account for why the bacteria appear in the measurements.

1. GelGreen creates a dimer with bacteria making them fluorescent and visible in the system, albeit not as prominent as plaques.
2. Some light is able to make it all the way through from the light source to the camera. As the light source is not positioned directly against the camera, it will not appear until it is refracted by the bacterial lawn.

To test these hypotheses, I grew a bacterial lawn on a Petri dish filled with M9 agar, applying Gelgreen only to half of the bacterial lawn. The results from this experiment are presented in figure 25. The left side is with GelGreen, while the right side is without. The first image was captured immediately after preparing the Petri dish, while the second was captured 19 hours later, when the bacterial lawn had appeared.

The average pixel value of the boxes in Figure 25 are presented in Table 8. The boxes are 600 times 600 pixels in size, which corresponds to roughly 69 mm² on the Petri dish. The pixel values given by Cellfiebooth are in 16-bit and contain only the green channel. This translates to none being completely dark and 65535 being completely green. Figure 25 is converted to grayscale for greater visibility. The results show that the presence of GelGreen in the

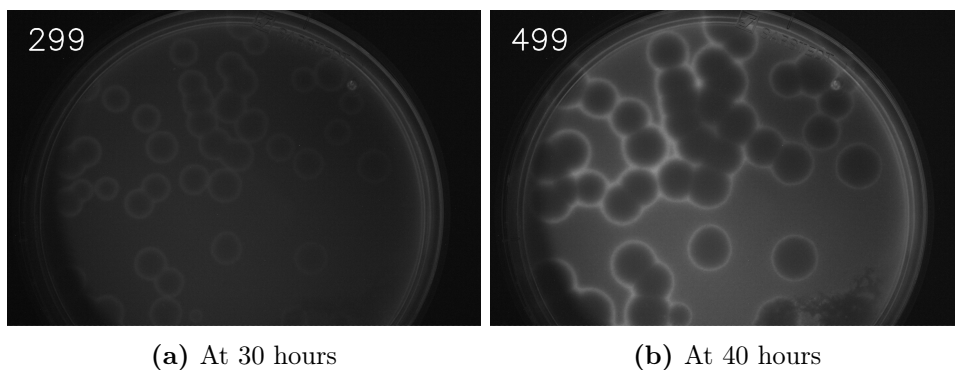
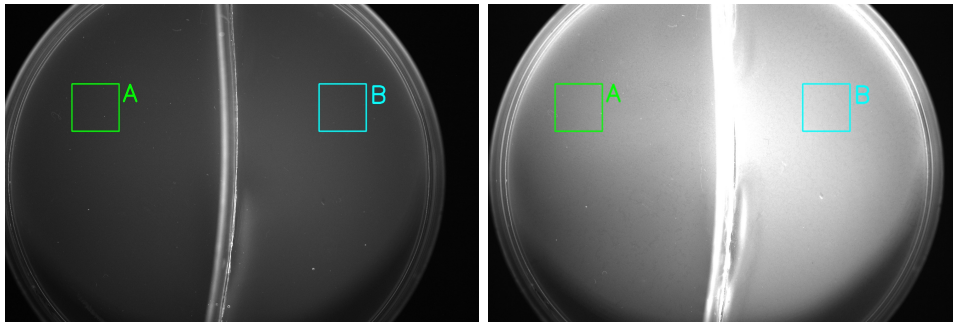


Figure 24: Cellfiebooth results at different time points. The number in the series is given in the left corner of the image.

soft agar overlay will result in a lower visibility of the bacterial lawn, which suggest that the observed effect is *not* caused by a fluorescence of GelGreen; the reason we see the bacterial lawn in the Cellfiebooth being light scattering. This has a couple of notable implications for the Cellfiebooth system as a whole. Firstly: analysing the experimental results, one must be aware of the fact that the source of the measured light intensity can be either fluorescence by free DNA or bacterial scattering, or both. Secondly: when analysing the experimental data, bacterial growth curve can be found by selecting an area of bacterial lawn that is unaffected by plaques throughout the experiment, and observe how the measured light intensity from this spot changes with time.

	Start	End
A - with GelGreen	321	900
B - without GelGreen	418	1338

Table 8: Average pixel value for the different boxes in Figure 25.



(a) Image captured in the beginning. (b) Image captured 19 hours later.

Figure 25: Both images were captured and processed with Cellfiebooth. The light intensity has been scaled by a factor of 40 to make the effect visible to the naked eye. The left side is with GelGreen and the right side is without.

4.4 Cellfiebooth and model results

Five experimental runs are selected from the ≈ 100 conducted experiments, of which many are "failed" experiments. Two are of the selected runs were done with BL21, three with DH5 α . The initial bacterial concentration of run 1.3 was not measured, but is included for interesting results that relate very much to the results in run 1.1 and run 1.2. The same phage strain is used for all selected experimental runs, and the initial phage concentration is not included. Phage concentration can however be calculated by counting the number of plaques on each Petri dish, and is left as an exercise for the curious reader. Note that experiment 1.1 was performed without the improvements to the Cellfiebooth mentioned in section 3.2.3. The temperature in the Cellfiebooth was measured to be 21 °C for all selected (and excluded) experiments.

Presentation of each experiment is initiated by showing six heat maps of the Petri dish during the experimental run. The heat maps range over time, from when the plaques first appear as faint dots to the point of development cessation. The last heat map shows boxes that encapsulate the plaques I studied closer and modelled. Subsequently, six heat maps of one of the chosen plaques over time are presented. Following that, intriguing results from the model are presented. The modelling results are presented by showing six surface plots per page. Each page show a time point in the model compared to the identical time point in the experimental results. The plot order for each page is the same, with the first plot being the experimental results, the following plots DNA, phage, bacteria, infected bacteria, and nutrient concentration in the model at the chosen time point.

Table 9: Overview of the experimental runs included in the thesis.

Name	Bacteria	Start OD ₆₀₀
1.1	DH5 α	0.086
1.2	DH5 α	0.333
1.3	DH5 α	not recorded
2.1	BL21	0.808

4.4.1 Experimental run 1.1 with DH5 α

The data were captured with the old camera and light filter. 700 images were captured with six minutes between each photograph in the run. The six photographs presented in figure 27 range from photo 150 to 549, where photo 150 is the first photo where traces of the plaques can be observed and at 549 the plaques have stopped expanding. A number of plaques appear in the Petri dish, and two sections were studied closer and modelled. These

sections are shown as box A and box B in figure 27f. We see a clear tilt in the surface plots of the later data of the experimental results (which can be observed in figure 33a). This has to do with the placement of the light source, as it is not directly beneath the Petri dish, but placed at an angle.

The graph in figure 26 shows the change in light intensity measured in a patch of bacterial lawn not affected by plaques. While it does not render an exact reading of the bacterial concentration, it does give us a good estimate of the growth curve of the bacteria. This growth curve is very similar to what we would expect, as it follows a typical Monod kinetics curve.

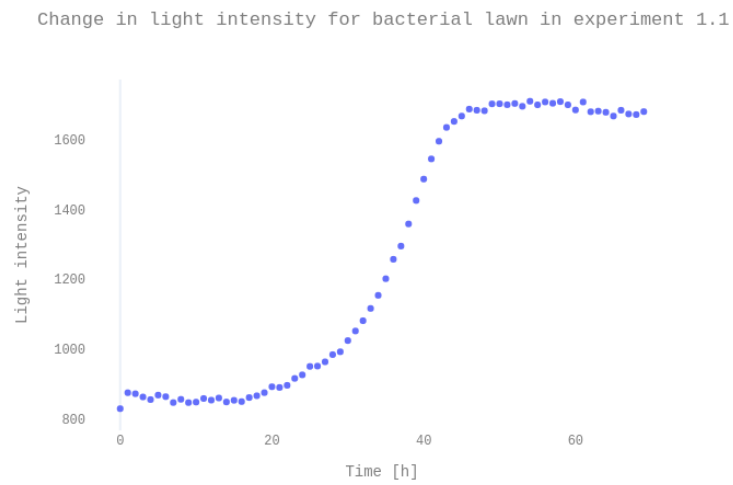


Figure 26: Change in light intensity over time in the bacterial lawn in experiment 1.1.

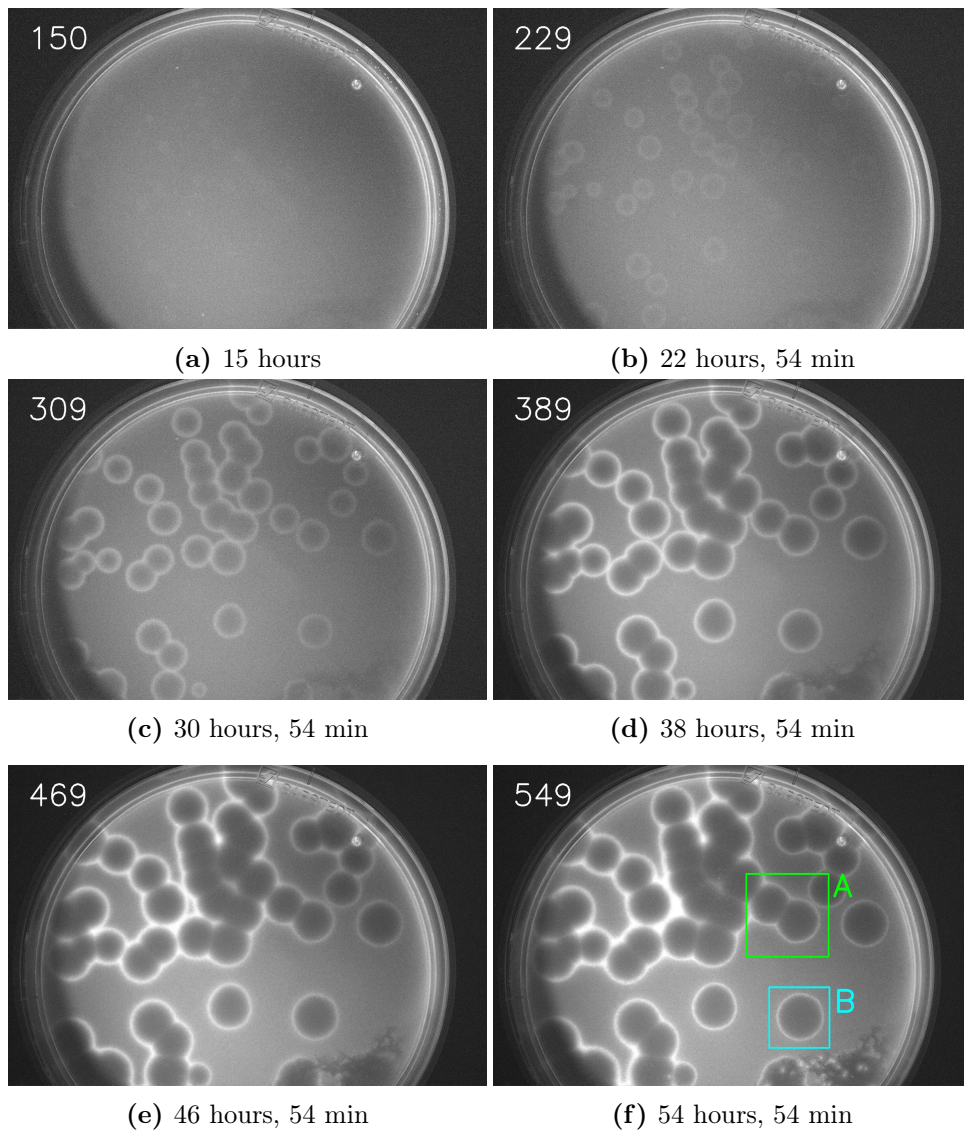
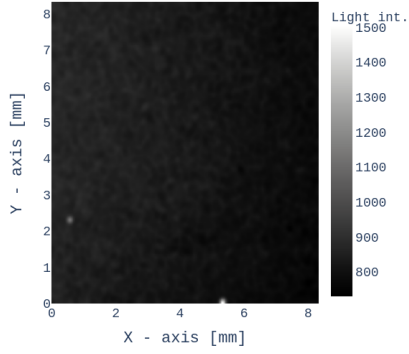


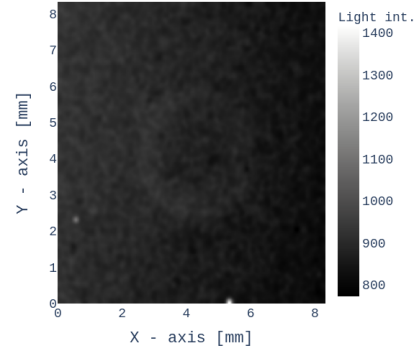
Figure 27: DH5 α with initial OD₆₀₀ = 0.086. The number in the series is given in the left corner of the image. There are six minutes between each number. Data were captured before the improvements mentioned in 3.2.3 A fungus started growing at the bottom of the Petri dish. The plaques in box A and B are studied. closer

Box B at picture 160



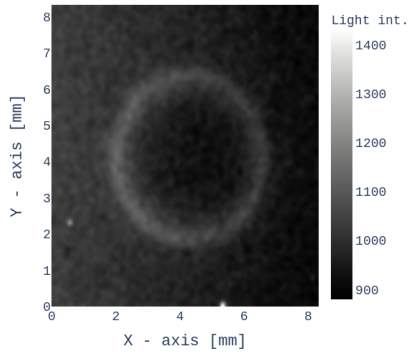
(a) 16 hours.

Box B at picture 238



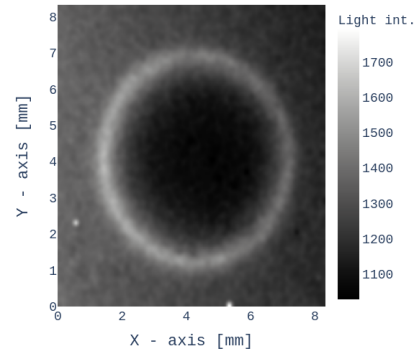
(b) 23 hours, 48 min.

Box B at picture 316



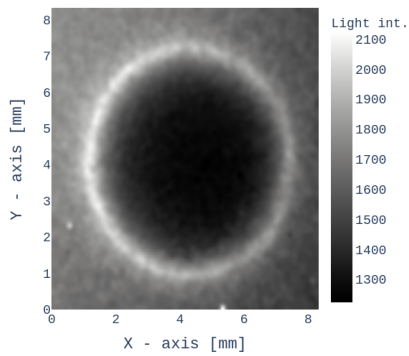
(c) 31 hours, 36 min.

Box B at picture 394



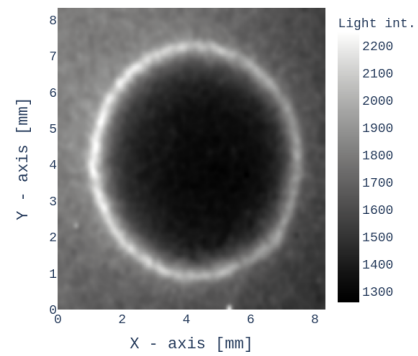
(d) 39 hours, 24 min.

Box B at picture 472



(e) 47 hours, 12 min.

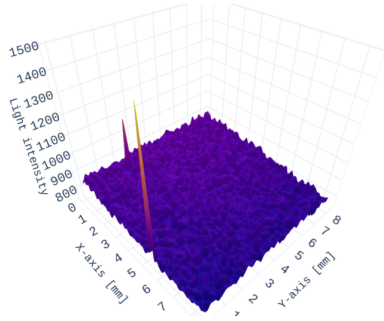
Box B at picture 550



(f) 55 hours, 48 min.

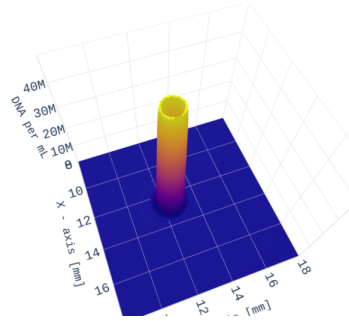
Figure 28: Closer look at the data from box b in figure 27 presented in a grayscale heatmap. The data were treated with a Gaussian filter with $\sigma = 5$.

Box B at picture 160



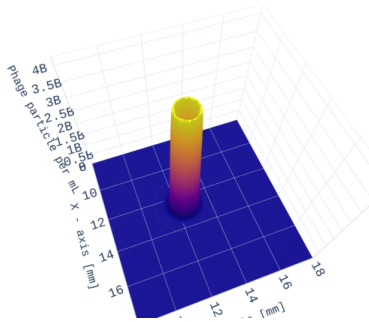
(a) Experimental results.

DNA in model of box B at 15 hours and 30 minutes



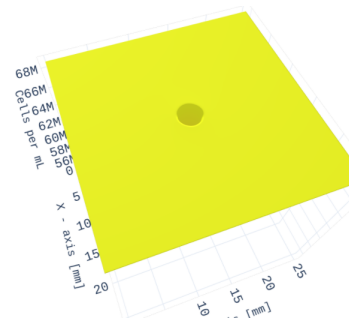
(b) Model - DNA concentrations.

Phage in model of box B at 15 hours and 30 minutes



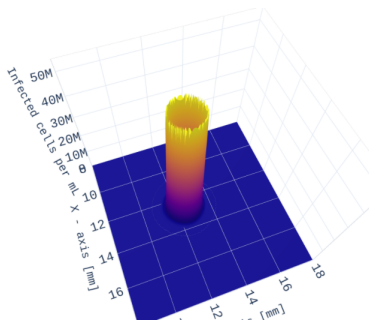
(c) Model - Phage concentration.

Bacteria in model of box B at 15 hours and 30 minutes



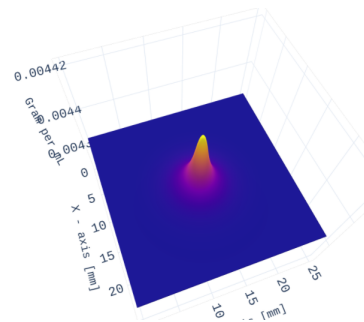
(d) Model - Bacteria concentration.

Infected in model of box B at 15 hours and 30 minutes



(e) Model - Infected bac. concentration.

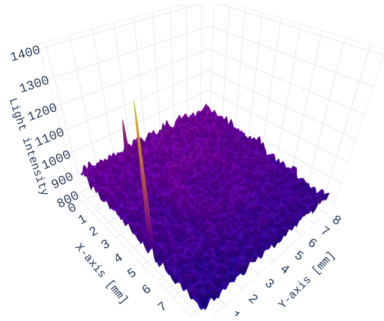
Nutrient in model of box B at 15 hours and 30 minutes



(f) Model - Nutrient concentration.

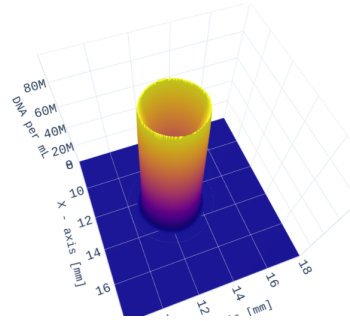
Figure 29: Experimental data in box B at 16 hours, compared to the model.

Box B at picture 238



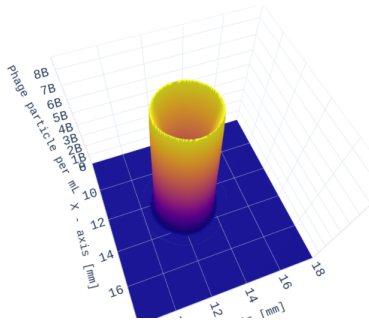
(a) Experimental result.

DNA in model of box B at 23 hours and 18 minutes



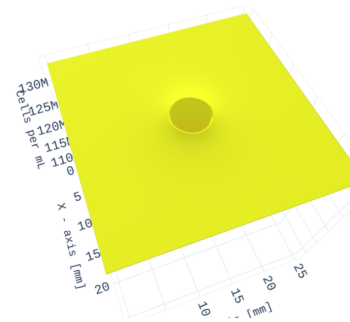
(b) Model - DNA concentration.

Phage in model of box B at 23 hours and 18 minutes



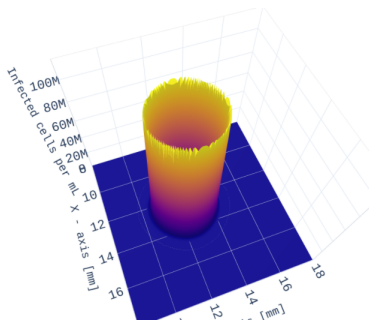
(c) Model - Phage concentration.

Bacteria in model of box B at 23 hours and 18 minutes



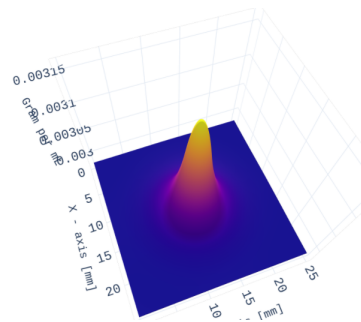
(d) Model - bacterial concentration.

Infected in model of box B at 23 hours and 18 minutes



(e) Model - Infected bac. concentration.

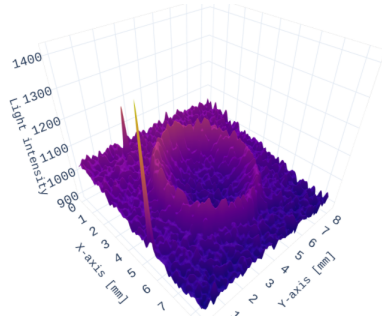
Nutrient in model of box B at 23 hours and 18 minutes



(f) Model - Nutrient concentration.

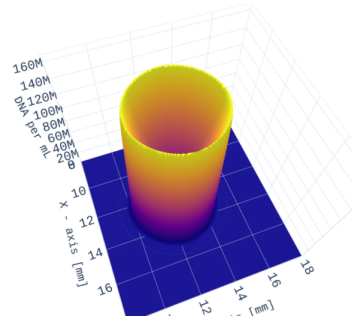
Figure 30: Experimental data in box B at 23 hours, 48 min compared to the model.

Box B at picture 316



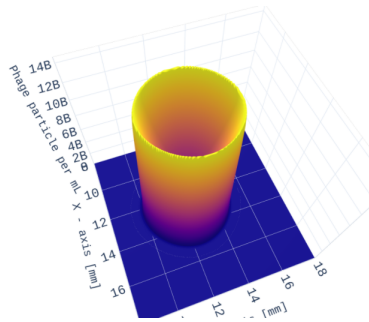
(a) Experimental result.

DNA in model of box B at 31 hours and 6 minutes



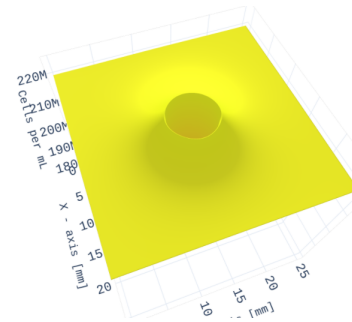
(b) Model - DNA concentration.

Phage in model of box B at 31 hours and 6 minutes



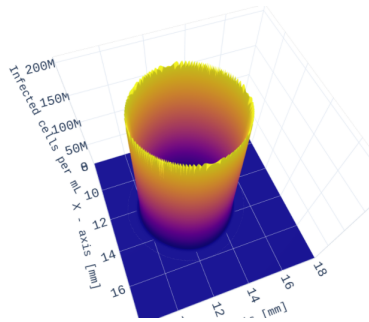
(c) Model - Phage concentration.

Bacteria in model of box B at 31 hours and 6 minutes



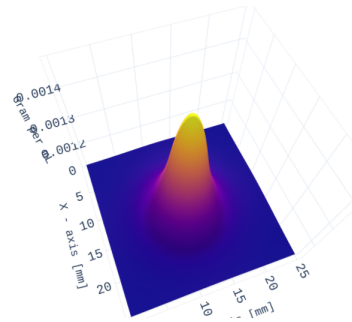
(d) Model - Bacterial concentration.

Infected in model of box B at 31 hours and 6 minutes



(e) Model - Infected bac. concentration.

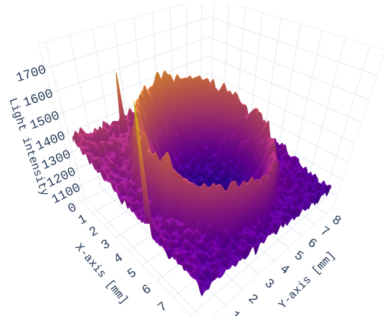
Nutrient in model of box B at 31 hours and 6 minutes



(f) Model - Nutrient concentration.

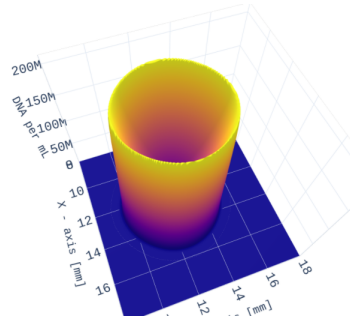
Figure 31: Experimental data in box B at 31 hours, 36 min compared to the model.

Box B at picture 394



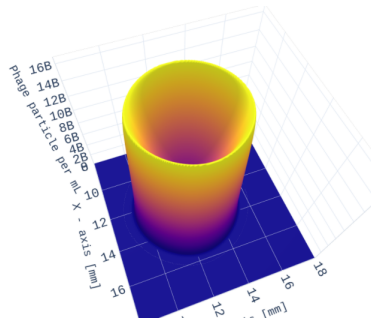
(a) Experimental result.

DNA in model of box B at 38 hours and 51 minutes



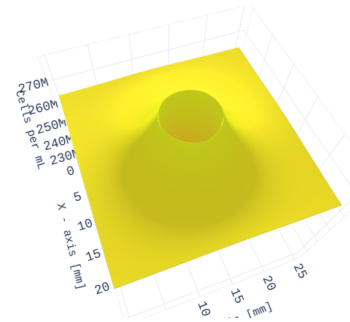
(b) Model - DNA concentration.

Phage in model of box B at 38 hours and 51 minutes



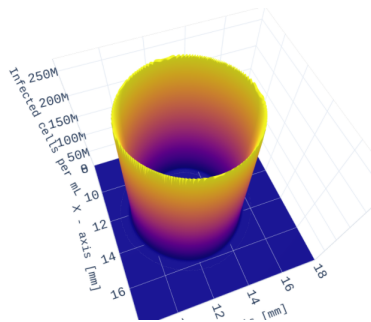
(c) Model - Phage concentration.

Bacteria in model of box B at 38 hours and 51 minutes



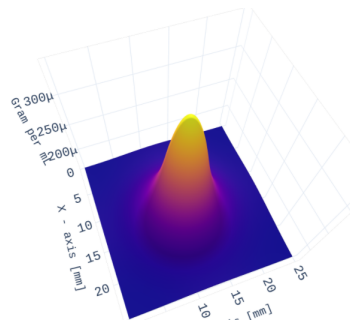
(d) Model - Bacterial concentration.

Infected in model of box B at 38 hours and 51 minutes



(e) Model - Infected bac. concentration.

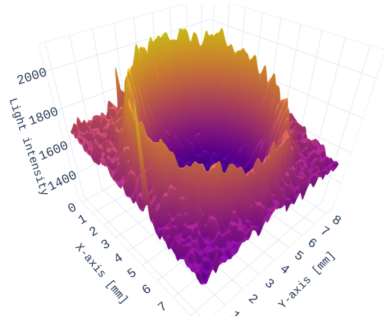
Nutrient in model of box B at 38 hours and 51 minutes



(f) Model - Nutrient concentration.

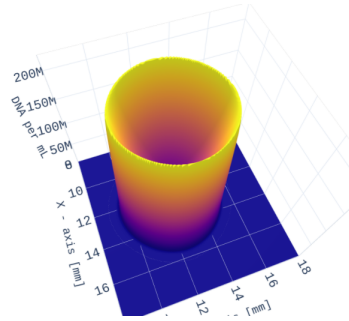
Figure 32: Experimental data in box B at 39 hours, 24 min compared to the model.

Box B at picture 472



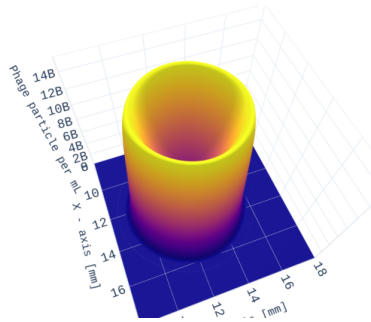
(a) Experimental result.

DNA in model of box B at 46 hours and 39 minutes



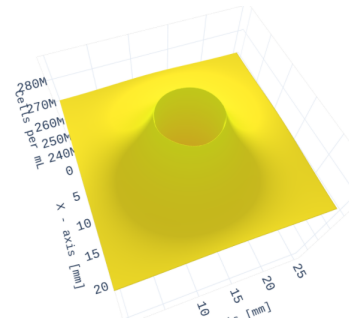
(b) Model - DNA concentration.

Phage in model of box B at 46 hours and 39 minutes



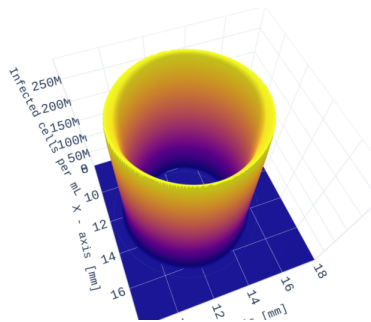
(c) Model - Phage concentration.

Bacteria in model of box B at 46 hours and 39 minutes



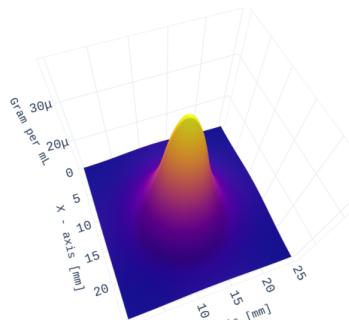
(d) Model - Bacterial concentration.

Infected in model of box B at 46 hours and 39 minutes



(e) Model - Infected bac. concentration.

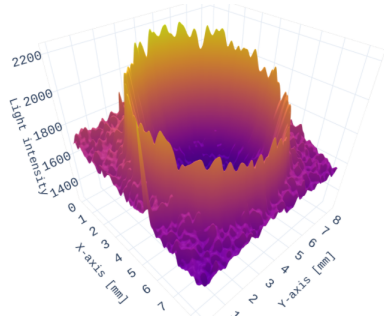
Nutrient in model of box B at 46 hours and 39 minutes



(f) Model - Nutrient concentration.

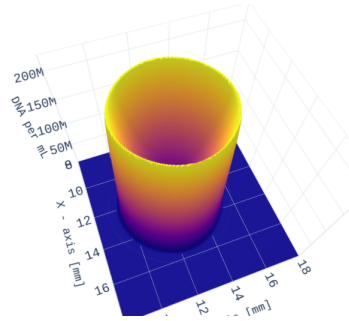
Figure 33: Experimental data in box B at 47 hours, 12 min compared to the model.

Box B at picture 550



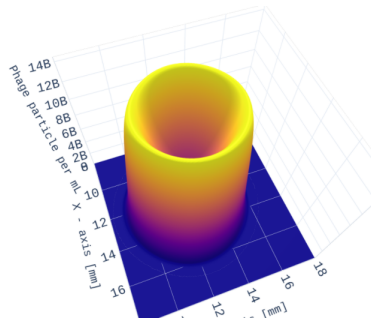
(a) Experimental result.

DNA in model of box B at 54 hours and 27 minutes



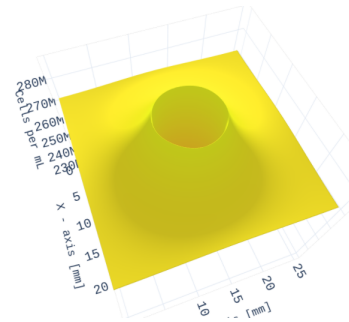
(b) Model - DNA concentration.

Phage in model of box B at 54 hours and 27 minutes



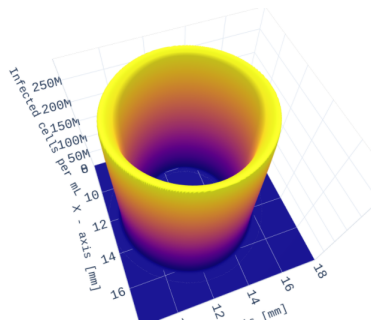
(c) Model - Phage concentration.

Bacteria in model of box B at 54 hours and 27 minutes



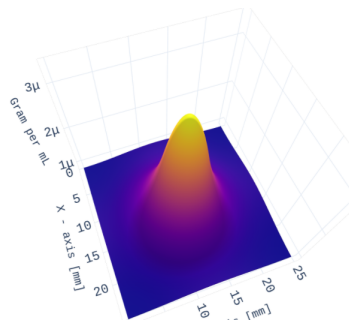
(d) Model - Bacterial concentration.

Infected in model of box B at 54 hours and 27 minutes



(e) Model - Infected bac. concentration.

Nutrient in model of box B at 54 hours and 27 minutes



(f) Model - Nutrient concentration.

Figure 34: Experimental data in box B at 55 hours, 48 min compared to the model.

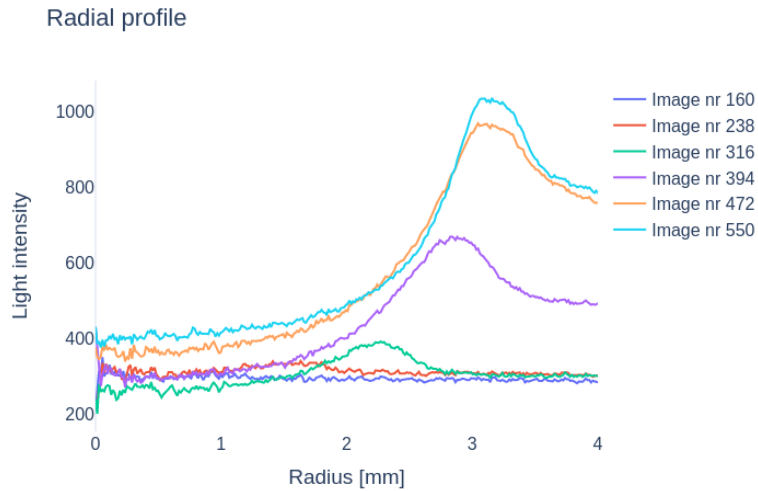


Figure 35: Radial profile of plaque in box B in the experimental result found by calculating the radial average.

A couple of immediate observations can be done by studying the results presented in figure 29 to 34 related the experimental results and the theoretical results from the model. The experimental results, which is supposed to measure the concentration of free DNA in the petri dish, and the models level of free DNA do indeed look alike. Both have a distinct hemisphere and both have notches. The hemisphere is an emergent property of the bacteria growing at the same time as the plaque expands. Since the Cellfiebooth measures the fluorescence of free DNA, the measurements are directly related to the concentration of lysed bacteria. In the early stages of plaque expansion, the immediate bacterial concentration is low and thus the amount of DNA released into the petri dish is low as well. As the plaque expands over time through cycles of infection and diffusion of phages, the bacterial concentration rises and there are more bacteria to lyse and thus more DNA is released. Another interesting observation is that the bacteria surrounding plaques are thriving and outgrowing the bacteria further from the plaques. This is due to diffusion of nutrient. There are no bacteria left alive in the middle of the plaques, and therefore no one left to consume the nutrient. The surrounding bacteria consume the nutrient immediately available to them, which causes a lower concentration i so the nutrient naturally diffuse from places of high concentration to the surrounding places of low concentration, which is outside the plaques where the bacteria has consumed nutrients. Due to this dynamic, the bacteria thrive by "living on the edge" of the plaques. The phage concentration has a similar shape as the DNA, but the edge of the hemisphere is shaped inwards. This is due to the diffusion of phages. The infected bacteria have a shape of hollowed out cylinder.

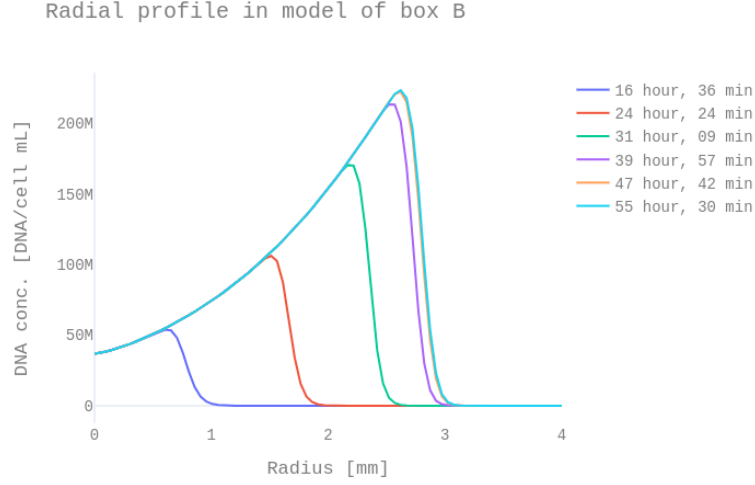


Figure 36: Radial profile for the theoretical results.

The notches observed in the experimental results are most likely data noise. The experimental data is treated with a Gaussian filter with $\sigma = 5$. A higher sigma or more precise measuring device would likely eliminate these notches. The notches in the model can be seen on the edges in infected bacteria, phage and DNA concentrations. These notches are a result of the spatial step-sizes being too large. A lower step-size would eliminate these notches, but also rise the modelling time exponentially.

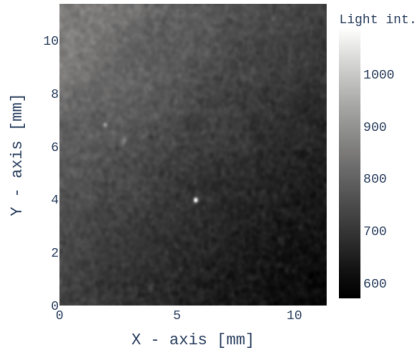
Another thing we can see from the experimental results is that the "base" level of light intensity rises as time progresses. This can be observed in all plaques found through the Cellfiebooth. We would expect this rise in the bacterial lawn, but the centre of the plaque, where there is no growth, rises as well. This is most likely a general light noise due to the light scattering from the bacteria. I believe this because I found the rise of light intensity in the plaque and bacterial lawn to behave linearly. This linearity, shown in equation 25, was taken into account when I calculated the radial profile of the plaque, shown in figure 35, and in all following radial profiles of plaques found experimentally.

$$x_{plaque} = x_{bacterial} \cdot 0.6468 \quad (25)$$

The radial profile of the experimental results, in figure 35, corresponds well with the radial profile of the theoretical results shown in figure 36. The DNA concentration in the model can be read as number of bacteria lysed by phages, while the experimental values are light intensity from free DNA

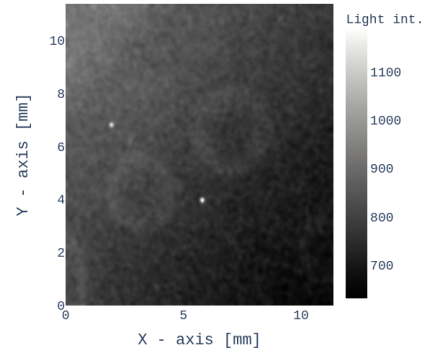
fluorescing and bacterial scattering, so the values are not completely comparable, but how they change are. The shape of the curve, the relative end point and the end size of the plaques are very similar. Both plaques end up having a radius of roughly 3 mm. The early peaks in the experimental data are further along than the peaks in the theoretical data, but it is hard to say if it is bacterial scattering that is causing these early peaks or if all peaks are due to fluorescence of free DNA.

Box A at picture 160



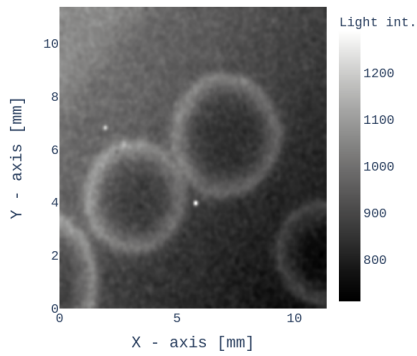
(a) 16 hours

Box A at picture 238



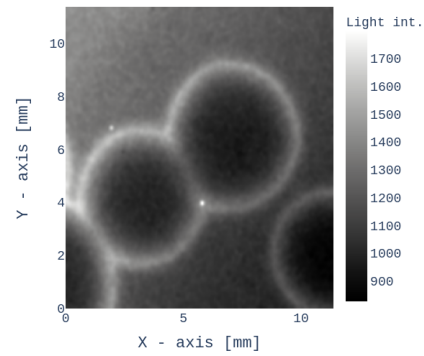
(b) 23 hours, 48 min

Box A at picture 316



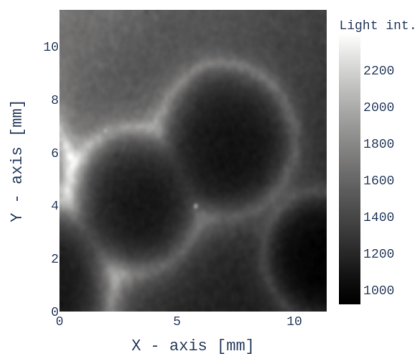
(c) 31 hours, 36 min

Box A at picture 394



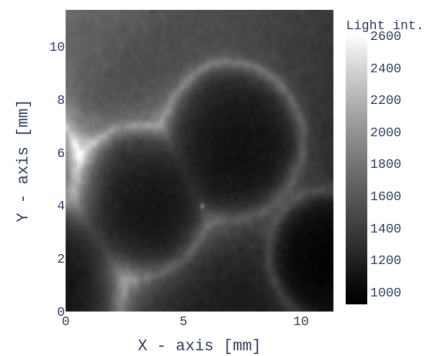
(d) 39 hours, 24 min

Box A at picture 472



(e) 47 hours, 12 min

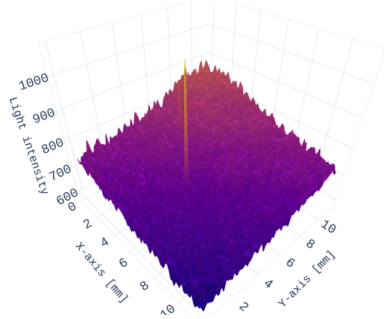
Box A at picture 550



(f) 55 hours

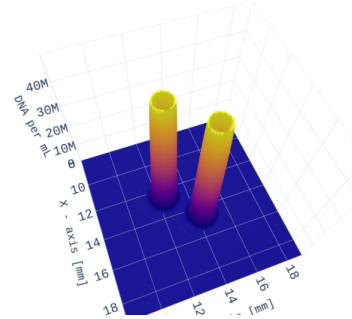
Figure 37: Closer look at the data from box A in figure 27 presented in a grayscale heatmap. The data were treated with a Gaussian filter with $\sigma = 5$.

Box A at picture 160



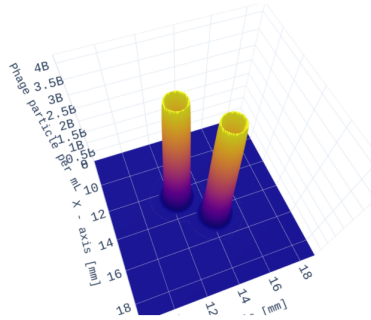
(a) Experimental result.

DNA in model of box A at 15 hours and 30 minutes



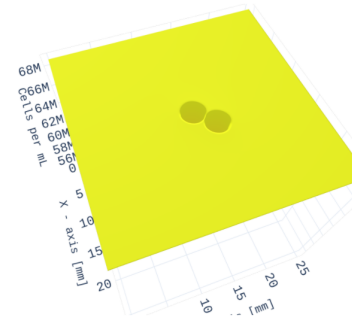
(b) Model - DNA concentration.

Phage in model of box A at 15 hours and 30 minutes



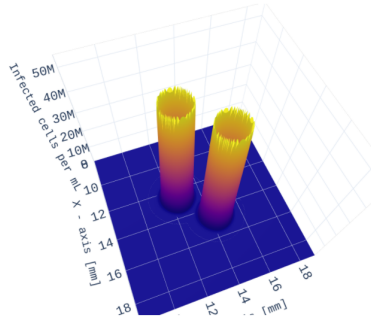
(c) Model - Phage concentration

Bacteria in model of box A at 15 hours and 30 minutes



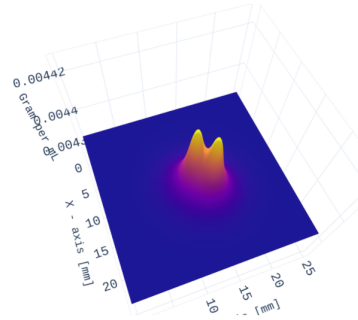
(d) Model - Bacteria concentration.

Infected in model of box A at 15 hours and 30 minutes



(e) Model - Infected bac. concentration.

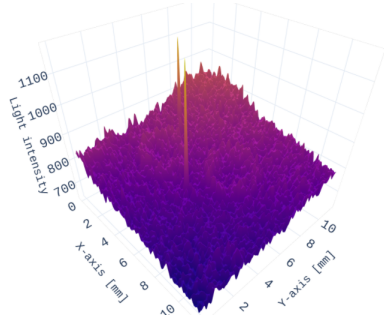
Nutrient in model of box A at 15 hours and 30 minutes



(f) Model - Nutrient concentration.

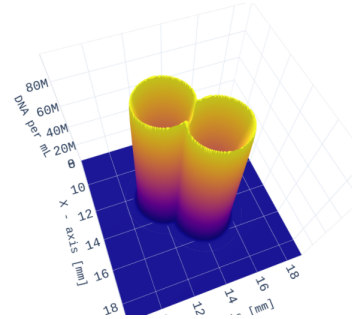
Figure 38: Experimental data in box A at 16 hours, compared to the model.

Box A at picture 238



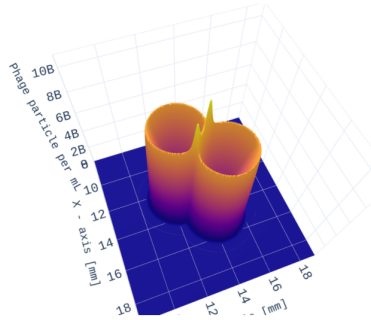
(a) Experimental result.

DNA in model of box A at 23 hours and 18 minutes



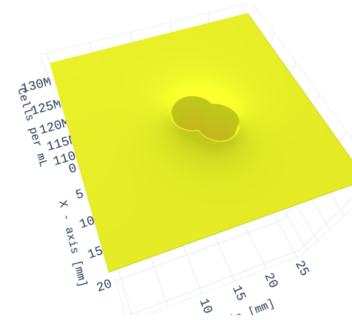
(b) Model - DNA concentration.

Phage in model of box A at 23 hours and 18 minutes



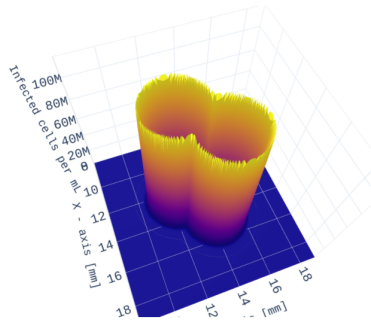
(c) Model - Phage concentration

Bacteria in model of box A at 23 hours and 18 minutes



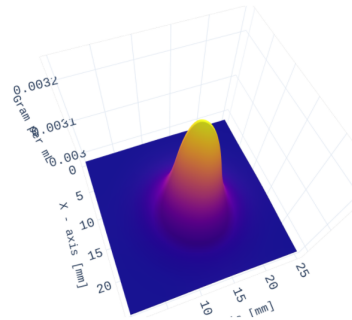
(d) Model - Bacteria concentration.

Infected in model of box A at 23 hours and 18 minutes



(e) Model - Infected bac. concentration.

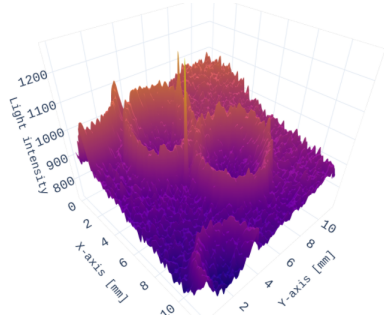
Nutrient in model of box A at 23 hours and 18 minutes



(f) Model - Nutrient concentration.

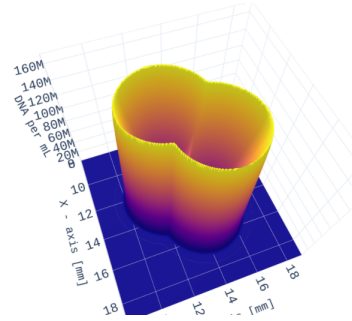
Figure 39: Experimental data in box A at 23 hours and 48 min, compared to the model.

Box A at picture 316



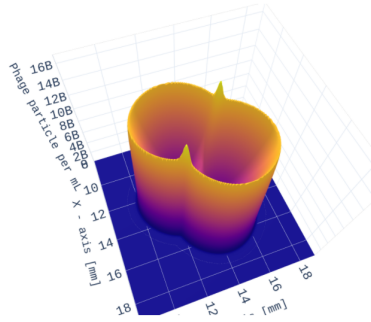
(a) Experimental result.

DNA in model of box A at 31 hours and 6 minutes



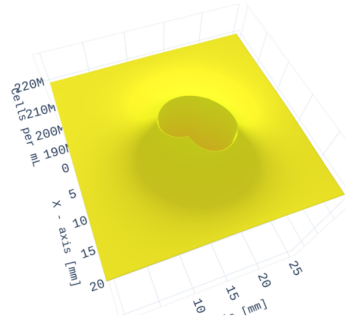
(b) Model - DNA concentration.

Phage in model of box A at 31 hours and 6 minutes



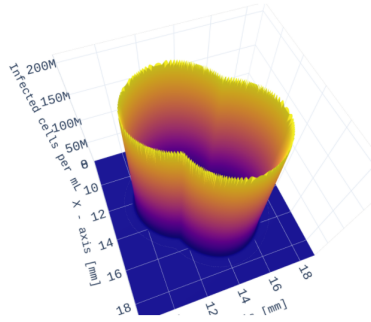
(c) Model - Phage concentration

Bacteria in model of box A at 31 hours and 6 minutes



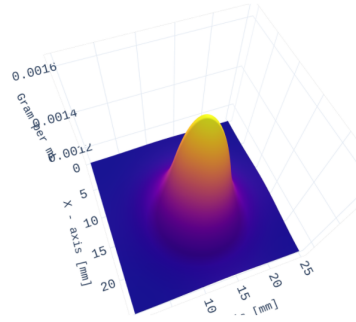
(d) Model - Bacteria concentration.

Infected in model of box A at 31 hours and 6 minutes



(e) Model - Infected bac. concentration.

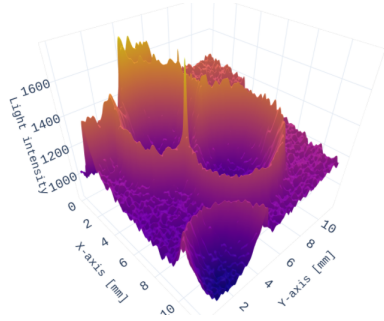
Nutrient in model of box A at 31 hours and 6 minutes



(f) Model - Nutrient concentration.

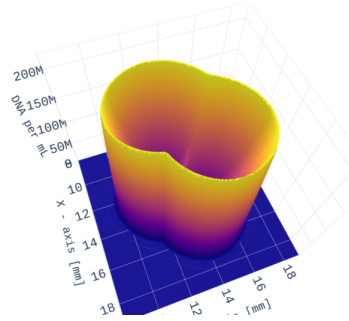
Figure 40: Experimental data in box A at 31 hours and 36 min, compared to the model.

Box A at picture 394



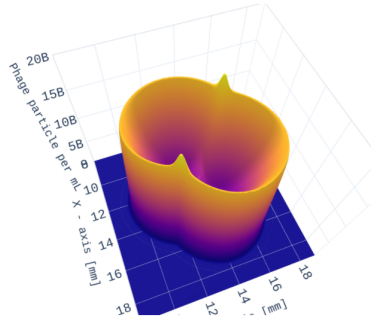
(a) Experimental result.

DNA in model of box A at 38 hours and 51 minutes



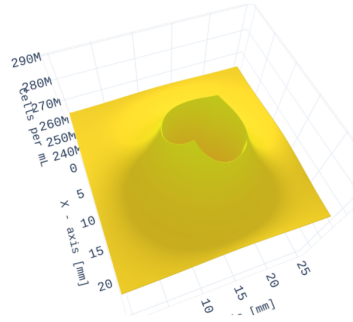
(b) Model - DNA concentration.

Phage in model of box A at 38 hours and 51 minutes



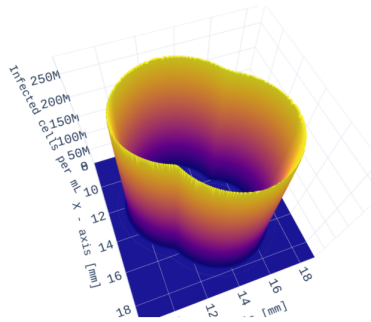
(c) Model - Phage concentration

Bacteria in model of box A at 38 hours and 51 minutes



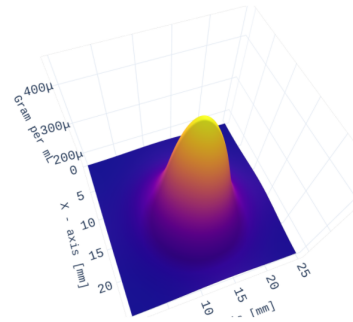
(d) Model - Bacteria concentration.

Infected in model of box A at 38 hours and 51 minutes



(e) Model - Infected bac. concentration.

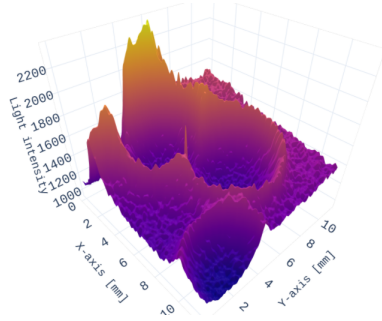
Nutrient in model of box A at 38 hours and 51 minutes



(f) Model - Nutrient concentration.

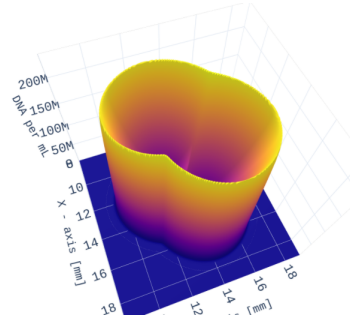
Figure 41: Experimental data in box A at 39 hours 24 min, compared to the model.

Box A at picture 472



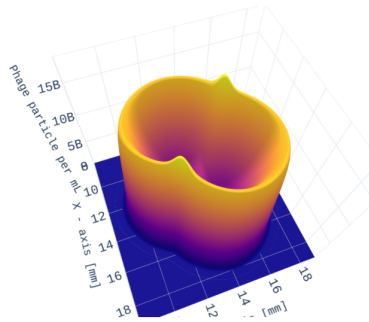
(a) Experimental result.

DNA in model of box A at 46 hours and 39 minutes



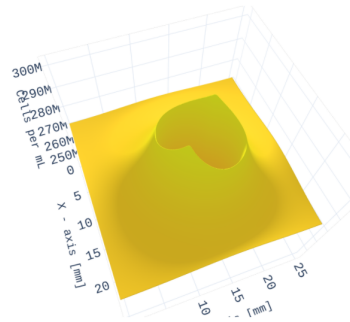
(b) Model - DNA concentration.

Phage in model of box A at 46 hours and 39 minutes



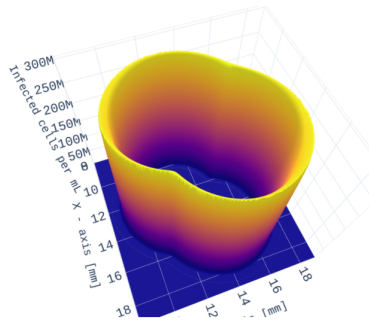
(c) Model - Phage concentration

Bacteria in model of box A at 46 hours and 39 minutes



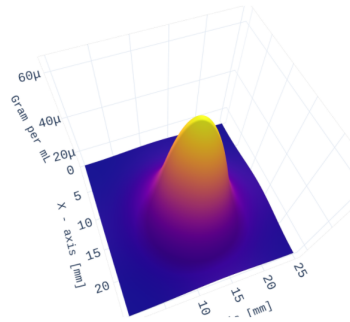
(d) Model - Bacteria concentration.

Infected in model of box A at 46 hours and 39 minutes



(e) Model - Infected bac. concentration.

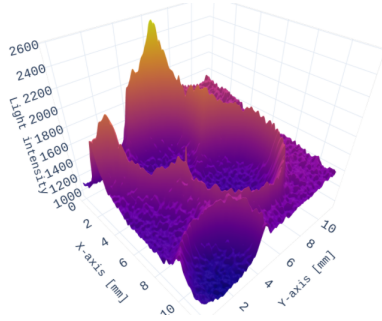
Nutrient in model of box A at 46 hours and 39 minutes



(f) Model - Nutrient concentration.

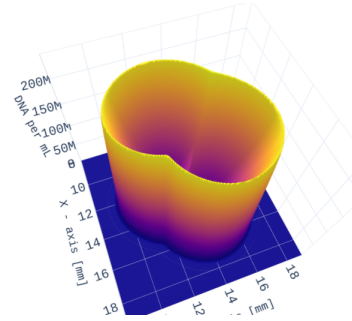
Figure 42: Experimental data in box A at 46 hours and 36 min, compared to the model.

Box A at picture 550



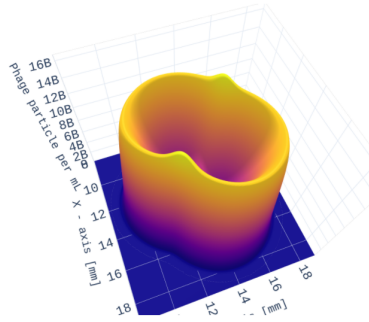
(a) Experimental result.

DNA in model of box A at 54 hours and 27 minutes



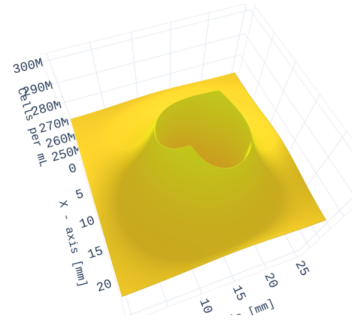
(b) Model - DNA concentration.

Phage in model of box A at 54 hours and 27 minutes



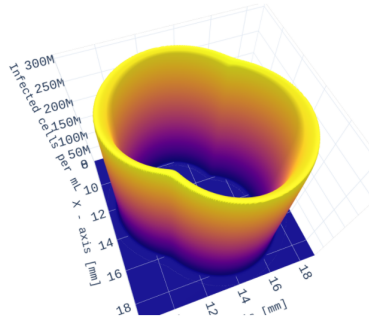
(c) Model - Phage concentration

Bacteria in model of box A at 54 hours and 27 minutes



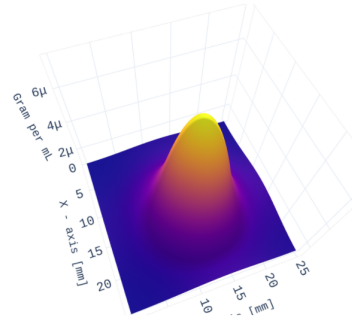
(d) Model - Bacteria concentration.

Infected in model of box A at 54 hours and 27 minutes



(e) Model - Infected bac. concentration.

Nutrient in model of box A at 54 hours and 27 minutes



(f) Model - Nutrient concentration.

Figure 43: Experimental data in box A at 55 hours, compared to the model.

The plaques were first modelled by having the seeding points for the two different phages the same distance from each other as the distance from the centre to the two plaques in the experimental run. This did not yield the desired results as the two plaques never met in the model. Instead the distance between the seeding points were halved. This did yield the desired result, but the model can not be read as literally as the previous one could be. The biggest difference is that the timing for when the plaques meet is not relevant, while the general behaviour, dynamic, and phenomena that occurs is still highly relevant.

The effects related to the diffusion of nutrient that we observed in the model of box B are even more prevalent in the model of box A. This makes sense as we are dealing with two expanding plaques in close vicinity of each other. As the plaques expand, the bacteria between the plaques will thrive and grow faster than other bacteria. This is because the bacteria will have a greater access to nutrient, since it will experience an influx of nutrient diffusing from the plaques on both side as well as the the nutrient that is already immediately available. As the plaques start to merge, the bacteria in the emergent "valley" have two sources where nutrient diffuse from. Now it is the bacteria in these valleys that outgrow the rest of the surrounding bacteria. Again due their greater access to nutrients. Due to this, we can see a line between the intersectional points where the plaques overlap, which contains an higher concentration of DNA, because it used to contain a higher concentration of bacteria at the time the phages reached the point. I believe this effect is the reason why many merging plaques don't seem to merge completely, but rather look like two bubbles pressed together without merging or bursting. The emergence of this bubble pressing effect is apparent in both the experimental results in figure 37, and the model in figure 43b.

4.4.2 Experimental run 1.2 with DH5 α

These data were generated with the Cellfiebooth improvements described in section 3.2.3. 1000 images were captured with six minutes between each photograph in the run. The six photographs presented in figure 45 range from photo 90 to 900, where photo 90 is the first photo in which traces of the plaques can be observed. At 900 the plaques have stopped expanding. A number of plaques appear in the Petri dish, and two sections were studied closer and modelled. These sections are shown as box C and box D in figure 45f.

The graph in figure 44 illustrates the change in light intensity measured in a patch of bacterial lawn not affected by the plaques. This gives us an estimate of the growth curve of the bacteria. This growth deviates slightly from the typical Monod kinetics. The bacteria seem to slow down after about 30 hours, before they speed up again, reaching approximately previous growth rate. This sort of growth behaviour is typical for microorganisms that change the main carbon source during growth. The only carbon sources available in the Petri dish are glucose and casamino acids, but the concentration of these nutrients should be equal throughout the Petri dish. The only thing differing this experimental run from run 1.1 in section 4.4.1, is the initial bacterial concentration.

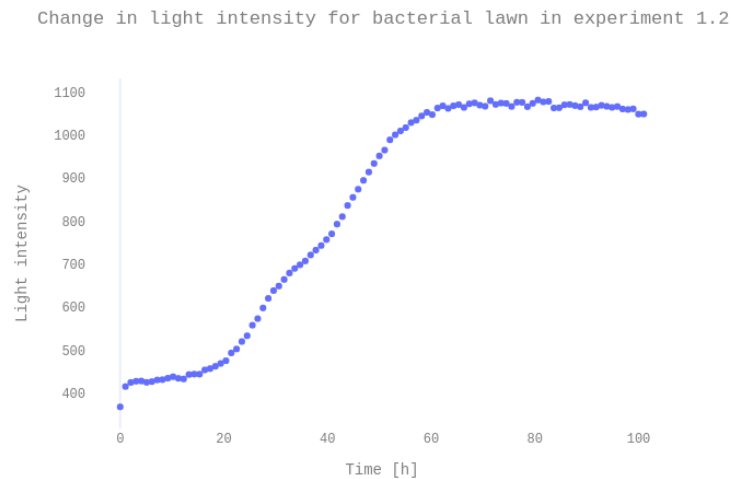


Figure 44: Change in light intensity over time in the bacterial lawn in experiment 1.2.

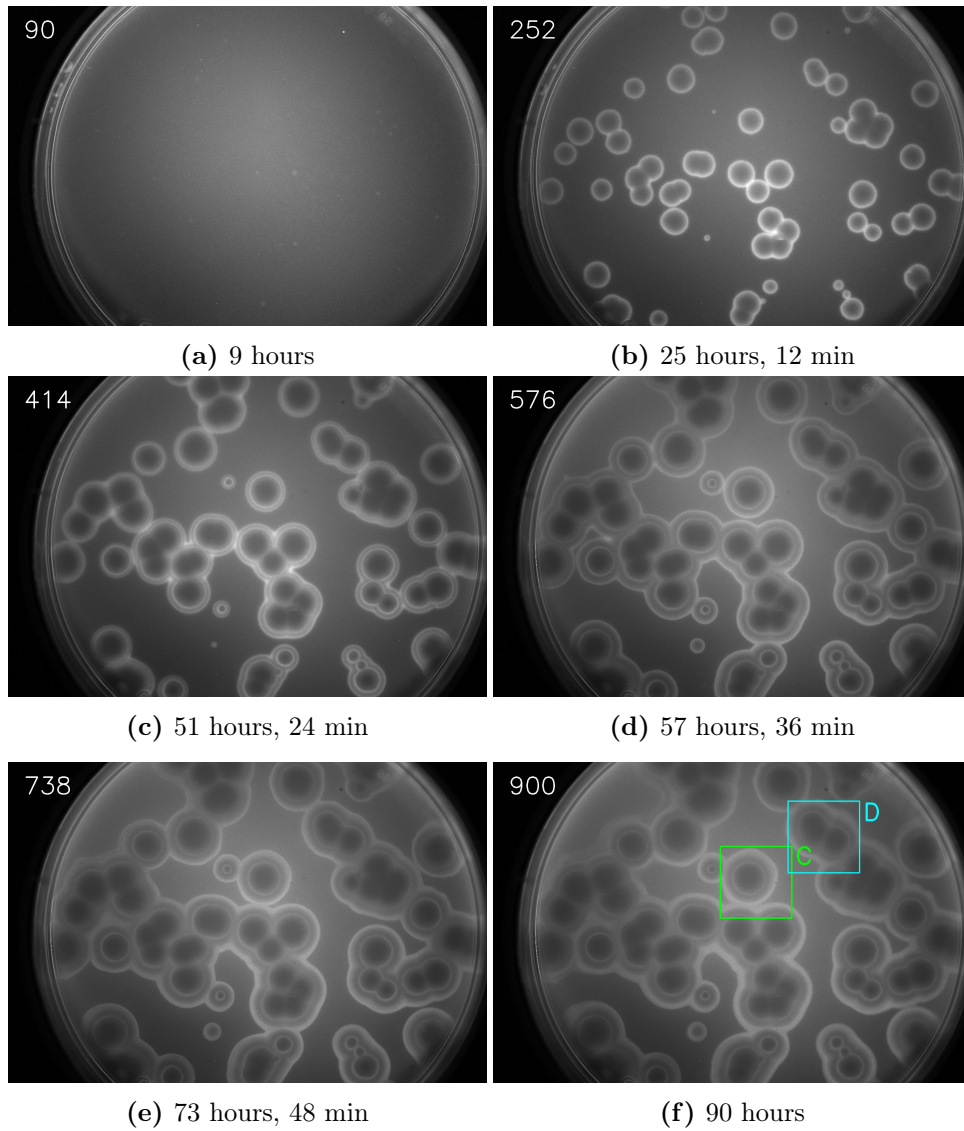
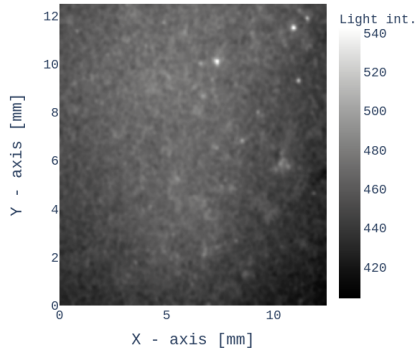


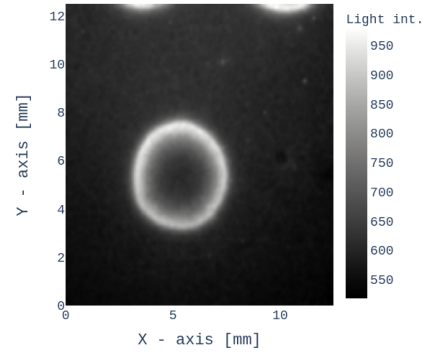
Figure 45: DH5 α with initial $OD_{600} = 0.333$. The number in the series is given in the left corner of the image. Six minutes between each number. The plaques in box C and D are studied closer

Box C at picture 90



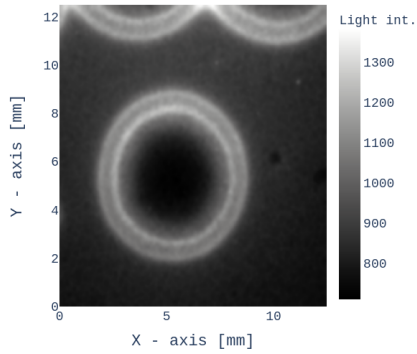
(a) 9

Box C at picture 252



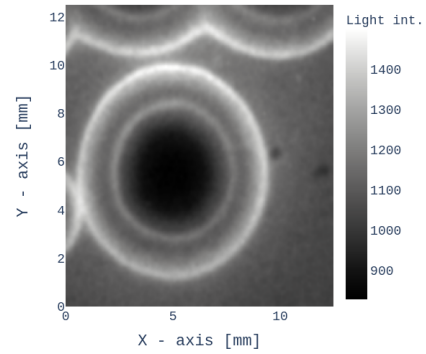
(b) 25 hours, 12 min

Box C at picture 414



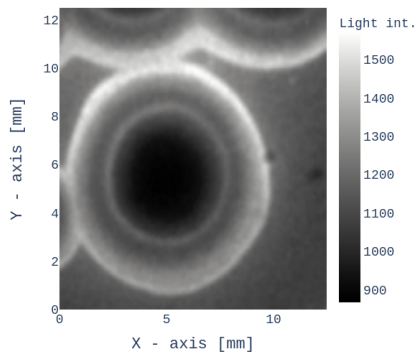
(c) 41 hours, 24 min

Box C at picture 576



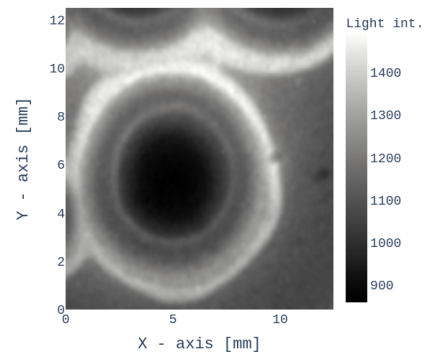
(d) 57 hours, 36 min

Box C at picture 738



(e) 73 hours, 48 min

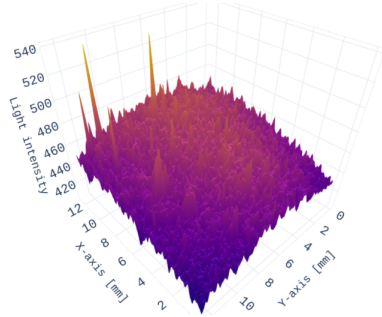
Box C at picture 900



(f) 90 hours

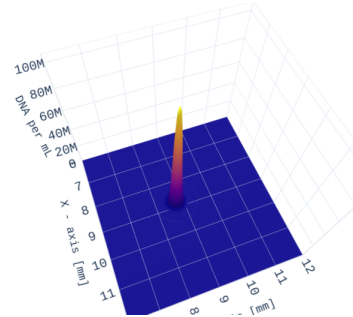
Figure 46: Closer look at the data from box C in figure 45 presented in a grayscale heatmap. The data were treated with a Gaussian filter with $\sigma = 5$.

Box C at picture 90



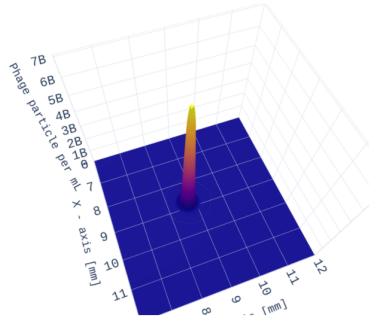
(a) Experimental result.

DNA in model of box C at 9 hours and 54 minutes



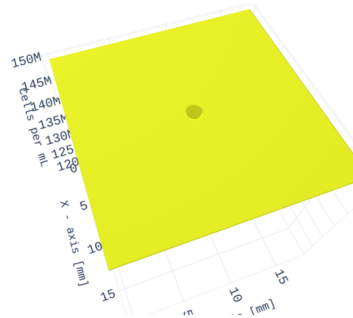
(b) Model - DNA concentration.

Phage in model of box C at 9 hours and 54 minutes



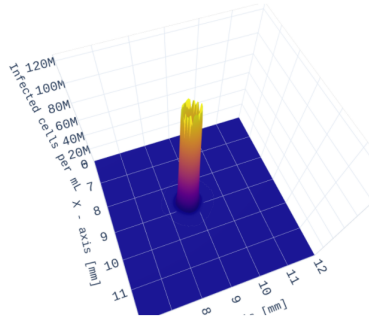
(c) Model - Phage concentration

Bacteria in model of box C at 9 hours and 54 minutes



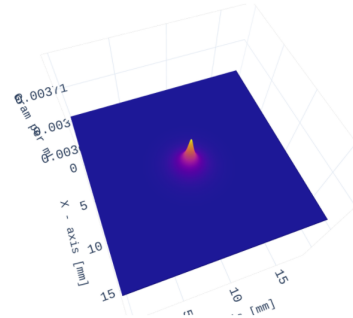
(d) Model - Bacteria concentration.

Infected in model of box C at 9 hours and 54 minutes



(e) Model - Infected bac. concentration.

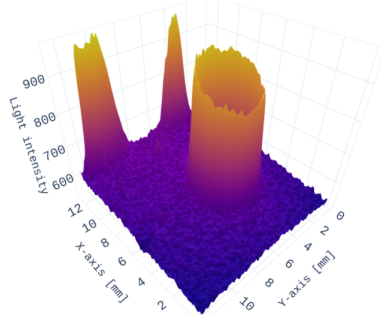
Nutrient in model of box C at 9 hours and 54 minutes



(f) Model - Nutrient concentration.

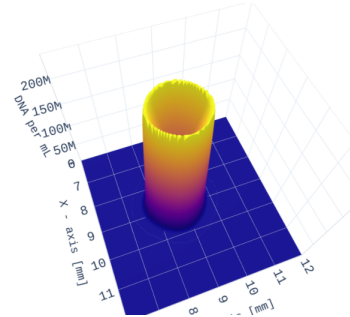
Figure 47: Experimental data in box C at 9 hours, compared to the model.

Box C at picture 252



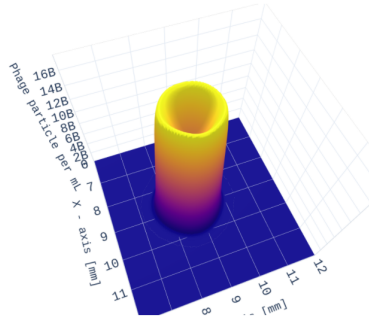
(a) Experimental result.

DNA in model of box C at 25 hours and 30 minutes



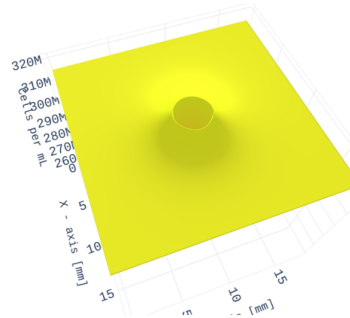
(b) Model - DNA concentration.

Phage in model of box C at 25 hours and 30 minutes



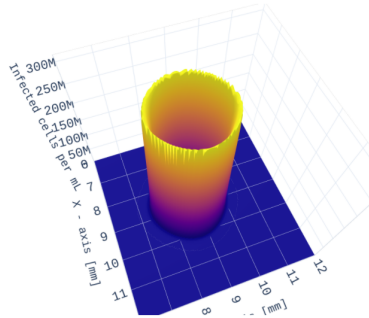
(c) Model - Phage concentration

Bacteria in model of box C at 25 hours and 30 minutes



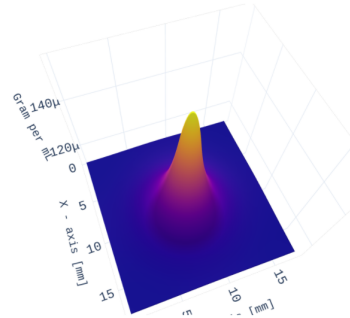
(d) Model - Bacteria concentration.

Infected in model of box C at 25 hours and 30 minutes



(e) Model - Infected bac. concentration.

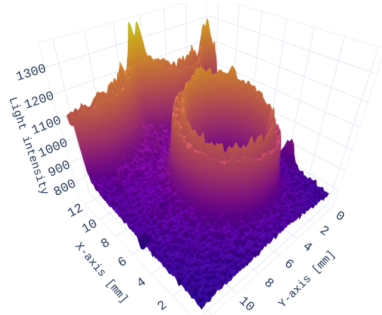
Nutrient in model of box C at 25 hours and 30 minutes



(f) Model - Nutrient concentration.

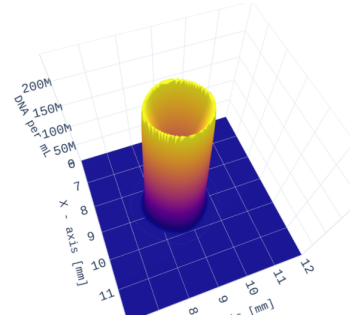
Figure 48: Experimental data in box C at 25 hours and 12 min, compared to the model.

Box C at picture 414



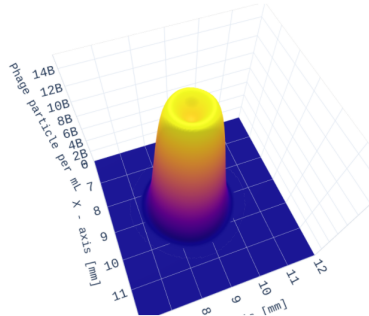
(a) Experimental result.

DNA in model of box C at 41 hours and 9 minutes



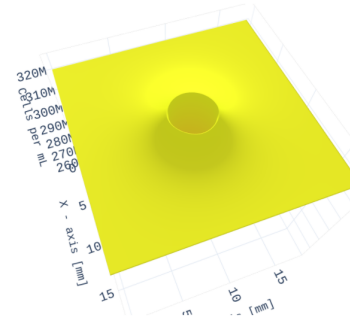
(b) Model - DNA concentration.

Phage in model of box C at 41 hours and 9 minutes



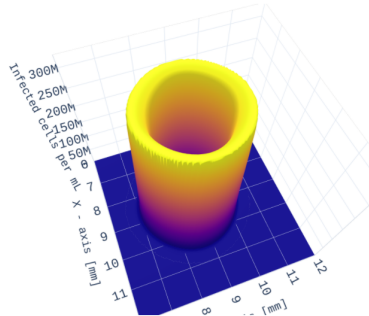
(c) Model - Phage concentration

Bacteria in model of box C at 41 hours and 9 minutes



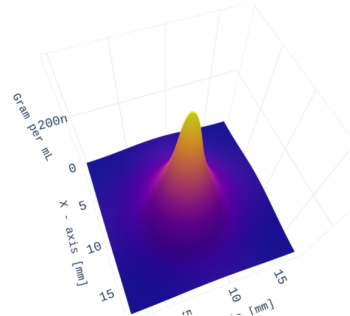
(d) Model - Bacteria concentration.

Infected in model of box C at 41 hours and 9 minutes



(e) Model - Infected bac. concentration.

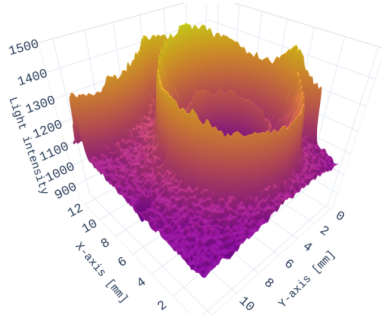
Nutrient in model of box C at 41 hours and 9 minutes



(f) Model - Nutrient concentration.

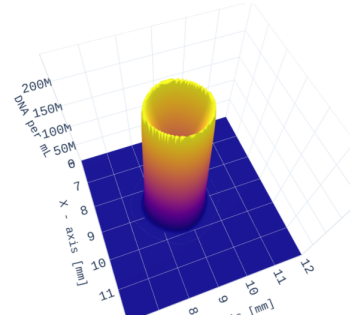
Figure 49: Experimental data in box C at 41 hours and 24 min, compared to the model.

Box C at picture 576



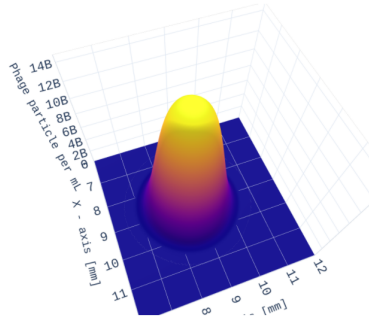
(a) Experimental result.

DNA in model of box C at 57 hours and 45 minutes



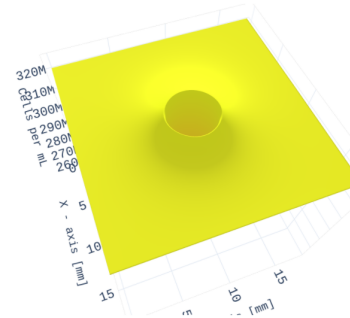
(b) Model - DNA concentration.

Phage in model of box C at 57 hours and 45 minutes



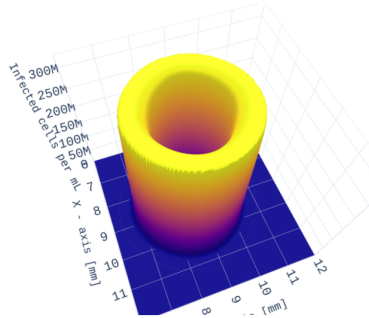
(c) Model - Phage concentration

Bacteria in model of box C at 57 hours and 45 minutes



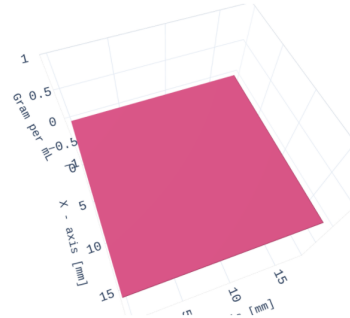
(d) Model - Bacteria concentration.

Infected in model of box C at 57 hours and 45 minutes



(e) Model - Infected bac. concentration.

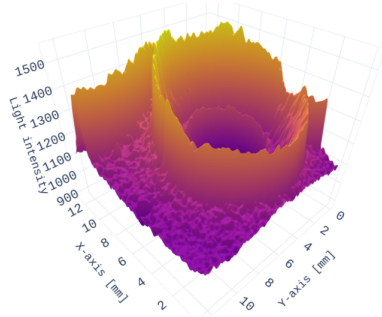
Nutrient in model of box C at 57 hours and 45 minutes



(f) Model - Nutrient concentration.

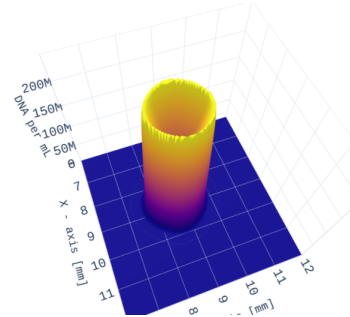
Figure 50: Experimental data in box C at 57 hours and 36 min, compared to the model.

Box C at picture 738



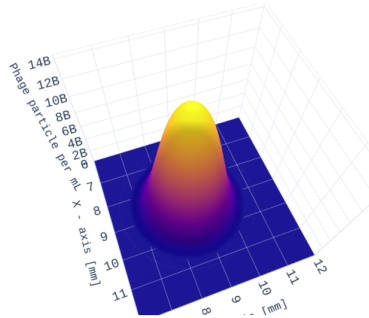
(a) Experimental result.

DNA in model of box C at 74 hours and 24 minutes



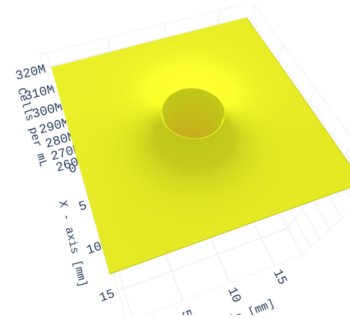
(b) Model - DNA concentration.

Phage in model of box C at 74 hours and 24 minutes



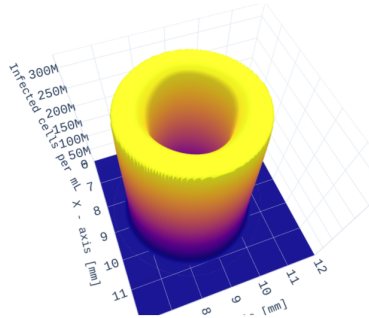
(c) Model - Phage concentration

Bacteria in model of box C at 74 hours and 24 minutes



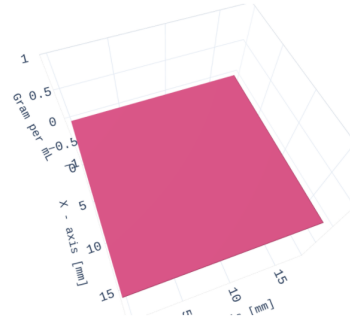
(d) Model - Bacteria concentration.

Infected in model of box C at 74 hours and 24 minutes



(e) Model - Infected bac. concentration.

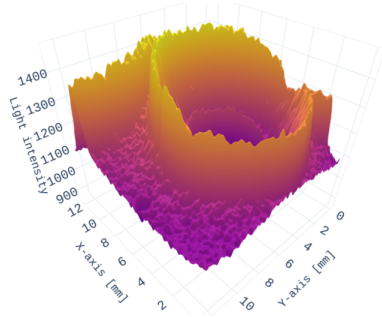
Nutrient in model of box C at 74 hours and 24 minutes



(f) Model - Nutrient concentration.

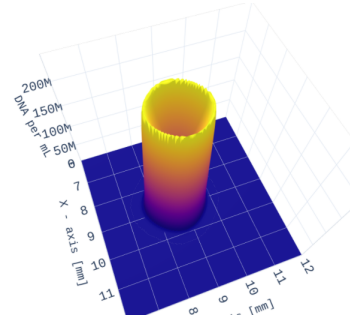
Figure 51: Experimental data in box C at 73 hours and 48 min, compared to the model.

Box C at picture 900



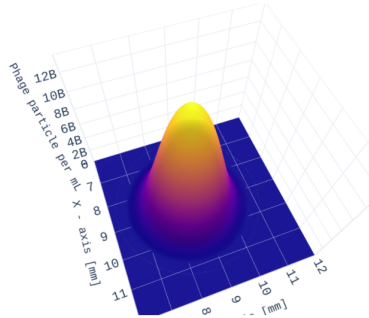
(a) Experimental result.

DNA in model of box C at 90 hours and 0 minutes



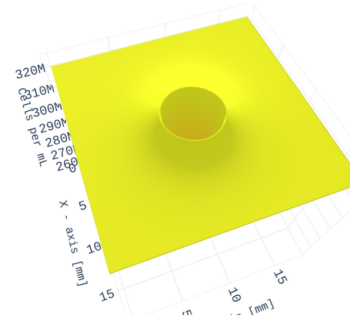
(b) Model - DNA concentration.

Phage in model of box C at 90 hours and 0 minutes



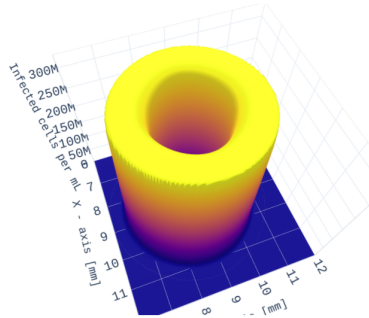
(c) Model - Phage concentration

Bacteria in model of box C at 90 hours and 0 minutes



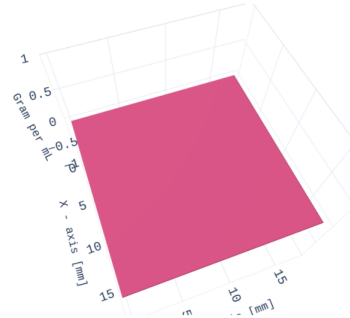
(d) Model - Bacteria concentration.

Infected in model of box C at 90 hours and 0 minutes



(e) Model - Infected bac. concentration.

Nutrient in model of box C at 90 hours and 0 minutes



(f) Model - Nutrient concentration.

Figure 52: Experimental data in box C at 90 hours, compared to the model.

The difference in initial bacterial concentration and the growth curve seem to have a huge impact on the plaque morphology. After about 40 hours the plaque formed a prominent ring, and a weaker ring started expanding beyond this ring. The formation of the prominent inner ring corresponds with the time of change in growth behaviour for the bacteria. It seems like something caused a change in the bacterial behaviour and this had a huge impact on the plaque morphology. The measurements from the bacterial lawn showed that the bacteria grew for considerably longer than expected. I would expect a discrepancy between the growth curve in the Cellfiebooth and the model as the bacterial growth rate used in the model is from measurements in bacteria growing in 28 °C, while the Cellfiebooth was kept at a steady 21 °C. This would cause the bacteria to grow slower, which again results in a longer period of time before the bacteria reaches a stationary growth phase. The discrepancy between the model and the experimental are, however, even larger than expected. The experimental results, shown in figure 44, show that the bacteria does not reach a stationary phase before 60 hours into the experiment. While the model predicted that even infected bacteria close to the plaque stopped maturing after 25 hours, which is shown in figure 55. The radial profile of the plaque is show in figure 53, and the radial profile predicted by the model is shown in figure 54. The experimental plaque radius ends up at ≈ 4.5 mm, while the plaque radius in the model ends up at ≈ 1.5 mm. I would also ask the reader to note the difference between this run and the previous run. The only parameter changed between this run and the previous one is that the initial bacterial concentration is $\approx 3.8x$ higher in this run. Yet the plaques continue to expand for 90 hours when the previous expanded for 55 hours, the end radius is ≈ 1.5 mm larger, which is a 50 % increase, and the plaque morphology is completely different, with a double ring where the previous had a single ring. What is going on here?

My hypothesis is that the bacteria is experiencing an influx of nutrients diffusing from the solid agar beneath the soft agar overlay. This vertical diffusion would affect all bacteria in the soft agar overlay equally and could explain the problems the model has had with predicting the progression in bacterial growth and plaque expansion. As already mentioned, the bacterial growth curve from figure 44 resembles that of a bacteria that changes growth tactic. I believe that the immediate available nutrient in the Petri dish starts to be exhausted about 40 hours inn, which causes the bacteria to initiate starvation related defence mechanisms. Diffusion is driven by change in concentration. And as the nutrient concentration at this point in time is considerably lower in the overlaying soft agar compared to the underlying agar, the nutrient will start to slowly diffuse upwards to the bacterial lawn. This influx of nutrient let the bacteria continue to grow, but is still so low that the bacteria will continue to be in "starvation" mode.

Many of the proteins related to the structure of *E. coli* DNA are highly de-

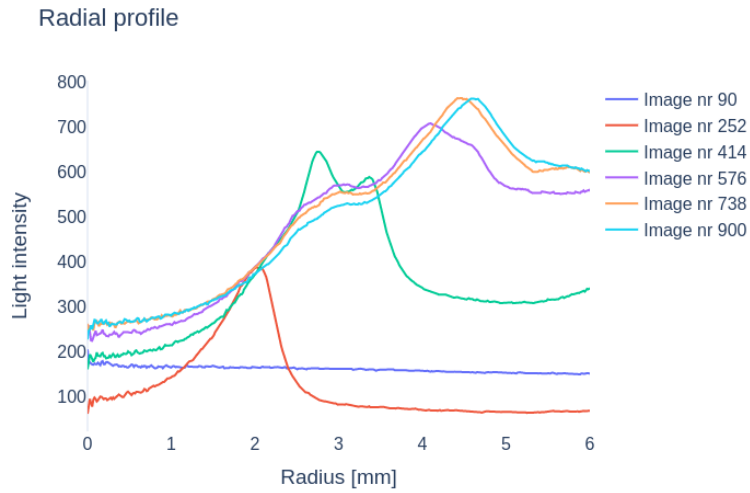


Figure 53: Radial profile of plaque in box C in the experimental result found by calculating the radial average. The radial profile for image nr. 414 show a clear double peak, and the following images show a saddle point where the first local maximum was measured.

pendent on the growth phase[104]. As the structure of the bacterial DNA changes, the affinity of GelGreen to create a dimer to this DNA could very well change as well. This would explain the double ring phenomena observed in this experimental run. We could look at the experimental result in figure 51a as some sort of historical document for the experiment. The light intensity corresponds to the number of bacteria infected and lysed by the phage. Moving radially outward from the centre of the plaque the intensity rises exponentially until we reach the inner ring, which shows the threshold where the available nutrient concentration was low enough to cause a starvation response in the bacteria. Moving outwards from this threshold again we the measured light intensity corresponds to the amount of lysed bacteria in starvation mode.

Radial profile in model of box c

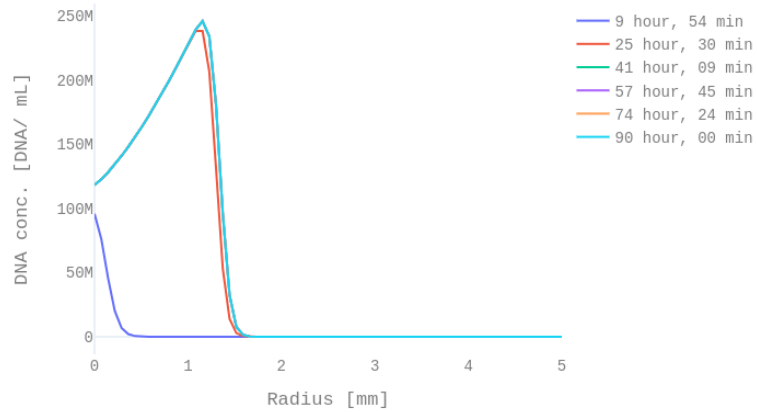


Figure 54: Radial profile of plaque in box C in the theoretical result. The model predicts that the plaque stops expanding completely after 25 hours, and little to no change happens past this point.

Radial profile in model of box c

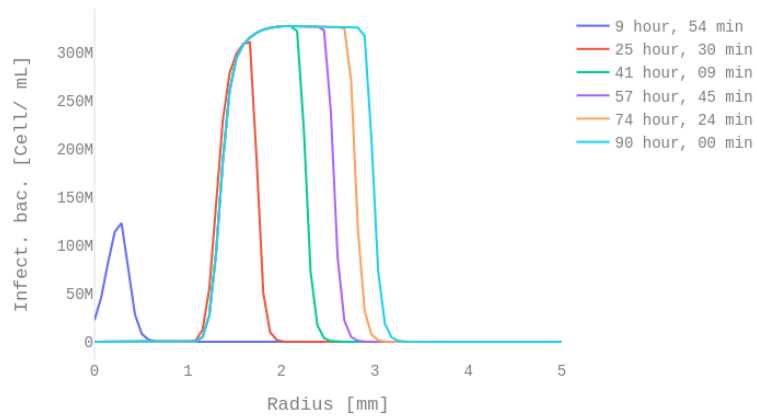
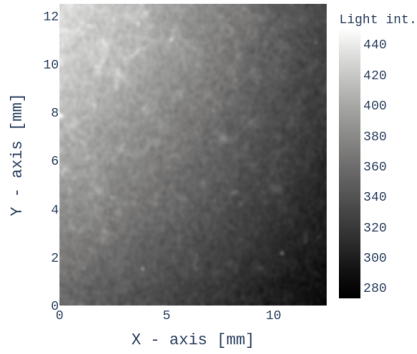


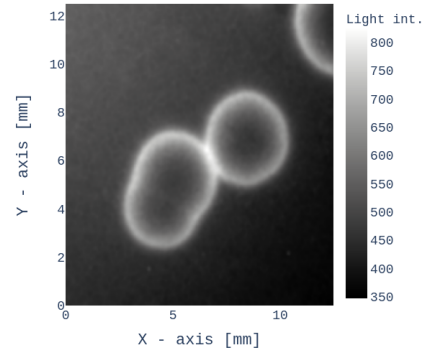
Figure 55: Radial profile of the infected bacteria in box C in the theoretical result. The model predicts that the bacteria continues to be infected, but as new phages are not produced and the amount of phages decrease for each bacteria that is infected the rate of expansion in infected bacteria decreases as well.

Box D at picture 90



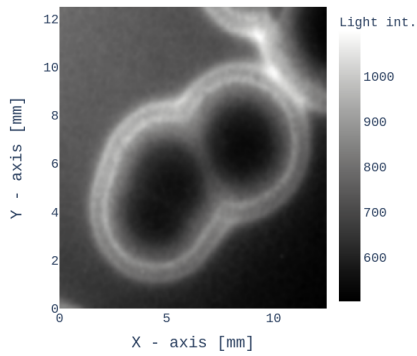
(a) 9 hours

Box D at picture 252



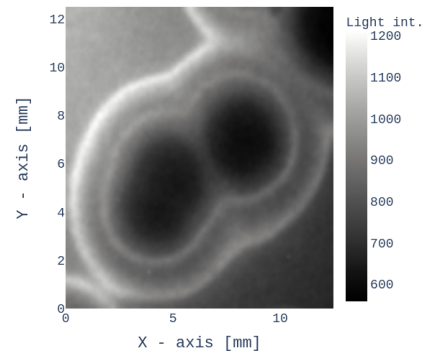
(b) 25 hours, 12 min

Box D at picture 414



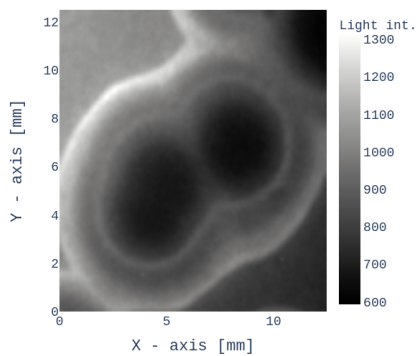
(c) 41 hours, 24 min

Box D at picture 576



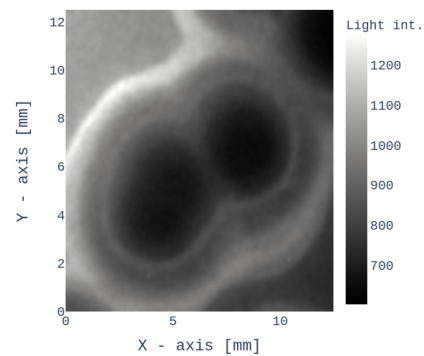
(d) 57 hours, 36 min

Box D at picture 738



(e) 73 hours, 48 min

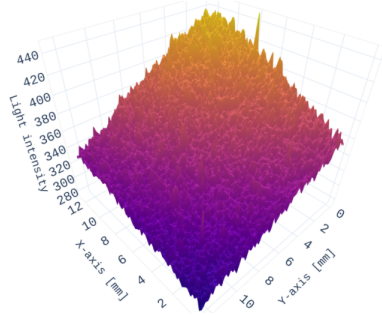
Box D at picture 900



(f) 90 hours

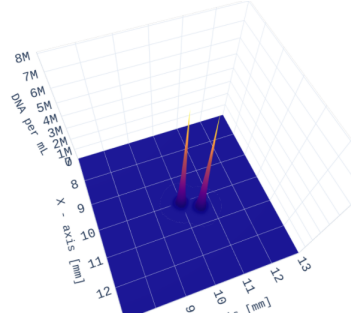
Figure 56: Closer look at the data from box D in figure 45 presented in a grayscale heatmap. The data were treated with a Gaussian filter with $\sigma = 5$.

Box D at picture 90



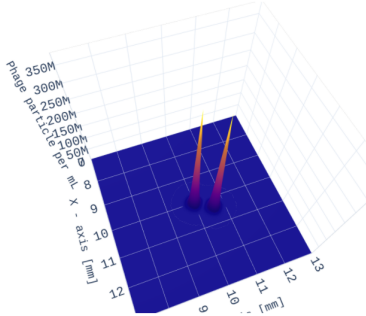
(a) Experimental result.

DNA in model of box E at 9 hours and 54 minutes



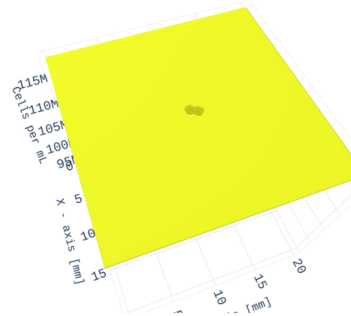
(b) Model - DNA concentration.

Phage in model of box E at 9 hours and 54 minutes



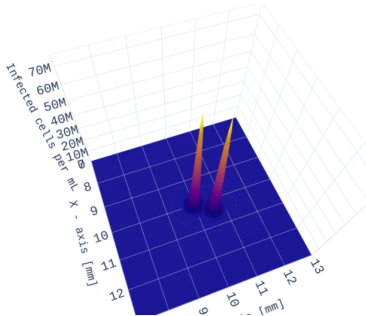
(c) Model - Phage concentration

Bacteria in model of box E at 9 hours and 54 minutes



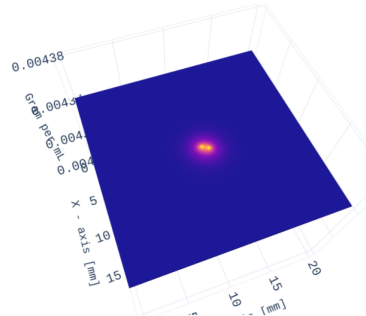
(d) Model - Bacteria concentration.

Infected in model of box E at 9 hours and 54 minutes



(e) Model - Infected bac. concentration.

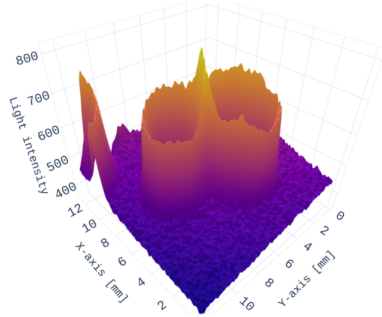
Nutrient in model of box E at 9 hours and 54 minutes



(f) Model - Nutrient concentration.

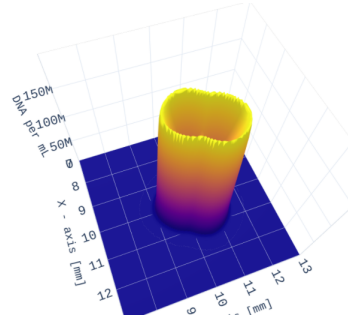
Figure 57: Experimental data in box D at 9 hours, compared to the model.

Box D at picture 252



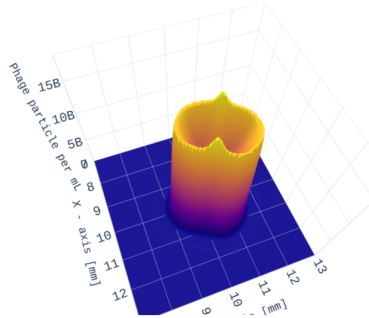
(a) Experimental result.

DNA in model of box E at 25 hours and 30 minutes



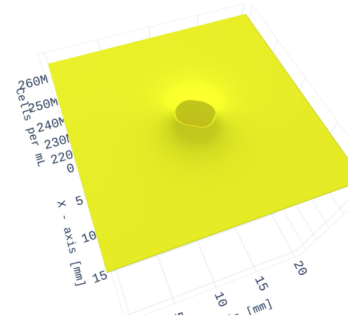
(b) Model - DNA concentration.

Phage in model of box E at 25 hours and 30 minutes



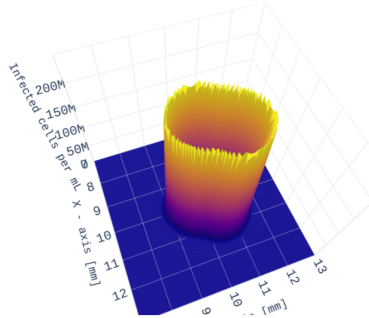
(c) Model - Phage concentration

Bacteria in model of box E at 25 hours and 30 minutes



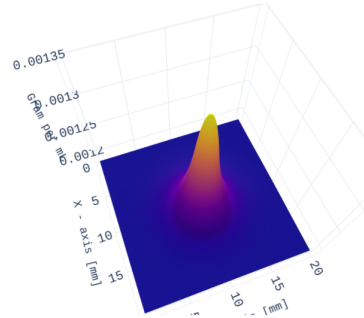
(d) Model - Bacteria concentration.

Infected in model of box E at 25 hours and 30 minutes



(e) Model - Infected bac. concentration.

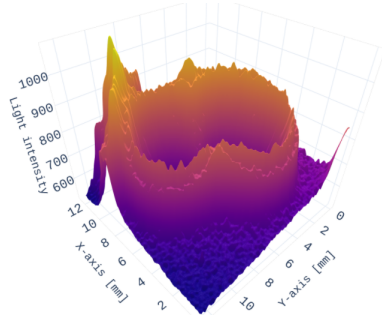
Nutrient in model of box E at 25 hours and 30 minutes



(f) Model - Nutrient concentration.

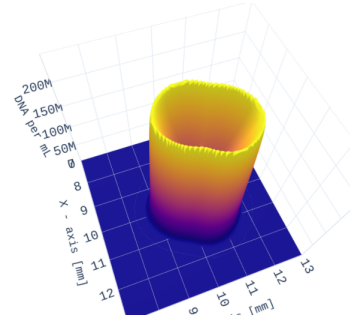
Figure 58: Experimental data in box D at 25 hours and 12 min, compared to the model.

Box D at picture 414



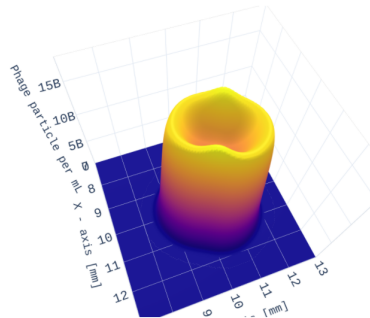
(a) Experimental result.

DNA in model of box E at 41 hours and 9 minutes



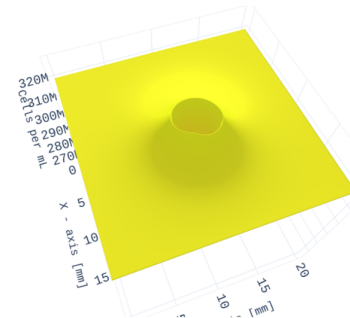
(b) Model - DNA concentration.

Phage in model of box E at 41 hours and 9 minutes



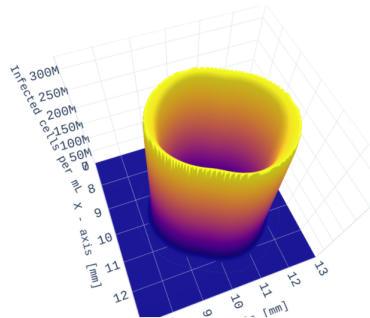
(c) Model - Phage concentration

Bacteria in model of box E at 41 hours and 9 minutes



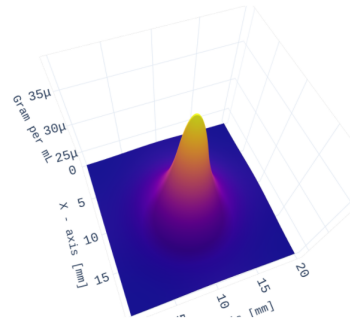
(d) Model - Bacteria concentration.

Infected in model of box E at 41 hours and 9 minutes



(e) Model - Infected bac. concentration.

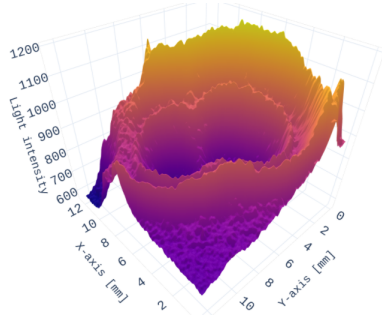
Nutrient in model of box E at 41 hours and 9 minutes



(f) Model - Nutrient concentration.

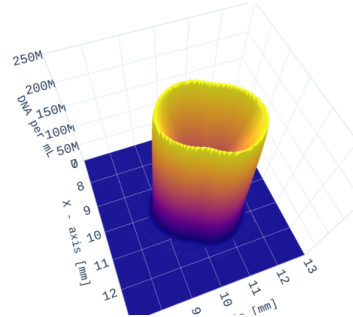
Figure 59: Experimental data in box D at 41 hours and 24 min, compared to the model.

Box D at picture 576



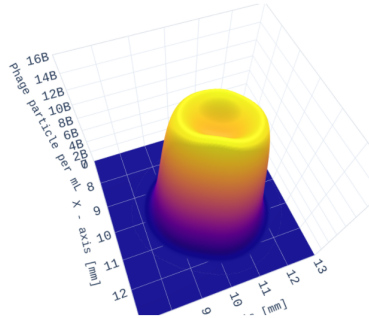
(a) Experimental result.

DNA in model of box E at 57 hours and 45 minutes



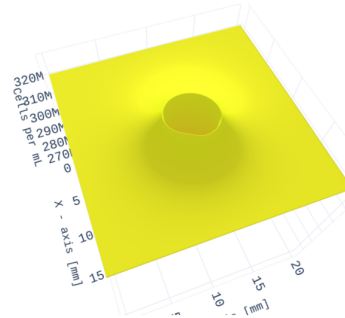
(b) Model - DNA concentration.

Phage in model of box E at 57 hours and 45 minutes



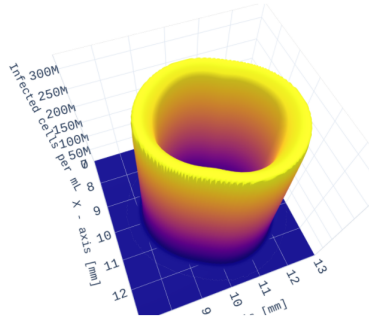
(c) Model - Phage concentration

Bacteria in model of box E at 57 hours and 45 minutes



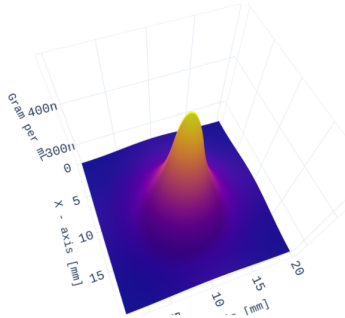
(d) Model - Bacteria concentration.

Infected in model of box E at 57 hours and 45 minutes



(e) Model - Infected bac. concentration.

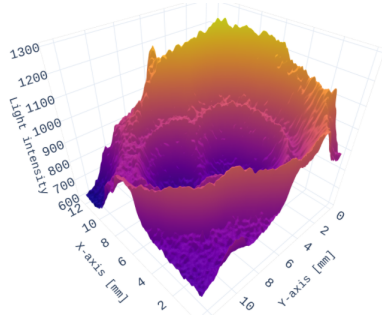
Nutrient in model of box E at 57 hours and 45 minutes



(f) Model - Nutrient concentration.

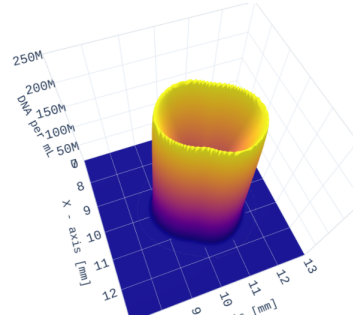
Figure 60: Experimental data in box D at 57 hours and 36 min, compared to the model.

Box D at picture 738



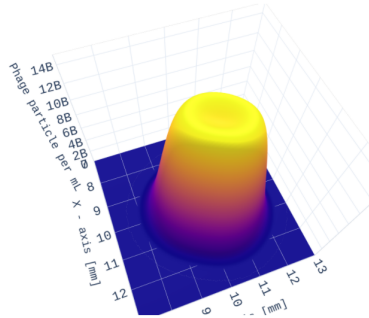
(a) Experimental result.

DNA in model of box E at 74 hours and 24 minutes



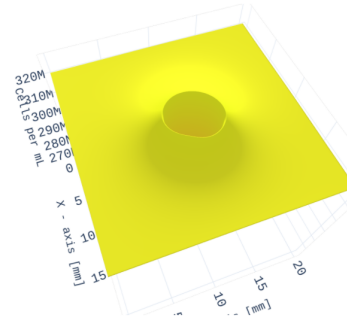
(b) Model - DNA concentration.

Phage in model of box E at 74 hours and 24 minutes



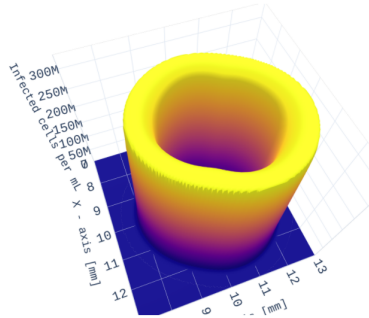
(c) Model - Phage concentration

Bacteria in model of box E at 74 hours and 24 minutes



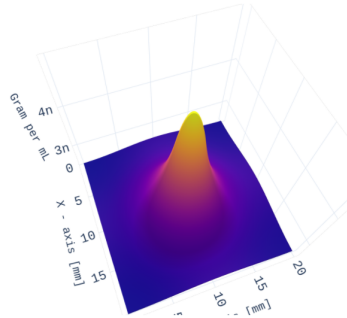
(d) Model - Bacteria concentration.

Infected in model of box E at 74 hours and 24 minutes



(e) Model - Infected bac. concentration.

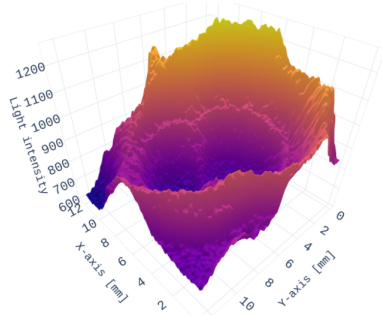
Nutrient in model of box E at 74 hours and 24 minutes



(f) Model - Nutrient concentration.

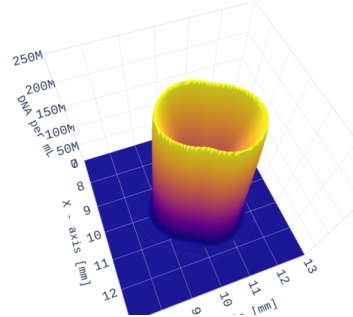
Figure 61: Experimental data in box D at 73 hours and 48 min, compared to the model.

Box D at picture 900



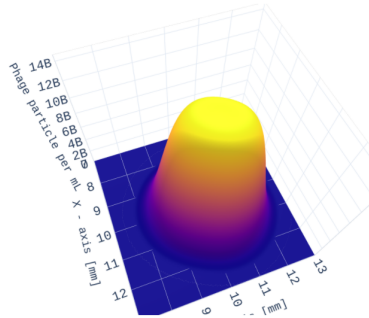
(a) Experimental result.

DNA in model of box E at 90 hours and 0 minutes



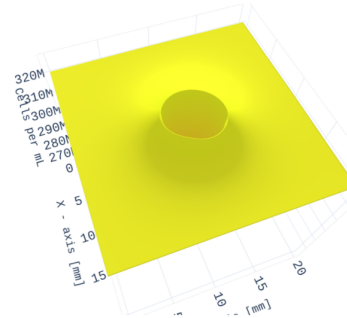
(b) Model - DNA concentration.

Phage in model of box E at 90 hours and 0 minutes



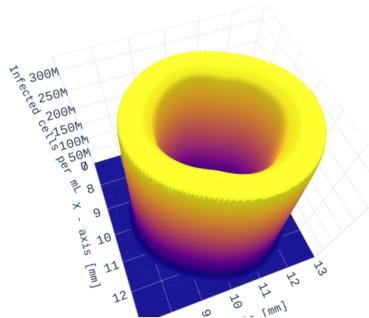
(c) Model - Phage concentration

Bacteria in model of box E at 90 hours and 0 minutes



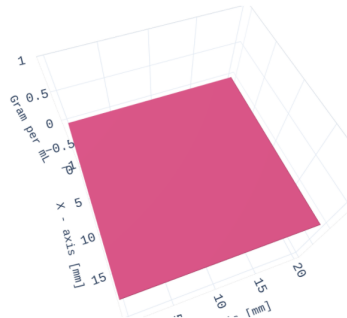
(d) Model - Bacteria concentration.

Infected in model of box E at 90 hours and 0 minutes



(e) Model - Infected bac. concentration.

Nutrient in model of box E at 90 hours and 0 minutes



(f) Model - Nutrient concentration.

Figure 62: Experimental data in box D at 90 hours, compared to the model.

The experimental plaques show three plaques merging, and not just two. The two first plaques merge between the first presented time points. I consider this merging to be so early that it is reasonable to only consider the two plaques that meet around 25 hours in when modelling.

Similar to box A, the plaques in the model never met when the phage seeding point was placed as far apart as the plaques found experimentally. Therefore the distance was halved and the results should not be read as literally as when a single plaque is considered.

The double plaques show many of the same characteristics that are already seen in box A, B, and C. The plaques merge and leave a line between the intersectional points. The bacteria close to the plaques experience better growth conditions due to an influx of nutrient from the centre of the plaque. Just like box C the infected bacteria continue to expand when the second ring begins to form. The model of box C showed that all nutrient in the model was consumed around 57 hours in. This was not the case in box D, as there were still nutrient diffusing 74 hours in. This is due to the two plaques merging leaving two nutrient peaks in close proximity to each other. The nutrient peaks experience a lower diffusion pressure from the front where the other nutrient peak is located, which amounts to lower total diffusion from the peaks.

4.4.3 Experimental run 1.3 with DH5 α

This experimental run was recorded after the above-mentioned improvements to the Cellfiebooth. Unfortunately the initial bacterial concentration was not recorded, which is why the plaques in this run are not modelled. The plaques in this run display an interesting variation in morphology: the two plaques that merge into each other to the left end up with a double ring, while the plaques that do not merge with others only have the one ring.

When trying to determine the bacterial growth curve in the experiment, I found that the growth curve was not equal for the whole Petri dish. Four points, X, Y, Z, and W, are presented in the graph in figure 63. The location of these points is shown in figure 64f. These points show two distinctly different growth rates. All growth rates follow the same trend until 40 hours in, where point X and Y deviate from Z and W. Point X and Y are close to the merging plaques that display a double ring. These points have a similar growth curve to run 1.2, where all plaques have a double ring. Point Z and W on the other hand are closer to the plaques that do not merge, and display a single ring. These points have a growth curve similar to run 1.1, where all plaques have a single ring.

The findings above support the hypothesis that plaque morphology is related to the bacterial growth curve. It is however difficult to pinpoint exactly what caused this change in bacterial growth rate in this particular experimental run. My efforts to recreate this run have not been fruitful, and none of my other runs showed double and single ringed plaques in the same Petri dish.

Change in light intensity for bacterial lawn in experiment 1.3

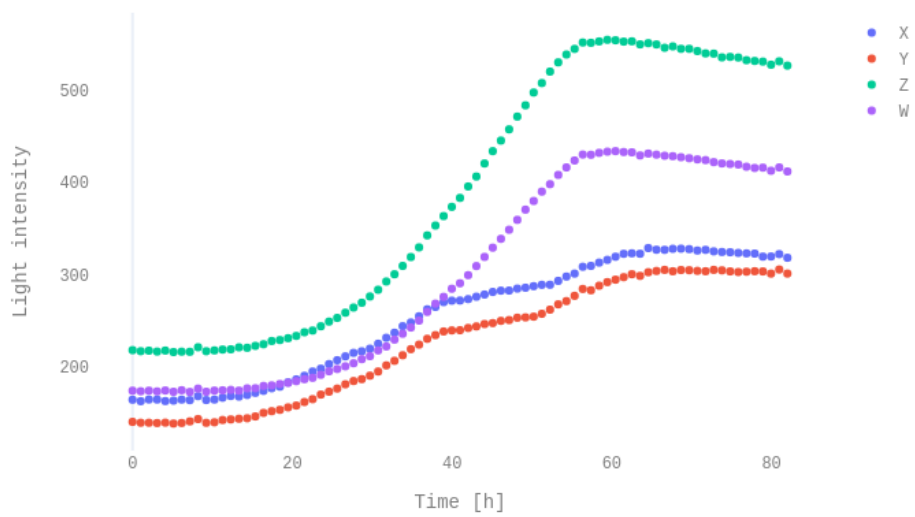


Figure 63: Change in light intensity over time in different parts of the bacterial lawn in experiment 1.3. The graph show local variations in the bacterial growth curve.

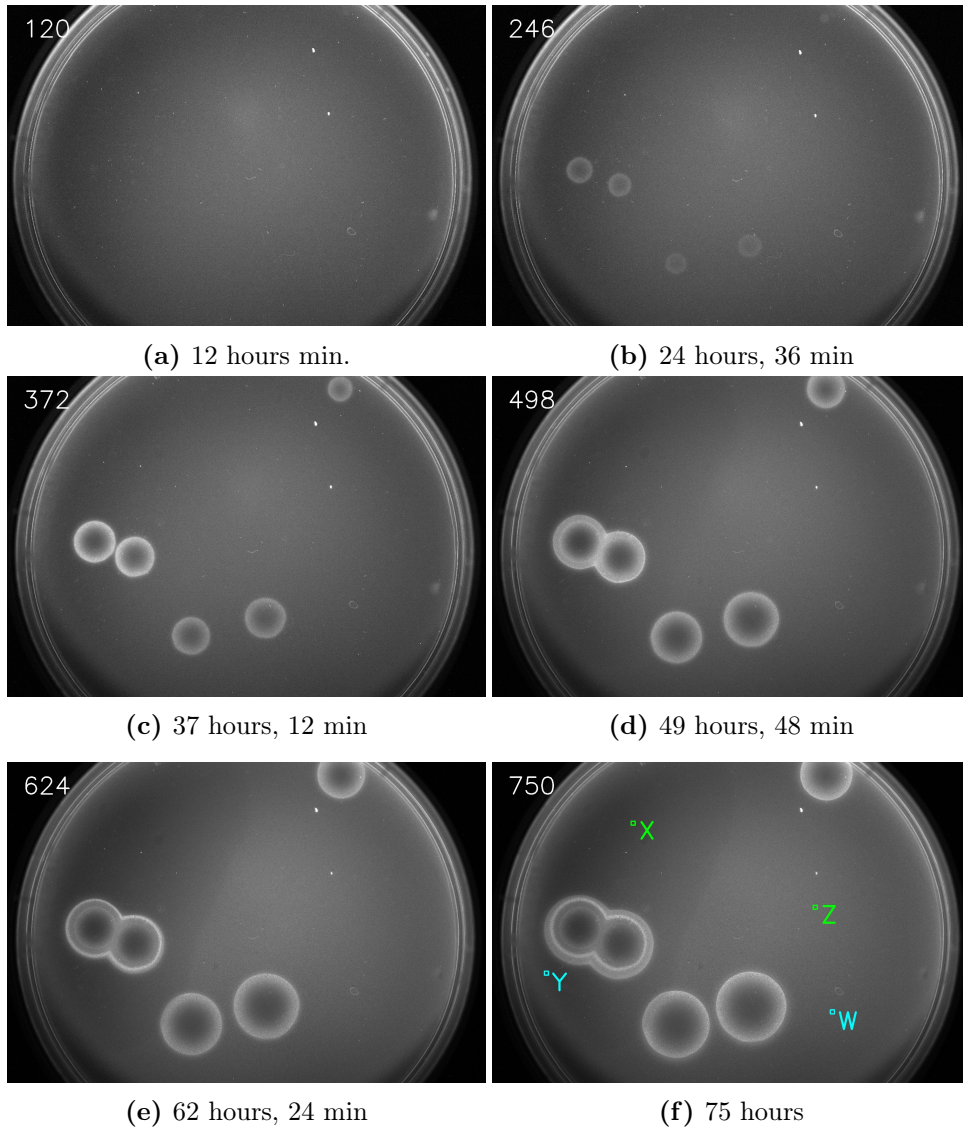


Figure 64: DH5 α with unknown initial bacterial concentration. The number in the series is given in the left corner of the image. Six minutes between each number. The two plaques that merge create a double ring while the plaques that are seemingly unaffected by neighbouring plaques do not.

4.4.4 Experimental run 2.1 with BL21

The data were captured with the Cellfiebooth improvements described in section 3.2.3. 1000 images were captured with six minute intervals. The six photographs presented in figure 45 range from photo 120 to 750, where photo 120 is the first photo where traces of the plaques can be observed. At 750 the plaques have stopped expanding. A number of plaques appear in the Petri dish, and one section was studied closer and modelled. This section is shown as box E in figure 66f.

While this is the only run with the *E. coli* strain BL21 presented in this thesis, I performed multiple experiments of this kind. These experiments were all conducted with an OD_{600} in the range 0.7 to 0.95, and all had similar results. None of the experiments performed with BL21 had plaques that visibly merged.

The graphs in figure 65 show the bacterial growth curve in the run. Looking back on the bacterial growth curve of the previous experimental runs I presented, we observe that run 1.1 stopped at around 40 hours in, while 1.2 and 1.3 stopped at 60 hours in. Dissimilarly, this run continued to grow even after 100 hours. The growth curve resembles the one for experimental run 1.2, where the plaques had double rings. This curve seems to have a steady growth for 30 hours before the growth rate changes to a lower rate and steadily declines. At the end of the experiment—100 hours in—the growth rate was still declining.

Change in light intensity for bacterial lawn in experiment 2.1

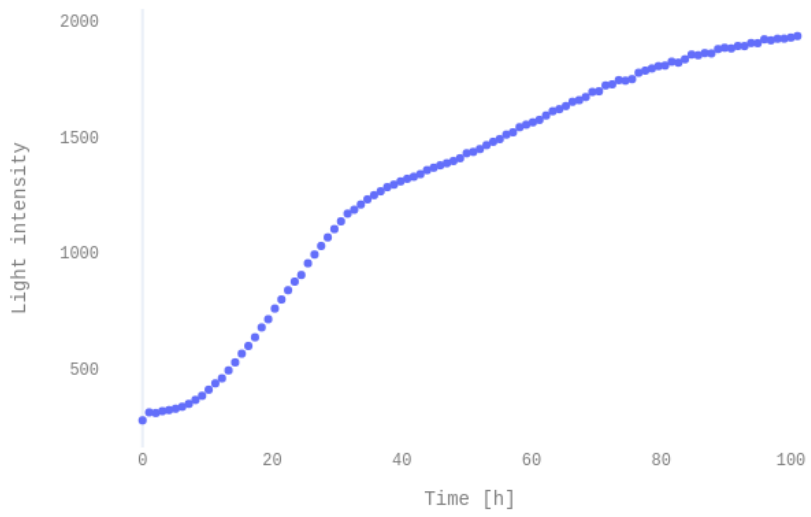


Figure 65: Change in light intensity over time in the bacterial lawn in experiment 2.1.

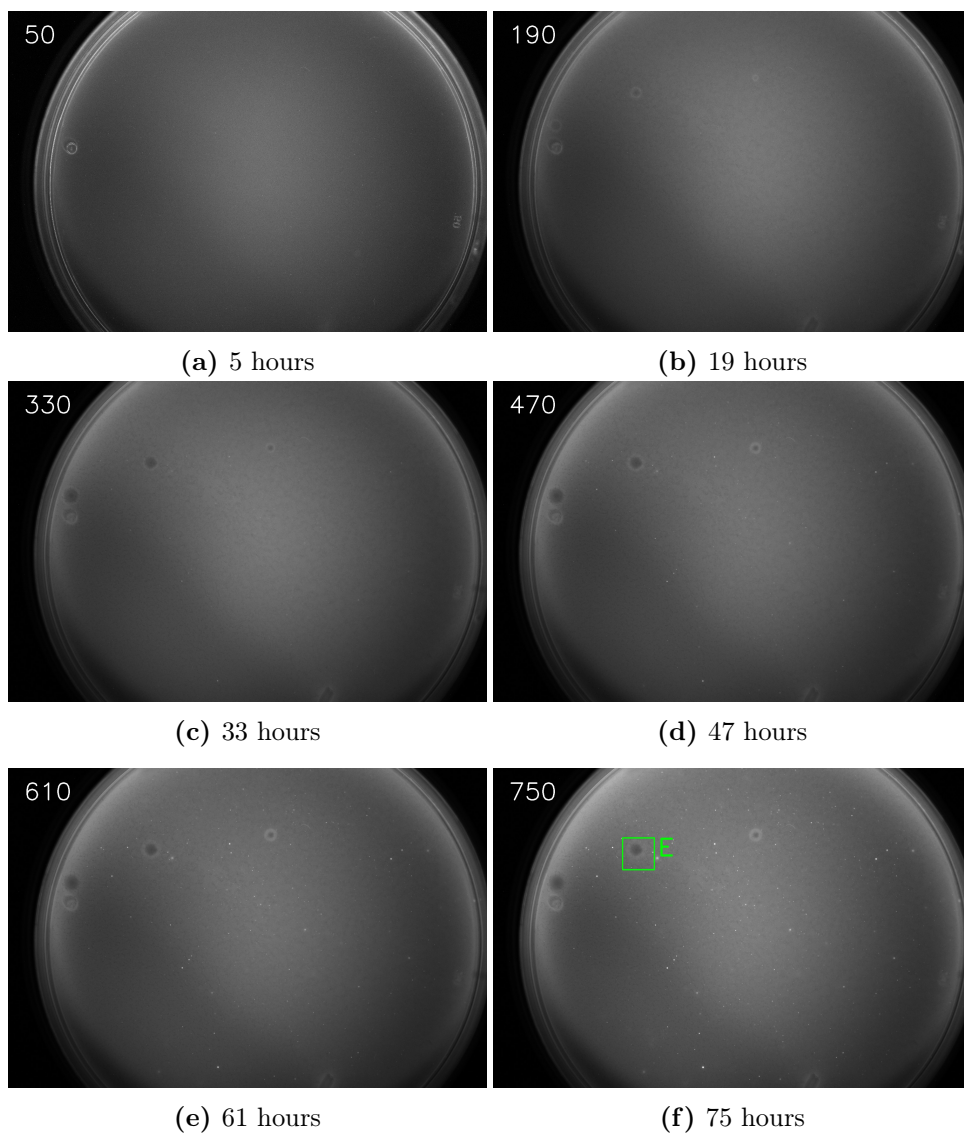
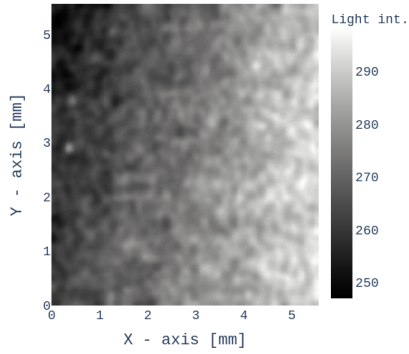


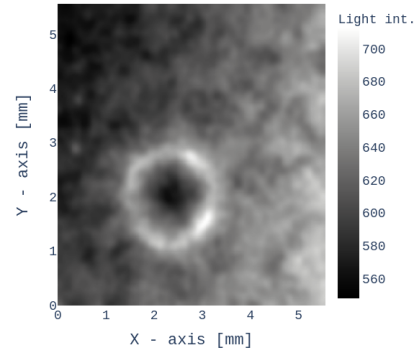
Figure 66: BL21 with initial $OD_{600} = 0.808$. The number in the series is given in the left corner of the image. Six minutes between each number. Data captured before the improvements mentioned in 3.2.3. Box E is studied closer.

Box E at picture 50



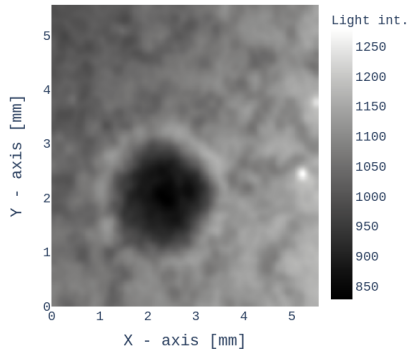
(a) 16 hours

Box E at picture 190



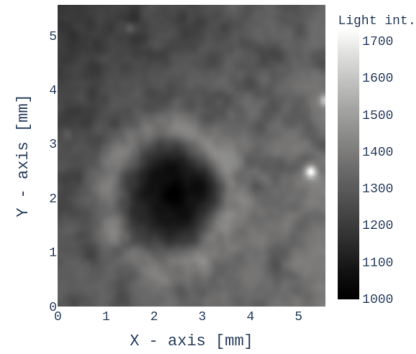
(b) 23 hours, 48 min

Box E at picture 330



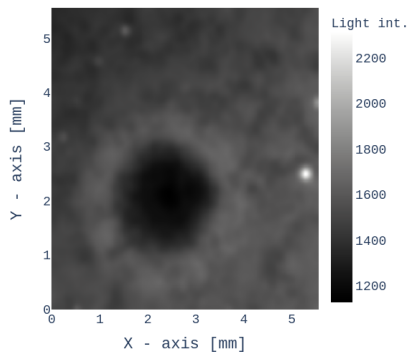
(c) 31 hours, 36 min

Box E at picture 470



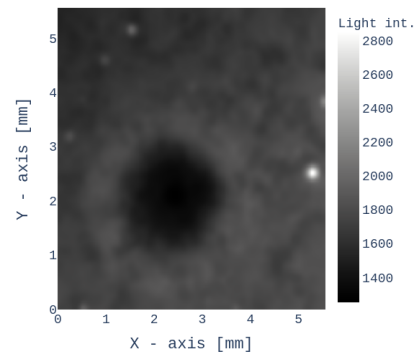
(d) 39 hours, 24 min

Box E at picture 610



(e) 47 hours, 12 min

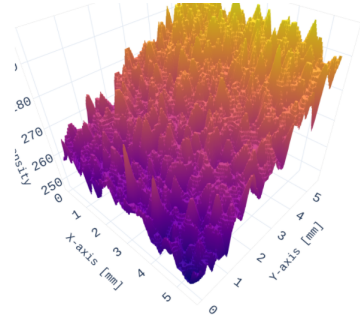
Box E at picture 750



(f) 55 hours

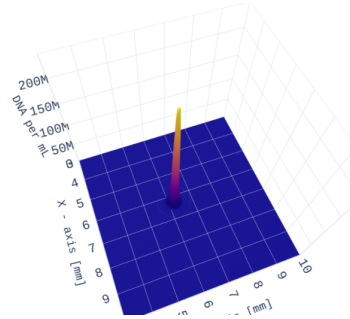
Figure 67: Closer look at the data from box E in figure 66 presented in a grayscale heatmap. The data were treated with a Gaussian filter with $\sigma = 5$.

Box E at picture 50



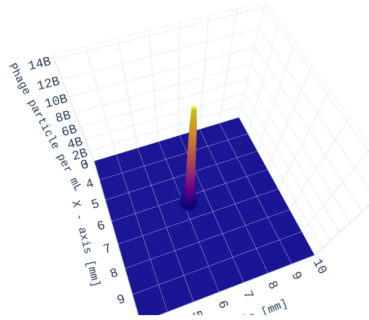
(a) Experimental result.

DNA in model of box E at 5 hours and 30 minutes



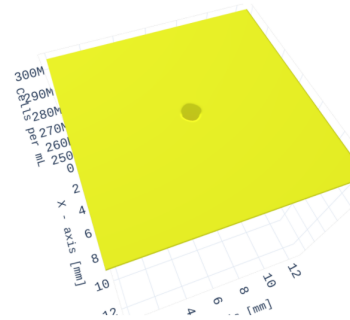
(b) Model - DNA concentration.

Phage in model of box E at 5 hours and 30 minutes



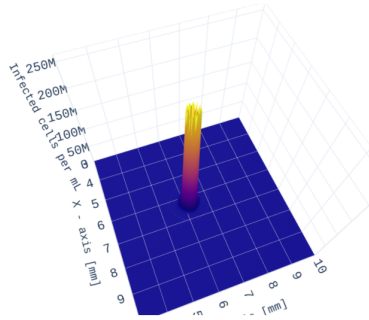
(c) Model - Phage concentration

Bacteria in model of box E at 5 hours and 30 minutes



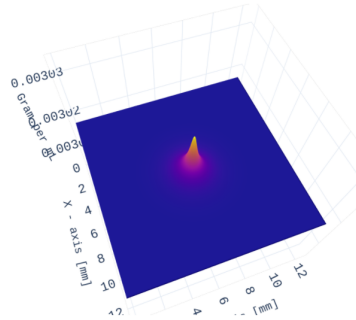
(d) Model - Bacteria concentration.

Infected in model of box E at 5 hours and 30 minutes



(e) Model - Infected bac. concentration.

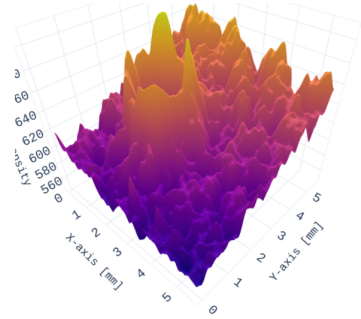
Nutrient in model of box E at 5 hours and 30 minutes



(f) Model - Nutrient concentration.

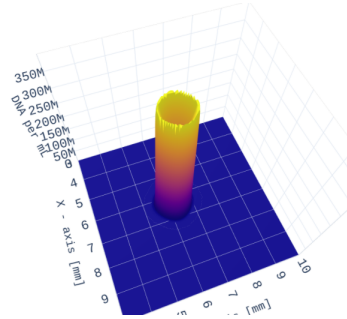
Figure 68: Experimental data in box E at 5 hours, compared to the model.

Box E at picture 190



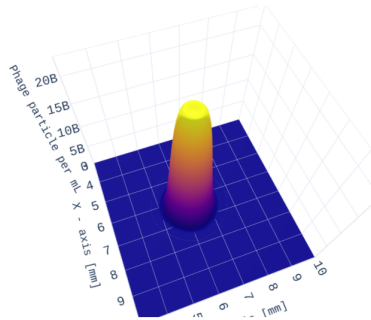
(a) Experimental result.

DNA in model of box E at 19 hours and 54 minutes



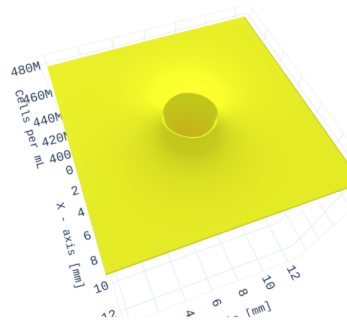
(b) Model - DNA concentration.

Phage in model of box E at 19 hours and 54 minutes



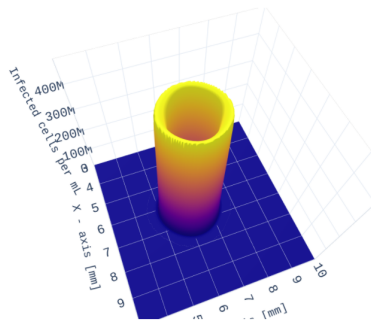
(c) Model - Phage concentration

Bacteria in model of box E at 19 hours and 54 minutes



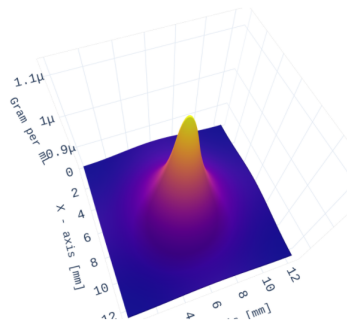
(d) Model - Bacteria concentration.

Infected in model of box E at 19 hours and 54 minutes



(e) Model - Infected bac. concentration.

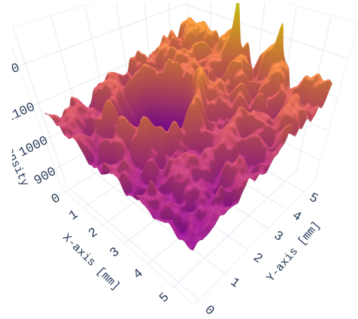
Nutrient in model of box E at 19 hours and 54 minutes



(f) Model - Nutrient concentration.

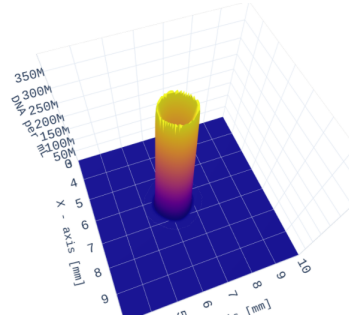
Figure 69: Experimental data in box E at 19 hours, compared to the model.

Box E at picture 330



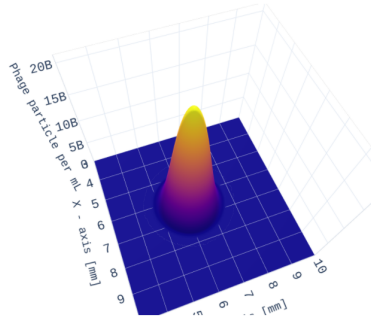
(a) Experimental result.

DNA in model of box E at 33 hours and 18 minutes



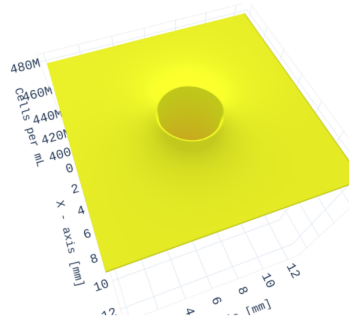
(b) Model - DNA concentration.

Phage in model of box E at 33 hours and 18 minutes



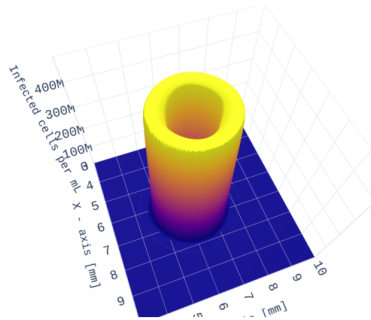
(c) Model - Phage concentration

Bacteria in model of box E at 33 hours and 18 minutes



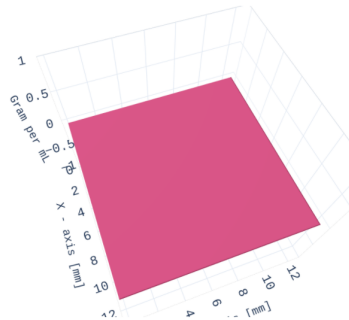
(d) Model - Bacteria concentration.

Infected in model of box E at 33 hours and 18 minutes



(e) Model - Infected bac. concentration.

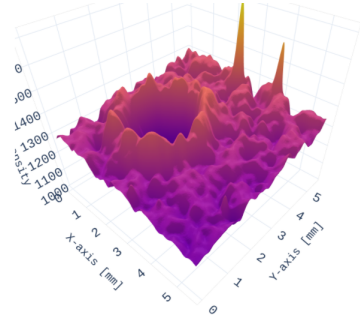
Nutrient in model of box E at 33 hours and 18 minutes



(f) Model - Nutrient concentration.

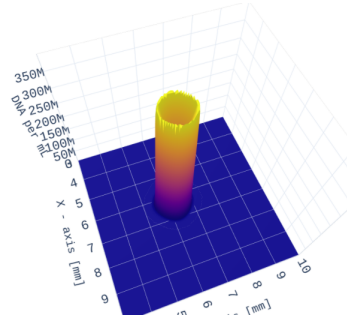
Figure 70: Experimental data in box E at 33 hours, compared to the model.

Box E at picture 470



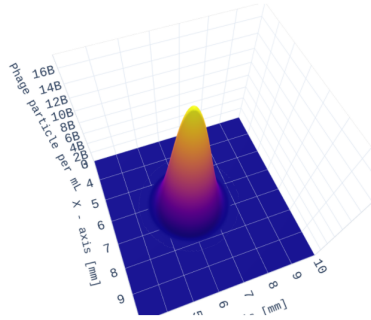
(a) Experimental result.

DNA in model of box E at 47 hours and 42 minutes



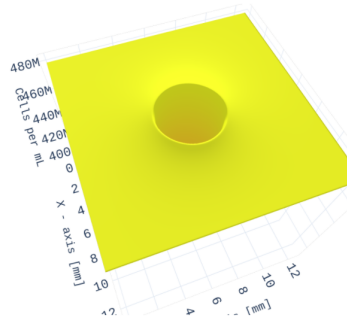
(b) Model - DNA concentration.

Phage in model of box E at 47 hours and 42 minutes



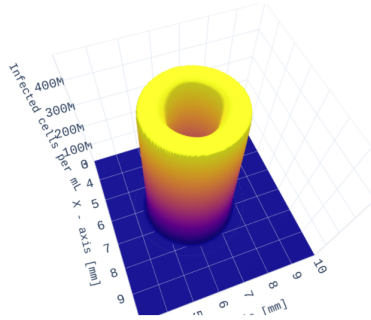
(c) Model - Phage concentration

Bacteria in model of box E at 47 hours and 42 minutes



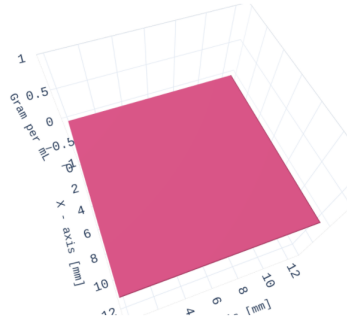
(d) Model - Bacteria concentration.

Infected in model of box E at 47 hours and 42 minutes



(e) Model - Infected bac. concentration.

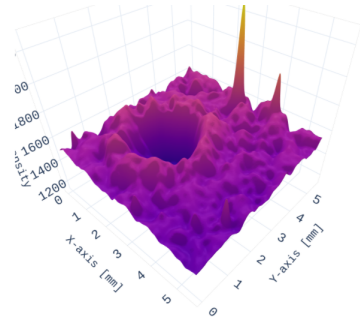
Nutrient in model of box E at 47 hours and 42 minutes



(f) Model - Nutrient concentration.

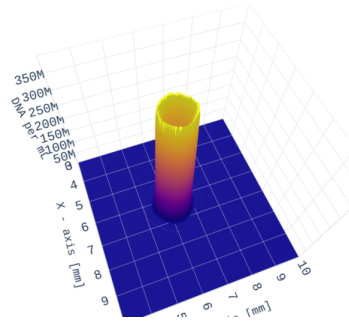
Figure 71: Experimental data in box E at 47 hours, compared to the model.

Box E at picture 610



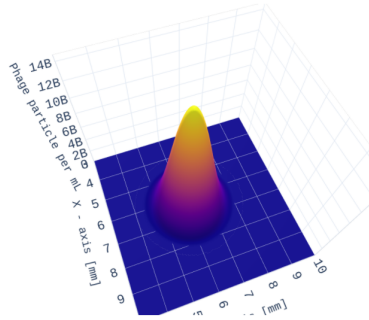
(a) Experimental result.

DNA in model of box E at 61 hours and 6 minutes



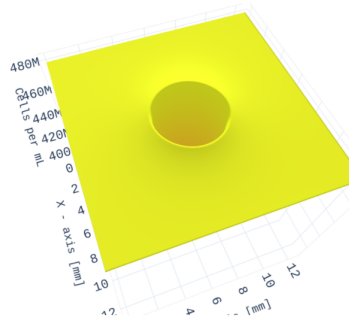
(b) Model - DNA concentration.

Phage in model of box E at 61 hours and 6 minutes



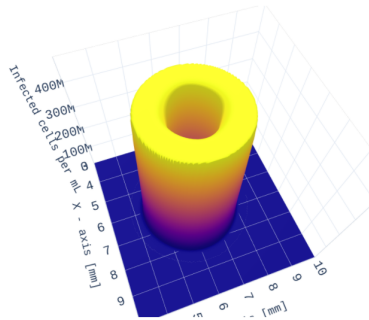
(c) Model - Phage concentration

Bacteria in model of box E at 61 hours and 6 minutes



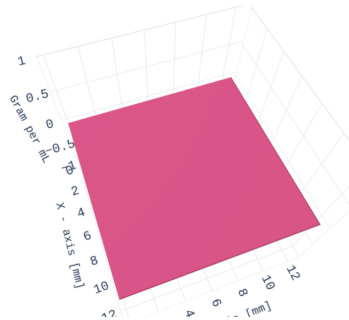
(d) Model - Bacteria concentration.

Infected in model of box E at 61 hours and 6 minutes



(e) Model - Infected bac. concentration.

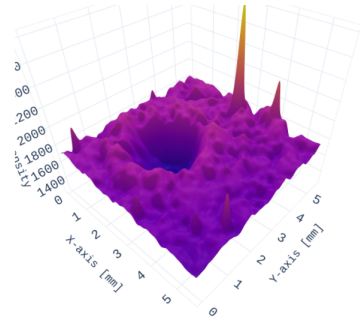
Nutrient in model of box E at 61 hours and 6 minutes



(f) Model - Nutrient concentration.

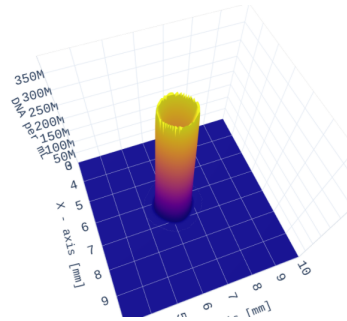
Figure 72: Experimental data in box E at 61 hours, compared to the model.

Box E at picture 750



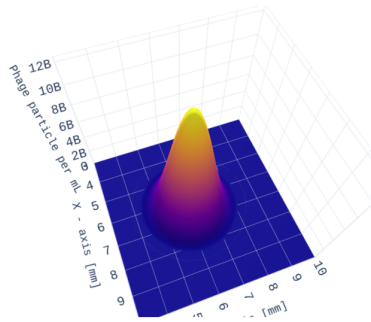
(a) Experimental result.

DNA in model of box E at 75 hours and 30 minutes



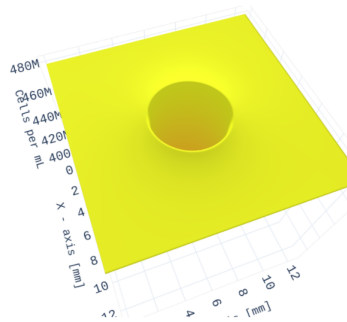
(b) Model - DNA concentration.

Phage in model of box E at 75 hours and 30 minutes



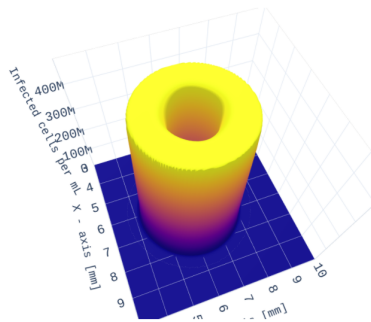
(c) Model - Phage concentration

Bacteria in model of box E at 75 hours and 30 minutes



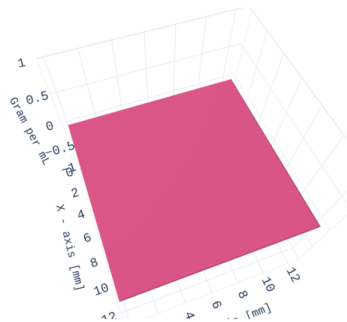
(d) Model - Bacteria concentration.

Infected in model of box E at 75 hours and 30 minutes



(e) Model - Infected bac. concentration.

Nutrient in model of box E at 75 hours and 30 minutes



(f) Model - Nutrient concentration.

Figure 73: Experimental data in box E at 75 hours, compared to the model.

Just like the previous runs with high initial bacterial concentration, the model predicts that the nutrient in the system run out early, with no nutrient left 33 hours in. What differs this experimental run from the runs performed with high concentration of DH5 α is the fact that there is that the plaques create a single ring despite a high initial bacterial concentration.

The radial profile of the plaque is shown in figure 74. This graph shows that the plaque morphology is quite different in this run compared to the ones earlier presented. The plaque seems to reach a peak at ≈ 1.25 mm 33 hours into the experiment. While the ring expands, this peak continues to be prominent throughout the experiment. Looking back to the growth rate curve in figure 65, the bacterial growth rate changed after about 40 hours. This shift coincides somewhat with when the peak in the plaque appears.

In section 4.4.2 I presented a hypothesis regarding how the diffusion of nutrient from the lower agar layer could affect the growth curve. Building on this, it seems like the bacteria ran out of nutrient in its immediate vicinity around 40 hours into the experiment. After this the bacteria continued to grow on the nutrient coming from the underlying agar layer. It seems reasonable to assume that the nutrient run out around 40 hours in, considering the high initial bacterial growth rate and the fact that BL21 has a higher bacterial growth rate than DH5 α . While the overlaying agar is pipetted and is always 3 mL soft agar + 1 mL bacterial broth, the underlying agar is poured by hand and can vary from Petri dish to Petri dish. Due to this, it is reasonable that the "second growth" driven by nutrient diffusion from underlying agar has a varying time span from experimental run to experimental run.

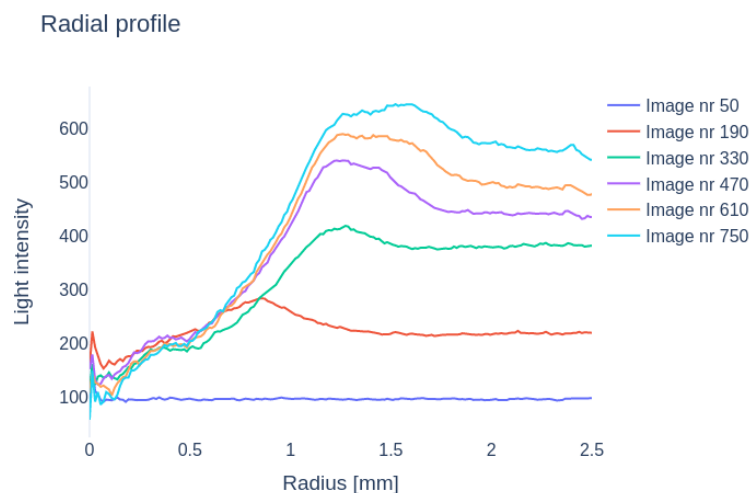


Figure 74: Radial profile of plaque in box E in the experimental result found by calculating the radial average.

Radial profile in model of box E

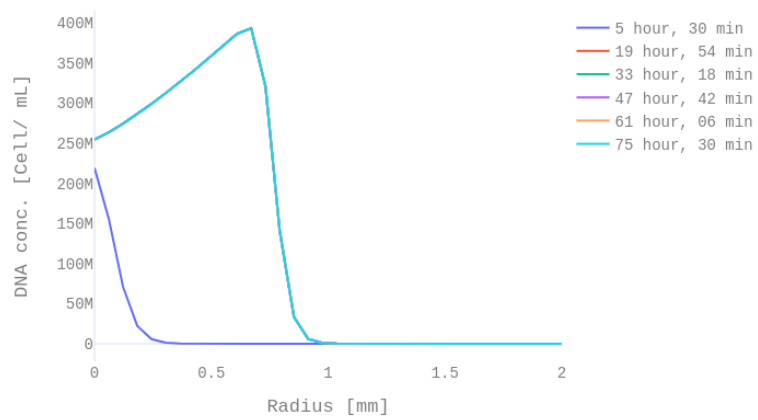


Figure 75: Radial profile of plaque in box in the theoretical result. The model predicts that the plaque stops expanding completely after 20 hours, and little to no change happens past this point.

5 Discussion

5.1 Burst size and lysis time

The burst sizes found were 95 for DH5 α and 85 for BL21. From the literature we see that the burst size varies for both host and phage, and that *E. coli* phages like the lambda phage have a burst size about 150 phages per cell [29, 105, 106]. This infers that the burst sizes found seem reasonable, comparing to other *E. coli* phages. I did not originally expect the burst size to be different for the different strains of *E. coli*, considering the same phage strain was used. The difference is not large, and is likely a result of the different growth rate the two strains have in the M9 growth media. This hypothesis is supported by the paper "Effect of bacterial growth rate on bacteriophage population growth rate", in which the burst size of phage T4 was investigated in a series of different *E. coli* hosts with growth rate ranging from 0.06 to 0.98h⁻¹. They found the increase in growth rate correlating linearly with the burst size, from 8 phages per cell to 89 phages per cell [107].

While the uncertainty of the burst size could have been decreased by repeating the experiment and acquiring more data for the range of interest, the results give me a sufficiently narrow range for my purposes.

The lysis time for the phage was found to be very different between the host strains, with the bacterial strain BL21 yielding almost half the lysis time of DH5 α . Again this is something that could be traced back to the difference in growth rate for the two bacterial strains, since the phage is dependent on the bacterial metabolism to proliferate, and the lysis itself is thought to be controlled by the accumulation of proteins [107]. The same factor limiting the growth rate of the bacteria is most likely also limiting the speed of phage production. Both determined lysis times were well within the range of what would be considered "normal" lysis times for a lytic phage preying on the *E. coli* [107].

I consider the protocol Martyushenko and I developed to be effective as it provided the burst time, lysis time and the standard deviation in the lysis time for a phage-host coupling, all in a single experiment. I also consider the protocol easier to perform than alternative protocols such as the widely used one-step growth curve [108]. The one-step growth curve requires the experimentalist to frequently perform actions with a precise timing over a couple of hours. In contrast, our protocol only requires the experimentalist to pour all the replicates of one phage dilution into the wells in the multiplate quickly, preventing the agar from hardening while pouring. The agar can be replaced with nutrient broth, which would eliminate this challenge. Neither can the one-step growth curve protocol be used to determine the standard deviation for the lysis time.

5.2 Characterisation of growth rate

My intentions for this experiment were to find the growth rate for the *E. coli* strains BL21 and DH5 α in the Cellfiebooth. To achieve this, I needed to grow the bacteria in an environment that permitted continuous measurement *and* could serve as an accurate representation of the environment in the soft agar overlay used in the Cellfiebooth. I chose to use a multiplate reader with a 96-well plate to investigate this, as this would allow me to do multiple accurate measurements for many different starting concentrations at the same time. The reader had the disadvantage of being equipped only with a heater but no cooler. Due to this inconvenience, all measurements were taken at 28 °C, which was the lowest temperature the machine could keep stable. *E. coli* grows slower as the temperature gets lower, and the max growth rate μ_{\max} was found most likely to be higher than the one in the Cellfiebooth, where the temperature was kept at 21 °C[109].

The growth rate was found by fitting a model that followed Monod growth kinetics to the experimental data. While I had the growth data for multiple dilutions (5 for BL21 and 7 for DH5 α), I only considered the three dilutions with the highest starting bacterial cell concentration. A series of assumptions follow when fitting a simple model to experimental data, and the smaller dilutions were not included in the model fitting. This was to escape the cases for which these assumptions no longer hold.

The model related to the bacterial growth is built on the assumption that the OD₆₀₀ can be directly translated to bacterial cell concentration by multiplying the OD₆₀₀ number with a constant. While this assumption seems to hold for the concentrations included in the results, it does not hold for lower concentrations. These were excluded here, but can be found in appendix B. When the bacterial concentration is low enough, the scattering from nutrients and agar has a greater effect on OD₆₀₀ than scattering from bacteria, and we get what may appear to be a long lag phase, but is most likely the time the bacteria needs to reach a concentration where it makes a visible impact on the OD₆₀₀ measurements. A possible solution for this could be to subtract the OD₆₀₀ contributed by the agar and nutrient alone, but that would not solve the problem of the bacterial results. Supported by the literature[110], the bacterial growth rate was assumed to be independent of the initial bacterial concentration.

From Table 4 and observing the graphs in figure 16 and 17, the Monod kinetics with the growth constants determined gave a good approximation for the growth that happens in the agar overlay. The two strains are known to have different growth characteristics, and they follow the same pattern seen in other growth characterisations done for these strains[106]. The strain BL21 is often used for protein expression since it is deficient in proteases Lon and

OmpT[111]. This protease deficiency could be the reason behind both the higher growth rate and higher maximum value for OD_{600} .

The results in section 4.3 suggest the visibility of the bacterial lawn in the Cellfiebooth data being due to light scattering. As OD_{600} measurements are based on light scattering as well, one could fit the model to the light intensity data for bacterial lawn unaffected by phages in the Cellfiebooth. This would yield a growth rate for the bacteria growing in the environment of interest. Pursuing this would require one to acquire precise calibration data in order to convert the light intensity values from the Cellfiebooth to cell concentration.

5.3 Cellfiebooth and model results

In general the Cellfiebooth and model performed well. The Cellfiebooth provided valuable insights into plaque development as well as the bacterial growth curves throughout the experimental run. The model was able to accurately predict the shape of the plaques as they appeared in the Cellfiebooth. In cases where the bacterial growth curve followed Monod kinetics throughout the experimental run, such as run 1.1, it was able to recreate the plaques at a very high precision. Considering no model fitting was performed on the mathematical model, this strongly suggests that the model considers all the major phenomena that affect the formation of viral plaques.

5.3.1 Cellfiebooth

As already described in section 4.3, the results related to the tests for bacterial fluorescence in the Cellfiebooth showed that the GelGreen-half of the Petri dish was less visible in the data than the control side. This was the case preceding as well as succeeding the appearance of a bacterial lawn. This strongly suggests that GelGreen is not the reason for the observed effect, and that the appearance of the bacterial lawn is most likely due to scattering from the light reaching the bacteria. I originally expected the light filters fitted on the light source and camera to block all light. To the naked eye, this seemed to be the case when observing the two filters together, and is demonstrated in appendix D. The light source is visible in the Cellfiebooth results when placed directly under the camera. The effect can be observed in figure 82 in appendix D. This shows that the two filters together are not able to hinder all light from the light source. Most likely a small amount of light is not stopped by both filters, and due to the long exposure time (100 seconds) used in the Cellfiebooth camera, this small amount of light makes an impact on the measured data. This implies that we should not interpret the mea-

sured light intensity in the Cellfiebooth as being solely from DNA, but also bacterial scattering.

These results may appear less than amazing at first sight, as the Cellfiebooth was built to measure *only* the fluorescence from the free DNA, as an indicator for the concentration of bacteria lysed by phages. However, the discovery that the Cellfiebooth also measures the light scattered by bacteria gives the researcher more valuable information to work with. Measuring an area that is not affected by plaque expansion gives me the shape of the bacterial growth curve throughout the experimental run, and is considered valuable insight into the host behaviour. While the plaques were affected by the scattered light, this effect was found to be linear, and therefore easy to account for when analysing the results. Although the measuring of bacterial scattering was first assumed an obstruction of my Cellfiebooth results, it turns out to be an advantage—an unintended upgrade/expansion of Cellfiebooth.

The Cellfiebooth system can be described as "general". It worked just as well for the *E. coli* strain BL21 as for DH5 α . While this thesis only considers a single phage strain, the U-phage, the Cellfiebooth system worked just as well for all other phage strains I tried, such as the Ubl21 and De2[1]. I see no reason the use of Cellfiebooth could not be expanded to other hosts and phages. As long as the host is able to grow on gel with non-fluorescent nutrients, it can be studied using my system.

5.3.2 Model

The model was solved using Euler's method with a constant step-size. This method was chosen because model had a stiff equation set and was multi-dimensional, with every time step represented by a large matrix. Established solvers available for python, like the `solve_ivp` function from the SciPy package, take in 1D arrays and check for instability by comparing the change to the average of the whole array. If I were to use this type of solver to solve the model, I would need to flatten the matrix and restructure it for every step. While this is doable, this means that the solver does not check for the type of local instability that can occur in reaction-diffusion models of the kind I have developed and used in this thesis. For example, if the nutrient matrix is suddenly unstable and yielding unreasonable results, the solver would not be able to detect this. The solver does not consider the instability locally, but rather averages all values in the model at the calculated time-step and checks if the average varies considerably from the average of the last time-step. Due to the large amount of values calculated for each time-step, the instability in a variable would not make big enough of an impact on the average value for it to be detectable as an instability, at least not before the instability propagated to the point of no return.

One of the biggest advantages of using an established solver would be that they offer dynamic step-sizes. From the Van Neumann stability analysis, we see that the step-sizes used in solving these equations need to be under a certain numerical threshold. As the solvers are incapable of effectively detecting instability in the system, one would have to force the solver to use steps that are lower than the threshold given by the Van Neumann analysis, effectively not utilising the dynamic step-size.

Without dynamic step-sizes there is little to gain time-wise from using the established solvers. I found it more practical to implement a simple forward Euler's method with a constant step-size to solve the equations set. There is little difference in the amount of time used for each iteration, and I achieved better control over what was happening during the calculations than I would using an established solver.

I did encounter some conflicts between my experimental and theoretical setup, most notably the model was not able to recreate the double rings phenomena observed in run 1.2 and 1.3. When presenting the results in section 4.4, I hypothesised that there are two phenomena affecting the plaque expansion I had not considered when developing the model. These are (i) the diffusion of nutrient from the underlying agar into the soft agar overlay, and (ii) the bacteria changing growth strategy during the experimental run. Both strategies could be incorporated into the model, but the question remains: would that be useful?

Incorporating the diffusion from the underlying agar up to the overlying soft agar would make the model a great deal more complicated. It would have to consider diffusion in three dimensions, instead of the two-dimensional diffusion considered now. The amount of agar in each Petri dish in the experimental runs would have to be standardised. I would also have to assess whether it is safe to presume the diffusion constants to be equal for both agar layers, or if the soft agar having half the agar concentration of the underlying agar would warrant different diffusion constants for the different layers. Having different diffusion constants for the different layers would add another layer of calculations to the model.

A more complex model is not intrinsically a worse model. The model I developed in this thesis is already too complex for algebraically deriving simple terms for effects, like the speed of plaque radius expansion³. The problem lies in that adding an extra dimension to the diffusion would slow down the calculations immensely. Each modelled "box" presented in this thesis took over two hours to solve numerically. Adding another dimension for diffusion would cause an exponential increase in time required to solve

³I am not claiming it is impossible per se—it might be doable for someone at a mathematician's skill level.

the model, hence making the model impractical to work with.

Another aspect to consider is that adding to a model does not automatically make it more precise. If the diffusion in the two layers needs to be considered differently, it could prove challenging to find sufficiently precise values for the diffusion in different agar layers. Not only should the diffusion constants be reasonable, but the ratio between the diffusion constants in the upper and lower layer needs to be reasonable as well. If not, the error could cascade and yield unrealistic predictions of the plaque formation and dynamics.

My suggested solution to this obstacle would be to remove the underlying agar from the experimental protocol. The underlying agar is an artefact from the original plaque assay protocol the Cellfiebooth protocol is based on. I also suggest the underlying agar not be included in any plaque assay unless there is explicit reason to do so, such as the plaque not appearing without the underlying agar. In my laboratory the agar is poured into the Petri dish by hand, and my observation is that the amount of agar effectively poured into Petri dishes varies greatly from person to person, and even between Petri dishes poured by the same person. These kinds of variations renders it challenging to compare the plaque morphology found. Notably, this is the case not only between different laboratories but also between different Petri dishes within the same laboratory.

The plaque morphology is often used as a basis for selection of phages for therapeutic use[48, 112]. My findings suggest that initial bacterial concentration, bacterial growth rate and diffusion largely affect the plaque morphology. If these are not considered, the plaque morphologies found in one lab will be incomparable to morphologies observed in another.

Exceptions are plaque assays performed with the intention of finding new phages. The underlying agar can aid in discovering a broader range of phages, e.g. lysogenic phages that only express the lytic pathway when the bacteria has changed its growth strategy to accommodate the lower influx of nutrient. My main sentiment is that an experimentalist should always be mindful about how different parts of a protocol affects the results. Following a protocol uncritically can yield undesirable results.

As mentioned in both the results in section 3.2 and earlier in this subsection, the results found using the Cellfiebooth show a pattern when experimental runs with high initial bacterial concentration experience a change in growth rate during the experimental run. While eliminating the underlying agar could hinder this phenomenon from reappearing, I still believe it should be considered to include the effect of the host changing growth strategy under the experimental run. The underlying agar is not the only repository of nutrient in a bacterial lawn containing plaques. Nutrient from the plaque centres will still diffuse out to the bacterial lawn, and I believe that this

effect, perhaps not as prominent, will make the second plaque ring appear in experimental runs with high initial bacterial concentration. I'm not sure what the most practical way to incorporate this would be, but in a perfect world, I would find what nutrient concentrations and environmental thresholds trigger this alternative growth strategy. I would characterise the growth kinetics for the bacteria under this alternative growth strategy. Then I would determine the burst size and lysis time for the phage infecting the bacteria under this growth strategy. Incorporating all this into the model could tell me if it was a change of growth strategy that caused the second ring, or if this hypothesis is a dead end. Nonetheless, this alternative model would be useful in the sense that it could provide me with answers.

I have spent many paragraphs examining the model and deliberating possible changes. But it should be clear that this model performed extremely well under "normal" conditions. I consider normal conditions to be when the bacterial growth rate follows Monod kinetics. This was the case in run 1.1 which displayed a bacterial growth curve typical to bacteria following Monod kinetics. Not only was the model able to accurately predict the shape and development of single plaques over time, but it also predicted most to all effects observed in the Cellfiebooth from two plaques merging. All these results suggest that the effects considered by the model are important for the development of plaques. The model also provides a reasonable explanation for the slowdown of plaque development.

5.3.3 Cellfiebooth and model in relation to previously experimental and theoretical attempts to characterise the formation of plaques

There are many differences between the model I developed, and comparable models published by other authors. The McCaskill-Yin model that was later revised by You and Yin is, as mentioned in section 2.3.3, is the first published reaction diffusion model for modelling plaque expansion in an bacterial lawn[113]. The model was made with the purpose of finding a term for the velocity of radial expansion in plaques. The model is a lot simpler than the one I derived, as they do not take available nutrition, growth of bacteria, or the time delay for bacterial lysis into account. They conclude that the rate of plaque enlargement is highly dependent on the adsorption rate, and they note that plaque enlargement slows down as the host-lawn reaches its growth limit and attribute this effect to hindered diffusion, which they incorporate into the model. These conclusions go against my findings, hindered diffusion was never considered in my model, but I achieved a slow down in plaque expansion that followed the experimental results greatly by coupling the rate of of which infected bacteria mature to the bacterial growth

with Monod kinetics. Changes in the adsorption rate has not been explored in this thesis, as the parameter is challenging to adjust experimentally. But I have been able to achieve a great variation in plaque morphology using a single phage strain. I believe it is safe to assume that the phage has the same adsorption rate and diffusion constant for both of the strains of *E. coli* used in this thesis, which strongly suggest that it is wrong to assume plaque formation is solely dependent on these two parameters.

In year 2000, Yih and Yin published a paper where they measured the propagation of a T7 plaque in agar[114]. They did this by photographing a plaque forming in a Petri dish every hour over a 24 hour period and found that the T7 phage expands radially with a speed of 0.059 mm/h. While they seemingly forgot to mention how the model Yin published the previous year played into this, they did mention that the plaque spreads in two stages. They mention that the radial expansion of the plaque reaches its "top speed" in the first stage, which consist of the first ten hours of the experiment, while it slows down in the second stage, which is the rest of the experiment. They note that T7 grows poorly on stationary hosts, and that it is surprising that the plaque expands at all in the second phase. They speculate that the second growth stage is due to the bacteria "cannibalizing" on the lysed bacteria remains. I did not consider the release of nutrient by lysed bacteria in the model, and I don't think it would be a considerable effect either, as phages would exhaust the infected cells for available relevant nutrients, and the neighbouring infected bacteria would require the exact same type of nutrients. In my model, this effect of plaque expanding after the bacteria has reached a stationary phase is explained by the diffusion of nutrients. I do, however believe that the way this effect is incorporated in my model could be improved. It has been showed that environmental effects that decrease the productivity of the host bacteria also decrease the productivity of viral infection and burst sizes[115–117]. While this supports my way of coupling the maturation of infected bacteria to the bacterial growth rate, it does infer that the assumption of a constant burst rate does not hold when the bacteria is in a stressed condition like starvation. This could be incorporated with either having different bacterial growth behaviours and viral burst sizes for starvation conditions, or finding a way to couple the burst size and number of infection stages to the bacterial growth rate. This would complicate the model and while it could make the model more realistic, I don't know if this sort of complication would improve the model enough to be worth it. To repeat George Box' aphorism "all models are wrong, some are useful", and complicating the model could make it less useful.

In 2002, Fort, et al [76], published their paper "Time-delayed spread of Viruses in growing plaques" that emphasised the importance of incorporating a time delay between the infection of a phage and the lysis of the infected bacteria. This was done by including the lysis time with a Dirac delta dis-

tribution, removing the infected bacteria from the model and adding phages after a time constant after the removal, effectively assuming all infected bacteria would have a constant and equal lysis time. I don't need to convince the reader that a constant lysis time is an assumption that will yield unrealistic predictions, because Fort, et al did just that in their 2006 paper[118]. Here they go in great lengths to argue for the use of a normally distributed lysis time, and why this would make the model more realistic. As mentioned in section 3.5, the way I incorporate the maturation of infected bacteria yield a lysis time which follows a gamma distribution, that tends towards a normal distribution under certain conditions.

Haseltine et al published their paper "Image-Guided Modeling of Virus Growth and Spread" in 2008, and the paper is focused on the spread of vesicular stomatitis virus in baby hamster kidney cells[119]. The paper consist of both photographing plaque expansion and modelling. The images are captured by staining plaques at different time points with fluorescent dye and photographing the plaques [120]. The experimental setup is quite different from mine, as their technique requires them to induce cellular arrest in the host cells which does not let them follow the same plaque through maturation. Instead they have to compare different plaques arrested at different time-points. I argue that my experimental setup achieves a much greater insight into the plaque formation and general host-virus dynamic as it gives us images of the same plaque over time at steady intervals.

While the model presented by Haseltine et al. builds on the previous mentioned reaction diffusion models, there are some considerable conceptual changes. The model is focused on explaining the infection dynamics observed in their images instead of focusing on explaining the velocity of plaque expansion like previous models have. Forces like host growth, limiting substrate and the maturation of infected host are considered in the model. The diffusion of nutrient are not considered, and the growth of host cells follow a constant rate multiplied by the concentration of nutrient and host cells. As I have little experience with cultivation of baby hamster cells I do not know if these modelling choices were done to mimic reality or as a simplification. But I know from my experience with developing my model and examining the experimental data that these simplifications would be detrimental to my model, as it would result in the loss of one of my most important discoveries which is the importance of nutrient diffusion in plaque formation. The model they presented takes the infection of already infected bacteria into account, which is something I did not consider when I developed my model. Some viruses change the structure of their host, so that an infected host will not adsorb more of the same type of virus, in an phenomena called superinfection exclusion [23, 121]. But I have not explored if the phage used in this thesis is capable of superinfection exclusion. Including superinfection to the model would likely cause the plaque expansion to slow down, as phages

would be "consumed" by infected bacteria instead of diffusion further to reach uninfected bacteria.

From the models found through my literature search, it was Haseltine model that was most similar to the one I developed, despite the model being focused on mimicking viral spread in baby hamster kidney cells. This suggests that both my model and my related findings are relevant beyond the scope of phages. These findings could help explain not only the spread of viruses in bacterial population but in plant-, animal-, and human-cells as well. All the models I have mentioned are expressed in terms of radial coordinates, which includes an assumption of radial symmetry in the plaques. The advantage of this is that the model only considers a single spatial dimension, which makes it faster to solve numerically. It also makes it easier to algebraically manipulate the model to find expressions for the speed of radial expansion. The drawback is that the models are not able to adequately mimic merging plaques, like my model does, which considers two spatial dimensions in Cartesian coordinates. The Haseltine model was developed further in a paper published in 2014, but this development was in the direction of incorporating interferons and the immunoresponse of baby hamster cells in relation to viral infections[122]. This made the model too distinct from the one developed in this thesis for any productive comparison to be made.

5.3.4 Run 1.3

The double circles displayed in the merging plaques in experimental run 1.3 are a curious case. At first I suspected a contamination from another phage, but soon realised that this was very unlikely. The plaques show a very similar morphology before the merge, and I have yet to experience an infection from another phage. A mutation also seems highly unlikely as that would imply that two phage particles got the exact same mutation, and coincidentally ended up next to each other. I also suspected the double ring being a result of diffusion of nutrients from the centre of the plaque out to the surrounding infected and uninfected bacteria. Since there are two merging plaques, the out-flux of nutrient from the plaque centres would be higher here than for single plaques. Perhaps there was a threshold for nutrient flux, and when the out flux is larger than this threshold, the infected bacteria is able mature and this is what causes the double ring? The discovery of local variations in bacterial growth rate suggests otherwise. The results from Cellfiebooth suggest that the double ring is expressed whenever the bacterial growth rate follows a growth curve that suggests the bacteria changes growth strategy during the run. This was found in the agar, but patches of bacteria lawn following the alternative growth curve were found far from the the merging plaques. I believe the local variation of growth rate caused the double ring

in the merging plaque, rather than the of the merging plaque causing local variation in growth curve. I suspect this difference of plaque morphology to be the result of human error in some way. Perhaps the agar or soft agar was poured in a way that left the agar hardening in a somewhat tilted state. Naturally this would cause one of the sides to end up with more agar or soft agar than the other. This would certainly distribute the diffusion of nutrient from the agar unevenly in the Petri dish. Which could again result in local variation of growth rate.

6 Conclusion

The aim of the research presented in this thesis was to explore the development of viral plaques as well as different factors that cause plaques to emerge from phages proliferating on a bacterial lawn. To do this, I utilised and improved the self-developed Cellfiebooth, first presented in my report "Fluorescence imaging of the pre-visible stage of bacteriophage plaque formation". I used this system to measure the distribution of free DNA on a Petri dish over time, which was used as an indicator of bacteria lysed by phages. In addition to this, I developed a mathematical model that predicts the formation of plaques, and used this to find that the diffusion of nutrient from within the plaque is a vital driver for the late expansion of plaques.

The Cellfiebooth is a "general" system as it worked well for all the phage and bacterial strains tested. The fluorescent dye used in the Cellfiebooth system does not disturb bacterial growth, and the system is able to measure the formation and expansion of every plaque throughout the course of its development. I performed 10 measurements each hour for the duration of all experiments. This provided us with deep insights into the formation of plaques, as it did not simply show the end result of a formed plaque, but how plaques develop and change over time. The Cellfiebooth also revealed how bacteria can change growth strategy during the experiment, and that this has a severe consequence on the morphology of plaques. These findings provided us with improved understanding of how plaques are formed and even served as a warning that parameters which are not always considered or taken for granted, can have drastic effects on the experimental results.

Without fitting any of the model parameters to the experimental results from the Cellfiebooth, the model I developed and presented in this thesis is able to reproduce the shape of both single plaques and multiple merging plaques. The model thus provides insight into how plaques develop over time, and explains many phenomena observed in the Cellfiebooth system. Comparing and analysing the results from the Cellfiebooth and the model, I found that many phenomena observed in the Cellfiebooth, most importantly how the plaques are able to expand even after most bacteria have reached a stationary phase, are largely driven by the diffusion of nutrients. This nutrient diffusion is driven by the difference of nutrient concentration between areas where the phages have lysed all bacteria, and areas unaffected by phages. Essentially this involves the diffusion of nutrient from the centre of plaques out to the newly infected as well as still uninfected bacteria. This enables them to continue to divide and grow when the bacteria on the dish have exhausted all surrounding nutrients and reached the stationary phase. This phenomenon also explains why the greatest bacterial concentrations are attained in areas between closely spaced plaques, which benefit the most from the diffusion

effects. The effect of a plaque expanding after the bacteria has reached a stationary phase has been previously speculated, by Yih and Yin, to be due to the bacteria surrounding the plaques "cannibalizing" on the lysed bacteria remains[114]. Previous models, such as the Yin-McCaskil model and Fort et al model assumed that the late slow down of plaque expansion was caused by hindered diffusion by the high concentration of bacteria[76, 113]. Unlike my model– the models considering the late slow down of plaque expansion to be caused by bacterial hindrance were not able to accurately predict the experimental results[77, 123].

In addition to this, I, together with Nikolay Martyushenko, developed a new protocol for using a multiplate reader to determine the burst size, lysis time and standard deviation of the lysis time of a phage strain in a single experiment. The new protocol, compared to established protocols like the one step growth curve, is easier to perform and provides more insight into the phage dynamics.

The implications for establishing and improving the methods for measuring viral plaque development are many. Perhaps most notable are the implications this research can have for the further development of phage therapy as an alternative to antibiotics. Today the selection of phages for therapeutic use is often based on plaque morphology[48, 112]. Progress in this field of research has the potential to significantly alter–if not revolutionise–the way bacterial infections are treated. As phage therapy is bacteria specific, the vast list of side effects associated with full-body antibiotics could be rendered irrelevant. This further implicates that the predicted harmful and fatal ramifications of the dangerous proliferation of the antibiotic-resistant bacteria.

References

1. Todal, A. *Fluorescence imaging of the pre-visible stage of bacteriophage plaque formation*. tech. rep. (NTNU, Trondheim, 2019).
2. Kepner, R. L., Wharton, R. A. & Suttle, C. A. Viruses in Antarctic lakes. *Limnology and Oceanography* **43**, 1754–1761 (Nov. 1998).
3. García-Ruiz, J. M., Villasuso, R., Ayora, C., Canals, A. & Otálora, F. Formation of natural gypsum megacrystals in Naica, Mexico. *Geology* **35**, 327–330 (Apr. 2007).
4. Zimmer, C. *A planet of viruses* (University of Chicago Press, 2015).
5. Pommerville, J. C. *Fundamentals of microbiology* (Jones & Bartlett Publishers, 2013).
6. Suttle, C. A. *The Suttle Lab* <http://www.ocgy.ubc.ca/~suttle/?p=projects>.
7. Bolduc, B., Wirth, J. F., Mazurie, A. & Young, M. J. Viral assemblage composition in Yellowstone acidic hot springs assessed by network analysis. *ISME Journal* **9**, 2162–2177 (Oct. 2015).
8. Suttle, C. A. *Viruses in the sea* Sept. 2005.
9. Willner, D. *et al.* Metagenomic Analysis of Respiratory Tract DNA Viral Communities in Cystic Fibrosis and Non-Cystic Fibrosis Individuals. *PLoS ONE* **4** (ed Gold, J. A.) e7370 (Oct. 2009).
10. Steward, G. F. *et al.* Are we missing half of the viruses in the ocean? *ISME Journal* **7**, 672–679 (Mar. 2013).
11. Magare, B., Nair, A. & Khairnar, K. Isolation of bacteriophages from air using vacuum filtration technique: an improved and novel method. *Journal of Applied Microbiology* **123**, 896–902 (Oct. 2017).
12. Nasir, A., Kim, K. M. & Caetano-Anollés, G. Viral evolution: Primordial cellular origins and late adaptation to parasitism. *Mobile Genetic Elements* **2**, 247–252 (2012).
13. Iyer, L. M., Balaji, S., Koonin, E. V. & Aravind, L. Evolutionary genomics of nucleo-cytoplasmic large DNA viruses. *Virus Research* **117**, 156–184 (2006).
14. Wessner, D. R. The Origins of Viruses. *Nature Education* **3**, 37 (2010).
15. Murphy, F. A. The evolution of viruses, the emergence of viral diseases: a synthesis that Martinus Beijerinck might enjoy. *Archives of virology. Supplementum* **15**, 73–85 (1999).
16. Summers, W. C. Félix Hubert d’Herelle (1873-1949): History of a scientific mind. *Bacteriophage* **6**, e1270090 (2016).

17. Fruciano, E. & Bourne, S. *Phage as an antimicrobial agent: d'Herelle's heretical theories and their role in the decline of phage prophylaxis in the West* in *Canadian Journal of Infectious Diseases and Medical Microbiology* **18** (Hindawi Limited, 2007), 19–26.
18. Summers, W. C. Bacteriophage Therapy. *Annual Review of Microbiology* **55**, 437–451 (2001).
19. Stent, G. *Nazis, women and molecular biology* (Routledge, 2019).
20. Karmakar, P. & Gaitonde, V. Promising Recent Strategies with Potential Clinical Translational Value to Combat Antibacterial Resistant Surge. *Medicines* **6**, 21 (2019).
21. Lin, D. M., Koskella, B. & Lin, H. C. Phage therapy: An alternative to antibiotics in the age of multi-drug resistance. *World Journal of Gastrointestinal Pharmacology and Therapeutics* **8**, 162 (2017).
22. Sulakvelidze, A., Alavidze, Z. & Morris, J. G. Bacteriophage Therapy. *Antimicrobial Agents and Chemotherapy* **45**, 649–659 (2001).
23. Erez, Z. *et al.* Communication between viruses guides lysis-lysogeny decisions. *Nature* **541**, 488–493 (Jan. 2017).
24. Mellegård, H. *Virusesenes hemmelige liv som spioner, leiemordere og martyrer* https://www.aftenposten.no/viten/i/zGbRVv/Virusenes-hemmelige-liv-som-spioner_-leiemordere-og-martyrer.
25. Keen, E. C. A century of phage research: Bacteriophages and the shaping of modern biology. *BioEssays* **37**, 6–9 (Jan. 2015).
26. Summers, W. C. In the beginning... *Bacteriophage* **1**, 50–51 (2011).
27. Jurczak-Kurek, A. *et al.* Biodiversity of bacteriophages: Morphological and biological properties of a large group of phages isolated from urban sewage. *Scientific Reports* **6** (Oct. 2016).
28. Gallet, R., Kannoly, S. & Wang, I. N. Effects of bacteriophage traits on plaque formation. *BMC Microbiology* **11**, 181 (2011).
29. Madigan, M. T., Martinko, J. M., Dunlap, P. V. & Clark, D. P. *Brock biology of microorganisms* (Pearson/Benjamin Cummings, San Francisco, CA, 2009).
30. Klein, J. *virus – Store medisinske leksikon* <https://sml.snl.no/virus>.
31. Lodish, H. *et al.* in *Molecular Cell Biology* 4th editio (W. H. Freeman, 2000). <https://www.ncbi.nlm.nih.gov/books/NBK21523/>.
32. Ofir, G. & Sorek, R. Contemporary Phage Biology: From Classic Models to New Insights. *Cell* **172**, 1260–1270 (Mar. 2018).
33. Tonjum, T. *bakteriofag – Store medisinske leksikon* 2018. <https://sml.snl.no/bakteriofag>.

34. *bacteriophage* <https://www.nature.com/scitable/definition/bacteriophage-phage-293>.
35. Clokie, M. R., Millard, A. D., Letarov, A. V. & Heaphy, S. Phages in nature. *Bacteriophage* **1**, 31–45 (2011).
36. Hyman, P. & Abedon, S. T. Practical methods for determining phage growth parameters. *Methods in molecular biology (Clifton, N.J.)* **501** (eds Clokie, M. R. J. & Kropinski, A. M.) 175–202 (2009).
37. Perlmutter, J. D. & Hagan, M. F. Mechanisms of Virus Assembly. *Annual Review of Physical Chemistry* **66**, 217–239 (Apr. 2015).
38. Fastrez, J. in *EXS* 35–64 (1996).
39. Talaro, K. *Foundations in microbiology* (McGraw-Hill Education, New York, NY, 2015).
40. Moons, P., Faster, D. & Aertsen, A. Lysogenic Conversion and Phage Resistance Development in Phage Exposed Escherichia coli Biofilms. *Viruses* **5**, 150–161 (2013).
41. Łoś, M. & Wkegrzyn, G. in *Bacteriophages, Part A* 339–349 (Elsevier, 2012).
42. Howard-Varona, C., Hargreaves, K. R., Abedon, S. T. & Sullivan, M. B. Lysogeny in nature: mechanisms, impact and ecology of temperate phages. *The ISME Journal* **11**, 1511–1520 (2017).
43. Hobbs, Z. & Abedon, S. T. Diversity of phage infection types and associated terminology: the problem with ‘Lytic or lysogenic’. *FEMS Microbiology Letters* **363** (ed Millard, A.) fnw047 (2016).
44. Citorik, R. J., Mimee, M. & Lu, T. K. *Bacteriophage-based synthetic biology for the study of infectious diseases* 2014.
45. HERSHEY, A. D. & CHASE, M. Independent functions of viral protein and nucleic acid in growth of bacteriophage. *The Journal of general physiology* **36**, 39–56 (1952).
46. Sambrook, J., Fritsch, E. F., Maniatis, T., *et al.* *Molecular cloning: a laboratory manual*. **Ed. 2** (Cold spring harbor laboratory press, 1989).
47. Baer, A. & Kehn-Hall, K. Viral concentration determination through plaque assays: Using traditional and novel overlay systems. *Journal of Visualized Experiments* (Nov. 2014).
48. Krylov, V. *et al.* *Modular approach to select bacteriophages targeting Pseudomonas aeruginosa for their application to children suffering with cystic fibrosis* Oct. 2016. <http://journal.frontiersin.org/article/10.3389/fmicb.2016.01631/full>.
49. Son, M. S. & Taylor, R. K. Growth and maintenance of Escherichia coli laboratory strains. *Current Protocols in Microbiology* (2012).

50. Grant, S. G., Jessee, J., Bloom, F. R. & Hanahan, D. Differential plasmid rescue from transgenic mouse DNAs into *Escherichia coli* methylation-restriction mutants. *Proceedings of the National Academy of Sciences of the United States of America* **87**, 4645–4649 (1990).
51. Jeong, H., Kim, H. J. & Lee, S. J. Complete genome sequence of *Escherichia coli* strain BL21. *Genome Announcements* **3** (2016).
52. Fotadar, U., Zaveloff, P. & Terracio, L. Growth of *Escherichia coli* at elevated temperatures. *Journal of Basic Microbiology* **45**, 403–404 (Oct. 2005).
53. Monod, J. The Growth of Bacterial Cultures. *Annual Review of Microbiology* **3**, 371–394 (Oct. 1949).
54. Pepper, I. L., Gerba, C. P. & Gentry, T. J. *Environmental Microbiology* Third Edit. <https://linkinghub.elsevier.com/retrieve/pii/C20110050299> (Elsevier, 2015).
55. Venkateshan, S. & Swaminathan, P. in *Computational Methods in Engineering* 1–15 (Elsevier, 2014). <https://linkinghub.elsevier.com/retrieve/pii/B9780124167025500016>.
56. Poirier, D. R., Geiger, G. H., Poirier, D. R. & Geiger, G. H. in *Transport Phenomena in Materials Processing* 419–461 (Springer International Publishing, Cham, 2016).
57. Bender, E. A. *An Introduction to Mathematical Modeling (Dover Books on Computer Science)* <https://www.xarg.org/ref/a/048641180X/> (Dover Publications (Educa Books), Mar. 2012).
58. Dubois, G. *Modeling and Simulation : Challenges and Best Practices for Industry* First edit. <http://gen.lib.rus.ec/book/index.php?md5=a5c71fa61badac3c24f70b0d025d0cbb> (CRC Press, 2018).
59. Box, G. E. P., Hunter, J. S. & Hunter, W. G. in *Wiley Series in Probability and Statistics* (Wiley Hoboken, NJ, USA, 2005).
60. Box, G. E. P. Science and statistics. *Journal of the American Statistical Association* **71**, 791–799 (1976).
61. Clapeyron, E. Mémoire sur la puissance motrice de la chaleur. *Journal de l'École Polytechnique* **XIV**, 153–90 (1834).
62. Raymond, K. W. *General organic and biological chemistry : an integrated approach* 648 (John Wiley & Sons, 2015).
63. Box, G. in *Robustness in Statistics* 201–236 (Elsevier, 1979).
64. Newton, I. *Philosophiae naturalis principia mathematica* (G. Brookman, 1833).
65. Maxwell, J. C. VIII. A dynamical theory of the electromagnetic field. *Philosophical Transactions of the Royal Society of London* **155**, 459–512 (Jan. 1865).

66. Turing, A. M. The Chemical Basis of Morphogenesis. *Philosophical Transactions of the Royal Society of London. Series B, Biological Sciences* **237**, 37–72 (1952).
67. Maini, P. K., Painter, K. J. & Chau, H. N. P. Spatial pattern formation in chemical and biological systems. *Journal of the Chemical Society - Faraday Transactions* **93**, 3601–3610 (Oct. 1997).
68. Pilipchuk, V. N. *Nonlinear Dynamics Between Linear and Impact Limits* (eds Pfeiffer, F. & Wriggers, P.) **0**, 265–273 (Springer-Verlag Berlin Heidelberg 2010, 2010).
69. Rossant, C. *IPython Cookbook - 12.4. Simulating a partial differential equation — reaction-diffusion systems and Turing patterns* <https://ipython-books.github.io/124-simulating-a-partial-differential-equation-reaction-diffusion-systems-and-turing-patterns/>.
70. Karig, D. *et al.* Stochastic Turing patterns in a synthetic bacterial population. *Proceedings of the National Academy of Sciences of the United States of America* **115**, 6572–6577 (June 2018).
71. Kauffman, S. A., Shymko, R. M. & Trabert, K. Control of sequential compartment formation in *Drosophila*. *Science* **199**, 259–270 (1978).
72. Yin, J. & McCaskill, J. S. Replication of viruses in a growing plaque: a reaction-diffusion model. *Biophysical Journal* **61**, 1540–1549 (1992).
73. Krone, S. M. in *Bacteriophage Ecology* (ed Abedon, S. T.) 415–438 (Cambridge University Press).
74. Koch, A. L. The growth of viral plaques during the enlargement phase. *Journal of Theoretical Biology* **6**, 413–431 (1964).
75. Ortega-Cejas, V., Fort, J., Méndez, V. & Campos, D. Approximate solution to the speed of spreading viruses. *Physical Review E - Statistical, Nonlinear, and Soft Matter Physics* **69** (Mar. 2004).
76. Fort, J. A comment on amplification and spread of viruses in a growing plaque. *Journal of theoretical biology* **214**, 515–8 (Feb. 2002).
77. Abedon, S. T. & Culler, R. R. Bacteriophage evolution given spatial constraint. *Journal of Theoretical Biology* **248**, 111–119 (Sept. 2007).
78. Kreyszig, E. *Advanced Engineering Mathematics, 10th Edition* (Wiley, 2009).
79. Hairer, E. & Wanner, G. *Solving Ordinary Differential Equations II. Springer Series in Computational Mathematics* (Springer-Verlag Berlin Heidelberg, 1996).
80. Hirsch, C. *Numerical Computation of Internal and External Flows: Volume 1: Fundamentals of Numerical Discretization* (Chichester [etc.]: John Wiley & Sons, 2001).

81. WESSELING, P. von Neumann stability conditions for the convection-diffusion equation. *IMA Journal of Numerical Analysis* **16**, 583–598 (1996).
82. Walpole, R., Myers, R., Myers, S. & Ye, K. *Probability & statistics for engineers & scientists* <https://sci-hub.se/http://bida.uclv.edu.cu/bitstream/handle/123456789/9724/probability-statistics-for-engineers-scientists.pdf?sequence=1> (2012).
83. Neuhauser, C. *Calculus for biology and medicine* 2nd editio (ed Yagan, S.) (Pearson Education, Inc, 2004).
84. Friedman, N., Cai, L. & Xie, X. S. Linking stochastic dynamics to population distribution: An analytical framework of gene expression. *Physical Review Letters* **97** (2006).
85. Huxley, J. Problems of relative growth. <https://archive.org/details/problemsofrelati033234mbp/page/n1> (1932).
86. Adams, C. J. & Bell, D. D. *A model relating egg weight and distribution to age of hen and season* tech. rep. (1998). <https://academic.oup.com/japr/article-abstract/7/1/35/729937>.
87. Cardinal, L. J. Central tendency and variability in biological systems: Part 2. *Journal of Community Hospital Internal Medicine Perspectives* **5**, 28972 (Jan. 2015).
88. Kernler, D. *User contributions for Mathprofdk - Wikimedia Commons* <https://commons.wikimedia.org/wiki/Special:Contributions/Mathprofdk>.
89. Hosch, W. L. *Gamma distribution | mathematics | Britannica* 2017. <https://www.britannica.com/science/gamma-distribution>.
90. Hitchcock, S., Hogg, R. V. & Craig, A. T. Introduction to Mathematical Statistics. *Journal of the Royal Statistical Society. Series A (General)* **129**, 589 (1966).
91. Belikov, A. V. The number of key carcinogenic events can be predicted from cancer incidence. *Scientific Reports* **7** (Dec. 2017).
92. Comtois, P. *The gamma distribution as the true aerobiological probability density function (PDF)* in *Aerobiologia* **16** (2000), 171–176.
93. Frank, S. A. *The common patterns of nature* Aug. 2009.
94. Peters, C. A. in *Environmental Engineering Processes Laboratory Manual* (ed S. E. Powers, E.) (Champaign, IL, 2001).
95. Pérez-Rodríguez, F. & Zwietering, M. H. Application of the Central Limit Theorem in microbial risk assessment: High number of servings reduces the Coefficient of Variation of food-borne burden-of-illness. *International Journal of Food Microbiology* **153**, 413–419 (Feb. 2012).

96. Tanushev, M. S. & Arratia, R. Central limit theorem for renewal theory for several patterns. *Journal of Computational Biology* **4**, 35–44 (1997).
97. Lange, K. Central limit theorems of pedigrees. *Journal of Mathematical Biology* **6**, 59–66 (1978).
98. Mao, F., Leung, W.-Y. & Van, T. *Methods of using dyes in association with nucleic acid staining or detection* 2014.
99. Nikon D750 - DxOMark <https://www.dxomark.com/Cameras/Nikon/D750>.
100. Canon EOS 500D - DxOMark <https://www.dxomark.com/Cameras/Canon/EOS-500D>.
101. Schantz, E. J. & Lauffer, M. A. Diffusion Measurements in Agar Gel. *Biochemistry* **1**, 658–663 (July 1962).
102. Müller-Merbach, M., Peter, K., Weidendorfer, K. & Hinrichs, J. Diffusion of bacteriophages in an agar gel and in a fermented milk matrix. *Milchwissenschaft* **62**, 24–27 (2007).
103. Monk, J. M. *et al.* Multi-omics Quantification of Species Variation of Escherichia coli Links Molecular Features with Strain Phenotypes. *Cell Systems* **3**, 238–251 (Sept. 2016).
104. Pletnev, P., Osterman, I., Sergiev, P., Bogdanov, A. & Dontsova, O. *Survival guide: Escherichia coli in the stationary phase* 2015.
105. Shao, Y. & Wang, I. N. Effect of late promoter activity on bacteriophage λ fitness. *Genetics* **181**, 1467–1475 (Apr. 2009).
106. Milo, R. & Phillips, R. *How many virions result from a single viral infection?* 2005. <http://book.bionumbers.org/how-many-virions-result-from-a-single-viral-infection/>.
107. Nabergoj, D., Modic, P. & Podgornik, A. Effect of bacterial growth rate on bacteriophage population growth rate. *MicrobiologyOpen* **7** (Apr. 2018).
108. Ackermann, H.-W. in *Bacteriophages* 127–140 (Springer, 2009).
109. Ratkowsky, D. A., Olley, J., McMeekin, T. A. & Ball, A. Relationship between temperature and growth rate of bacterial cultures. *Journal of Bacteriology* **149**, 1–5 (1982).
110. Jouenne, T., Bonato, H., Mignot, L. & Junter, G. A. Cell immobilization in composite agar layer microporous membrane structures: growth kinetics of gel-entrapped cultures and cell leakage limitation by a microporous membrane. *Applied Microbiology and Biotechnology* **38**, 478–481 (Jan. 1993).

111. neb.com. *BL21 Competent E. coli* / NEB 2018. <https://international.neb.com/products/c2530-bl21-competent-e-coli#Product%20Information%20https://www.neb.com/products/c2530-bl21-competent-e-coli#Product%20Information>.
112. Weber-Dabrowska, B. *et al. Bacteriophage procurement for therapeutic purposes* Aug. 2016.
113. You, L. & Yin, J. Amplification and spread of viruses in a growing plaque. *Journal of Theoretical Biology* **200**, 365–373 (Oct. 1999).
114. Lee, Y. & Yin, J. Imaging the propagation of viruses. *Biotechnology and Bioengineering* **52**, 438–442 (Mar. 1996).
115. Fister, S. *et al.* Influence of environmental factors on phage-bacteria interaction and on the efficacy and infectivity of phage P100. *Frontiers in Microbiology* **7** (July 2016).
116. Chibani-Chennoufi, S., Bruttin, A., Dillmann, M. L. & Brüßow, H. *Phage-host interaction: An ecological perspective* June 2004.
117. Denes, T. & Wiedmann, M. *Environmental responses and phage susceptibility in foodborne pathogens: Implications for improving applications in food safety* Apr. 2014.
118. Fort, J., Pérez, J., Ubeda, E. & García, F. J. Fronts with continuous waiting-time distributions: Theory and application to virus infections. *Physical Review E - Statistical, Nonlinear, and Soft Matter Physics* **73** (2006).
119. Haseltine, E. L., Lam, V., Yin, J. & Rawlings, J. B. Image-guided modeling of virus growth and spread. *Bulletin of Mathematical Biology* **70**, 1730–1748 (Aug. 2008).
120. Lam, V., Duca, K. A. & Yin, J. Arrested spread of vesicular stomatitis virus infections in vitro depends on interferon-mediated antiviral activity. *Biotechnology and Bioengineering* **90**, 793–804 (June 2005).
121. Adams, R. H. & Brown, D. T. BHK cells expressing Sindbis virus-induced homologous interference allow the translation of nonstructural genes of superinfecting virus. *Journal of Virology* **54**, 351–357 (1985).
122. Swick, A., Baltes, A. & Yin, J. Visualizing infection spread: Dual-color fluorescent reporting of virus-host interactions. *Biotechnology and Bioengineering* **111**, 1200–1209 (2014).
123. Gallet, R., Kannoly, S. & Wang, I.-N. Effects of bacteriophage traits on plaque formation. *{BMC} Microbiology* **11**, 181 (2011).

A Protocol for making M9 broth

The following protocols were first printed in my report "Fluorescence imaging of the pre-visible stage of bacteriophage plaque formation".

A.1 M9 5x stock

Following reagents are added to a 2-litre flask:

- 30 g Na_2HPO_4
- 15 g KH_2PO_4
- 2.5 g NaCl
- 1 L High quality distilled water

Once the ingredients are added, stir with heating until all everything is dissolved. Make sure the cap is loosened and autoclave at 15 psi, 121 C° for 20 minutes.

A.2 M9 1x working solutions

Following reagents are added aseptically to make 1 litre 1x working solution:

- 200 mL M9 salt (sterile 5x)
- 200 μL MgSO_4 (sterile 1 M)
- 50 mL Glucose (sterile 100 % w/v solution)
- 50 mL Casamino (sterile 10 % w/v solution)
- 699.8 mL High quality distilled water

For agar and soft agar; the agar is dissolved and autoclaved in the high quality distilled water before the other reagents are added. The temperature of the agar should be kept at 50 °C or over until it is poured to keep it from hardening too early. To achieve this, I recommended to heat the 5x M9 salt before mixing it in with the agar solution.

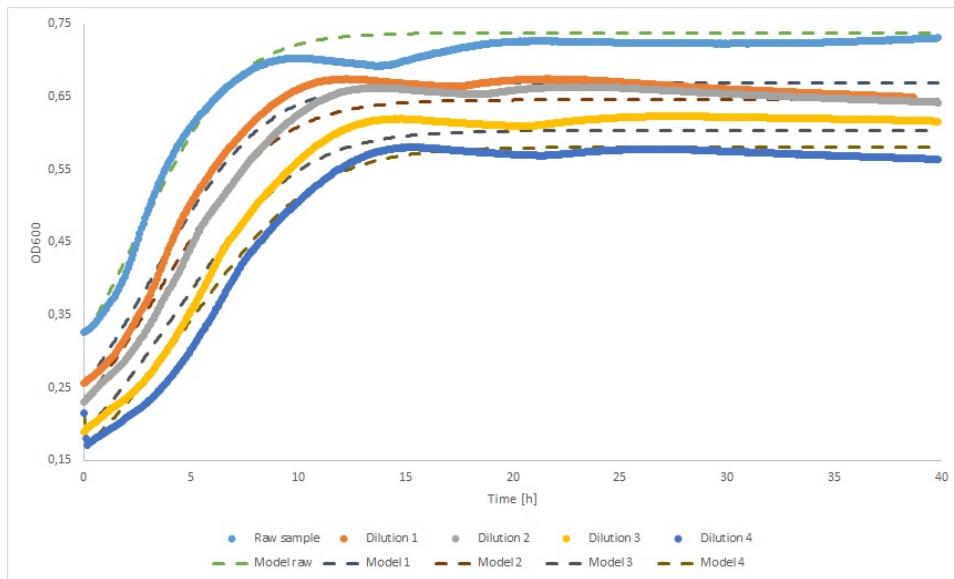


Figure 76: Growth curve for *E. coli* BL21. The dashed line shows the modelled growth for the same seeding OD. All models have the same constants related to growth kinetics.

B Characterisation of growth rate - additional data

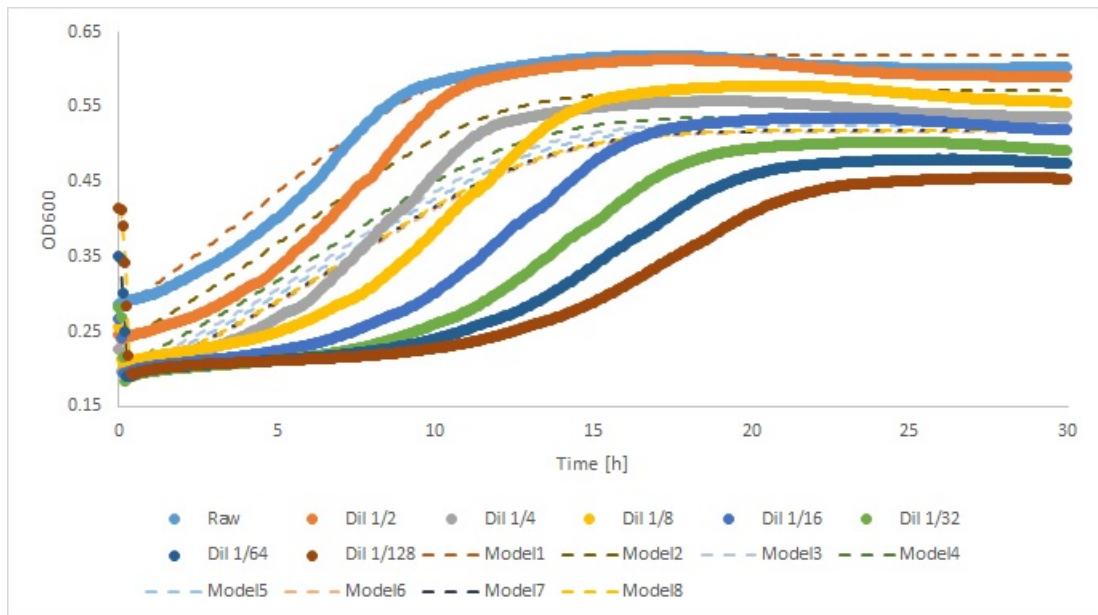


Figure 77: Growth curve for *E. coli* DH5 α . The dashed line shows the modelled growth for the same seeding OD. All models have the same constants related to growth kinetics.

C Burst size and lysis time - additional data

The graphs in figure 78 and 79 show the odd number dilutions

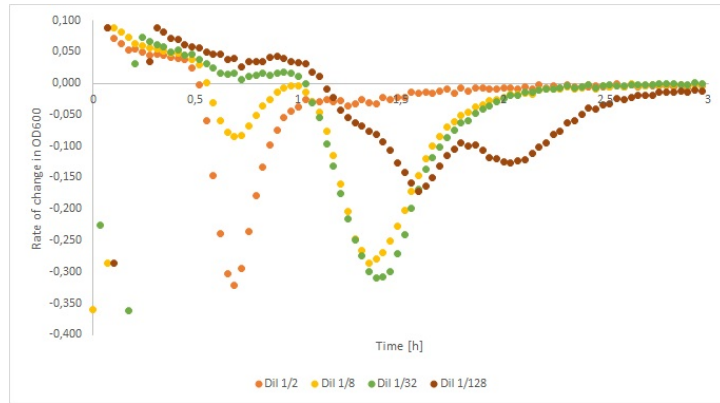


Figure 78: Rate of change in OD₆₀₀ over time for BL21 introduced to different concentrations of phages. Odd number dilutions.

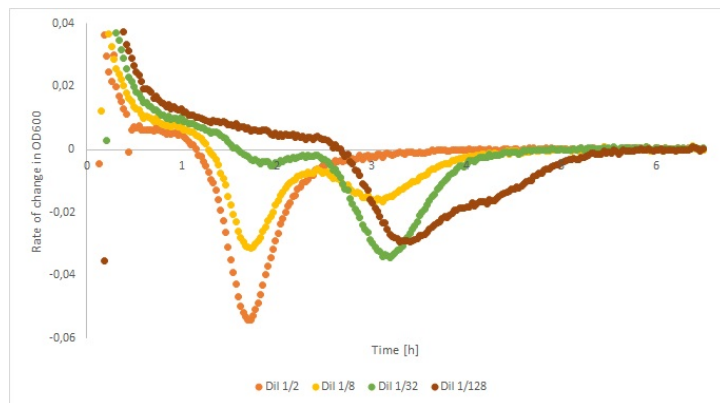


Figure 79: Rate of change in OD₆₀₀ over time for DH5a introduced to different concentrations of phages. Data filtered with 5 point average. Odd number dilutions.

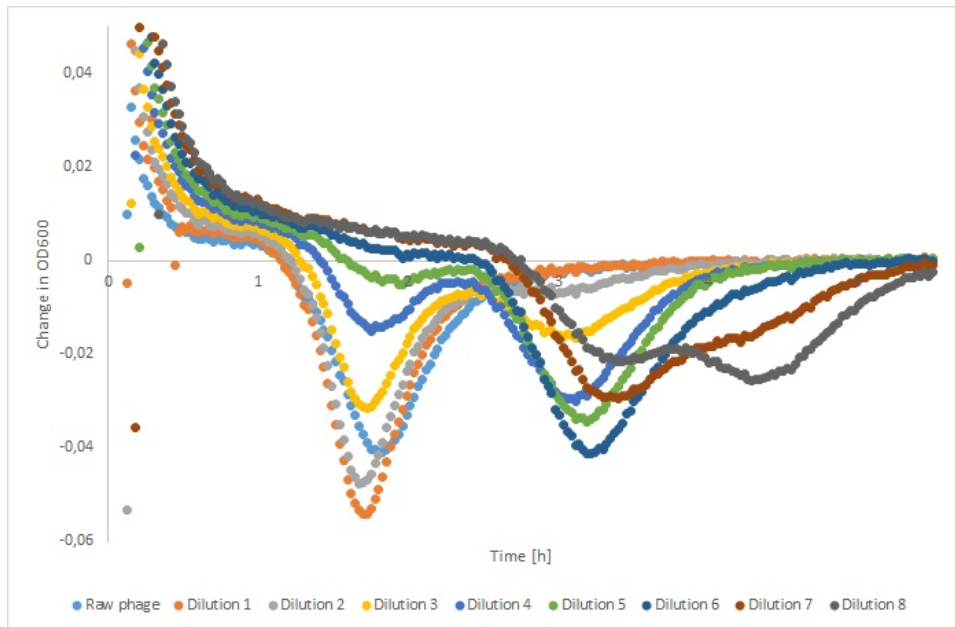


Figure 80: Change in OD when the *E. coli* strain DH5 α is introduced to different concentrations of the UP phage.

D Observed effects from Cellfiebooth regarding measurement of light

Figure 81 and 82 are from my report "Fluorescence imaging of the pre-visible stage of bacteriophage plaque formation"[1]. Figure 81 shows how the two filters together stop all light visible to the naked eye. Reflection of my hand photographing the effect can be observed where the two filters overlap. Figure 82 show how the light source is visible in the Cellfiebooth when it is placed directly under the camera. The lightsource can be observed in the middle of the Petri dish as a square brighter than the rest of the photograph. Reflection of the LED lights appear in the lower left corner of the image inside the Petri dish as bright circles.

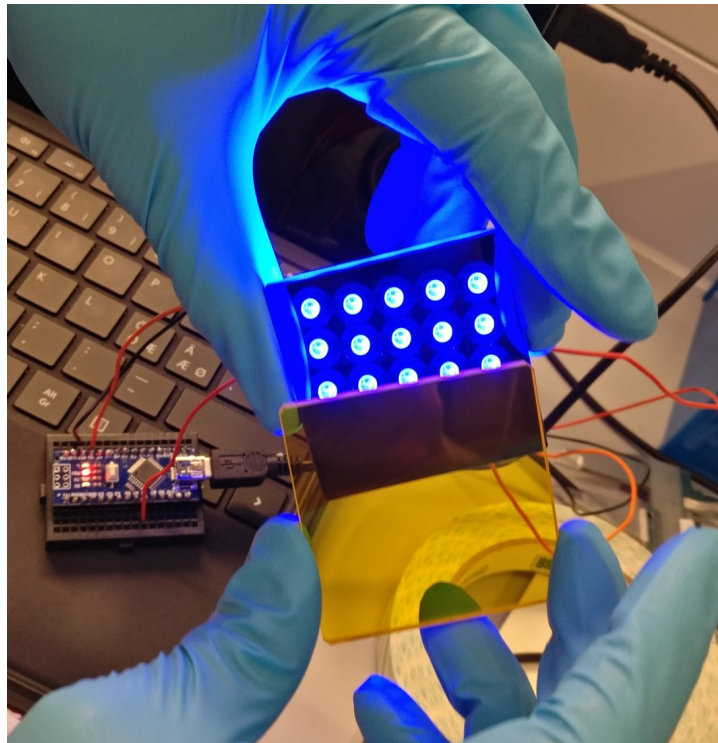


Figure 81: 515 nm longpass filter on top of 465 nm shortpass filter with LED lights on behind.

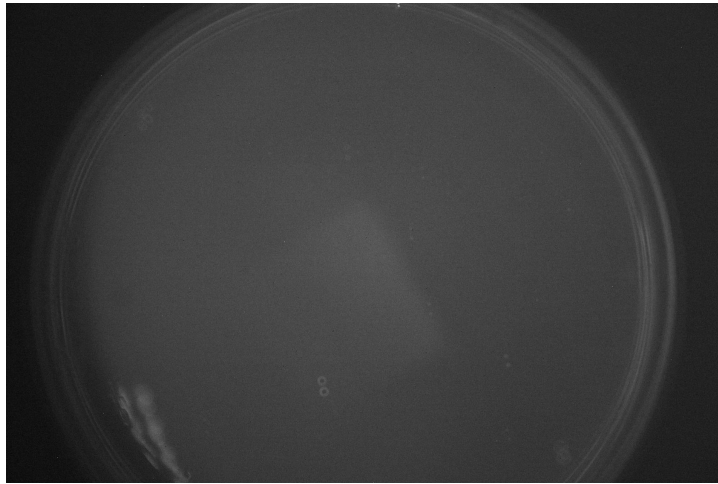


Figure 82: Light source directly under Petri dish in Cellfiebooth.